A CELLULAR AND MOLECULAR STUDY OF CORNEAL SCARRING

By

DANIEL JAMES GIBSON

A DISSERTATION PRESENTED TO THE GRADUATE SCHOOL
OF THE UNIVERSITY OF FLORIDA IN PARTIAL FULFILLMENT
OF THE REQUIREMENTS FOR THE DEGREE OF
DOCTOR OF PHILOSOPHY

UNIVERSITY OF FLORIDA

2011

To Prometheus – thanks for the fire

ACKNOWLEDGEMENTS

I thank the chair and members of my supervisory committee for their mentoring and guidance through the jungle of ambiguity that medical research can be. I would like to thank the National Eye Institute for its financial support through a Ruth L. Kirschstein National Research Service Award pre-doctoral training grant. I would like to give special thanks to my in-laws, whose tireless efforts helping with my children, granted my wife and I enough time for us both to finish our doctoral research, writing, and dissertation defense. And finally, I would like to thank my wife, Soojung Seo, for the two healthy boys she has provided me and the love and support she continues to provide me.

TABLE OF CONTENTS

page

LIST OF TABLES

LIST OF FIGURES

LIST OF ABBREVIATIONS

ASO	Antisense oligonucleotide, a short single stranded oligonucleotide with a sequence which is complimentary to a portion of a targeted mRNA sequence.
bp	Base pair, referring to a number of hybridized nucleic acids in a polynucleic acid.
EDTA	Ethylenediaminetetraacetic acid, a chelating agent used to inhibit metalloenzymes.
ELISA	Enzyme-linked immunosorbent assay, an assay for quantifying the presence of a particular antigenic substance using antibodies and dye processing enzymes.
HEPES	4-(2-hydroxyethyl)-1-piperazineethanesulfonic acid, a biologically compatible buffering agent.
LASIK	Laser-assisted in situ keratomileusis, one of many methods for reshaping the cornea with an excimer laser. Consists of creating a corneal flap, which is then lifted, and the underlying stroma is reshaped by the laser.
mAb	Monoclonal antibody, an immunoreactive solution composed of a single molecular species of an antibody directed against a molecular target.
pAb	Polyclonal antibody, an immunoreactive solution composed of a mixture molecular species of antibodies directed against a molecular target.
pCTGF-eGFP	A genetically engineered mouse with the promoter of connective tissue growth factor driving the transcription of enhanced green fluorescent protein.
PMSF	Phenylmethylsulfonyl fluoride, a serine proteinase inhibitor which alkylates the serine in the active site of the enzyme.
PTK	Phototherapeutic keratectomy, one of many methods for reshaping the cornea with an excimer laser. PTK removes a cylindrical or trapezoidal profile of tissue from the anterior surface of the cornea.
PBS	Phosphate buffered saline, a common biologically tolerable buffer.
Tris	Tris(hydroxymethyl)aminomethane, a biologically tolerable buffer.

Abstract of Dissertation Presented to the Graduate School
of the University of Florida in Partial Fulfillment of the
Requirements for the Degree of Doctor of Philosophy

A CELLULAR AND MOLECULAR STUDY OF CORNEAL SCARRING

By

Daniel James Gibson

August 2011

Chair: Gregory S. Schultz
Co-chair: Susan C. Frost
Major: Medical Sciences

Fibrosis of damaged tissue is the basis for many chronic pathologies. Insights from the scarless healing of mammalian fetuses and marsupial pouch young have revealed that transforming growth factor-β (TGF-β) has a central role in adult fibrosis. Additional work has revealed that connective tissue growth factor (CTGF) is a mediator of TGF-β induced, fibrosis-like, activities *in vitro*; including the key activities of proliferation, collagen synthesis, and cellular differentiation. Fibrosis in the cornea resulting from acute injury can lead to the generation of a light scattering scar. While it is known that CTGF is necessary for TGF-β to induce pro-fibrotic activities in cell cultures, it is not known whether this is the case for the formation of light scattering scars *in vivo*. The experiments reported herein are separated into two general categories; those centered on studying a molecular effector of fibrosis (CTGF) and those studying the process of fibrosis itself. Throughout all of the experiments, a surgical excimer laser is used to generate an acute wound in the cornea of one of three animal models: 1) a normal rabbit, 2) a transgenic reporter mouse with enhanced green fluorescent protein under control of the promoter found upstream of CTGF, and 3) a

transgenic reporter mouse in which the corneal epithelium is genetically labeled with β-galactosidase activity.

First, the role of CTGF in corneal fibrosis was tested by down regulation using an iontophoretically delivered antisense oligonucleotide (ASO). Following bilateral wounding, one cornea received a CTGF ASO while the contralateral cornea received a scrambled sequence control ASO. The ability of the CTGF ASO to reduce corneal haze was measured by photographing the wound and measuring the intensity of light reflection by the scar. The down-regulation of CTGF was measured by enzyme-linked immunosorbant assay (ELISA) analysis of homogenized corneas. The iontophoresis was well tolerated with an immediate increase in edema as the only observed side effect. The source of edema was confirmed to be caused by the transfer of the highly anionic ASOs themselves, and not iontophoresis ($p = 0.01$). The amount of haze was slightly, but not significantly reduced at day 7 ($p = 0.23$), but was significant by day 14 ($p = 0.04$). Iontophoresis of CTGF ASO was capable of reducing CTGF protein in the cornea at both days 7 ($p = 0.05$) and 14 ($p = 0.002$). The reduction of CTGF protein and corneal haze following treatment with a CTGF ASO validated that CTGF has a role in corneal fibrosis.

In order to better understand the role of CTGF in fibrosis, the location of its synthesis and accumulation was measured in healing corneas. First, the location of CTGF protein was observed during healing in rabbit corneas using immunofluorescent staining with a monoclonal antibody to CTGF. Next, a transgenic reporter mouse with enhanced green fluorescent protein transcription driven by CTGF's promoter was used to observe which cells are actively transcribing the CTGF gene. The corneas of the

reporter mouse were wounded, and the eyes were harvested and histologically sectioned. The location of CTGF protein was observed by staining the reporter mouse sections with a biotinylated form of the same monoclonal antibody used in the rabbit experiments. Since the synthesis was reported with a green fluorescent protein, the CTGF protein was detected using a Texas Red labeled avidin, thereby enabling simultaneous observation of CTGF synthesis (green) and protein localization (red). During healing, CTGF protein was detected in all three cellular layers of the cornea, but was most abundant in the basal epithelium. Surprisingly, the predominant source of CTGF synthesis in the cornea was the endothelium, with the levels of synthesis in the epithelium and stroma being so low that they could not be observed in the reporter mouse. These observations invalidated the initial hypothesis of fibroblast derived synthesis and binding of CTGF during fibrosis, and gave rise to a new, more complex, theory that CTGF is synthesized by the endothelium and then bound by the epithelium to have its pro-fibrotic effect.

Following re-epithelialization the cornea is still clear, but within the weeks that follow it can become opaque. Not much is known about how and where the opacification starts and how it matures to its final level of intensity. The next project investigated how and where haze starts, and how it changes with time using a novel photographic technique which enables visualization of the entire scar with standard photographic equipment. The emergence of haze was observed by daily photography of wounds as they developed haze. Next, a series of haze images were compared with the immunofluorescent localization of light reflecting myofibroblasts during the period of haze maturation. Haze consistently began as a thin ring at the wound periphery.

Occasionally, another separate region of haze emerged in the center of the wound with a haze-less region in between the center-region haze and the ring of haze at the margin. The haze spread with time from the these regions of nucleation into the adjacent haze-less regions with time. The regions with haze present intensified with time as well. The overall distribution of α-smooth muscle actin (α-SMA) staining in the wound, mirrored the pattern of haze initiation and spread during haze formation. Unexpectedly, α-SMA was also substantially present in the basal epithelium, but had a different intracellular distribution that that of the cells in the stroma. Finally, the intensification of haze was reflected in the number of myofibroblast layers that accumulated below the epithelium. These observations required a drastic change in the theory of haze fibrogenesis following acute injury; directing attention away from the fibroblasts in the underlying stroma towards either the fibroblasts in the peripheral stroma or even the epithelial cells themselves.

Finally, some previously known facts about wound healing and the new data generated by some of the work presented herein led to a conundrum concerning the current theory of fibrosis in the cornea. Given that epithelial cells are the first cells to contact the non-wounded stromal surface, that they are the primary source of CTGF binding, that they possess significant amounts of α-SMA, and that the formation and spread of haze mirror the pattern of re-epithelialization, a hypothesis that the epithelial cells themselves differentiate into the stromal myofibroblasts was formed to resolve the conundrum. An alternative hypothesis, that the peripheral stromal cells migrate into the wound area and displace the epithelium in a manner reminiscent of *de novo* stromagenesis was also formed. A reporter mouse with a genetically labeled epithelium

was used to observe whether cells from the epithelium are present in the stromal scar following acute injury. Concurrently, gross histological analysis was performed on hematoxylin and eosin stained rabbit corneal wounds from the period prior to haze formation to seek evidence of any interchange of cells between the epithelium and stroma, or of epithelial displacement by the stroma-derived cells. Finally, the presence and localization of tenascin-C, a candidate marker for the process of epithelial-to-mesenchymal transition (EMT), was observed in wounded rabbit corneas during the period of haze formation via immunofluorescent staining. Epithelium-derived cells were found below the scar in the wounded reporter mouse cornea, but were surrounded on all sides by stroma-derived cells. The gross histological analysis revealed that during re-epithelialization some epithelial cells invaded the residual stroma along incompletely removed stromal lamellae (days 1 and 2). The gross histological data also provided evidence for the migration of peripheral fibroblasts into the wound (day 3) and displacement of the epithelium by a blistering-like mechanism (day 5). Tenascin-C was present during haze formation and its distribution and spread mirrored both the spread of haze and the previously observed spread of α-SMA. In total, these data support the hypothesis that epithelial cells do become part of the stroma, but only to a minor degree. The data support a mechanism similar to the *de novo* stromagenesis with the peripheral fibroblasts as the primary source of cells that become light reflecting haze. The data also cast the use of protein markers as indicators of the EMT process.

In conclusion, the work reported here validates the proposed role of CTGF in the generation of light reflecting scars, but it calls into question the source of the pro-fibrotic CTGF and its locus and mechanism of action. The current evidence suggests that

CTGF synthesized by the endothelium could possibly diffuse through the edematous stroma and then bind to the basal epithelium. While, epithelial cells were found in the stroma following wound healing, they were vastly outnumbered by stroma-derived cells, undercutting an EMT-based theory for haze formation. With the new data presented here, the best supported theory explaining the formation of haze is that the peripheral fibroblasts migrated towards the basal epithelium, differentiate into the light reflecting α-SMA positive cells. The epithelium is then displaced by a blistering-like mechanism and the haze myofibroblasts populate the sub-epithelial space and proliferate, leading to the spread and intensification of the light reflecting scar.

CHAPTER 1
INTRODUCTION

Corneal Fibrosis

Fibrosis is the biological response to damage or disruption of cellularized tissue whereby the cells proliferate, differentiate, and synthesize new extracellular matrix (ECM) molecules to patch the damage. While this response does replace or bridge lost or rent tissue, the newly regenerated tissue typically does not possess the same structure as the uninjured tissue, nor does it regain the function of the once intact tissue. Fibrotic healing is responsible for prolonged pathological conditions in the kidneys[1,2], liver[3], heart[4,5], peritoneum[6], skin[7], and in the eye[8-11]. While not life threatening, fibrosis anywhere in the eye as a result of injury, infection, or surgery is highly problematic for the quality of one's life considering that sight is the most crucial of our senses providing an estimated 80% of all sensory input[12].

The eye provides at least three visual functions, it refracts and focuses incident light, it transduces the light into a neurological signal, and it provides some initial visual information processing. The eye is functionally divided into two segments, the posterior segment where photo-transduction and information processing take place, and the anterior segment where refraction and focus/accommodation take place. While fibrosis can impair each of these functions[9,13-15], the scope of this project will be restricted to fibrosis affecting the clarity of the cornea.

The cornea is a highly innervated, avascular, tissue composed of three cellular layers (Figure 1-1). Each of the layers has a critical function in the overall health and/or stability of the cornea. The epithelium provides a highly impermeable barrier to external contaminants, the stroma is largely responsible for the mechanical strength and stability

of the cornea, while the endothelium is responsible for actively maintaining the cornea's dehydrated state, and thereby its clarity.

Trauma to the cornea can lead to detrimental consequences to both the shape and clarity of the cornea. The shape of the cornea can be perturbed by the irregular replacement of the excised or injured tissue; this process is largely blamed for refractive regression following refractive surgery. Trauma can also lead to decreased light transmission by one of three mechanisms: 1) turbidity caused by edema, 2) matrix protein denaturation/coagulation and/or chemical modification or 3) by light occlusion and scattering due to phenotypic changes in the cells in the cornea.

In its normal clear state, the cornea is highly dehydrated. The dehydrated state is maintained primarily though the active transportation of ions out of the cornea by the endothelium. Diseases or defects that impact the endothelium can decrease the ion transport activity and cause the cornea to retain water and become less clear[16-18]. While chronic cases do exist, edema following stroma penetrating wounds (Figure 1-2A) tends to resolve once the epithelial barrier is re-established (Figure 1-2B). This class of light interference does not require a viable cornea and can occur on the time scale of minutes in *ex vivo* corneal tissue that is permitted to absorb water. The turbidity that accompanies edema is transient and reversible if the cornea is dehydrated once again.

Another class of light interfering lesions in the cornea can be attributed to denaturation of the proteinaceous matter within the cornea. Alkali chemical or thermal burns to the cornea can create light obscuring lesions within a minute or two in both viable (Figure 1-2C) and non-viable tissue (not shown). Coagulative opacification can also occur as a consequence of bacterial keratitis, though the mechanism is drastically

slower than the chemical and thermal burn based wound. At present, coagulative lesions are the most severe corneal opacifying lesions and are at present completely irreversible.

While the previous two types of opacification can interfere with light transmission through the cornea, neither is an example fibrosis. The fibrotic response requires a specific level of damage to the tissue and is a process that requires weeks of wound healing activity to diminish the cornea's transparency. The formation of a cellular scar is a much slower process than the other two classes and is therefore more amenable to therapeutic intervention. In the cornea, lesions only affecting the corneal epithelium don't elicit the fibrotic wound healing response. They do however, result in apoptosis of the stromal fibroblasts directly beneath the injury[19,20]. The scrape is healed by proliferation of the epithelial cells and the newly acellularized zone in the stroma is once again repopulated by proliferation and migration of fibroblasts leaving no vision impairing artifacts[21,22]. Injuries which penetrate into the stroma also result in apoptosis of the immediately juxtaposed fibroblasts. However, the cells which eventually repopulate the acellularized zone synthesize excessive extracellular matrix and can transdifferentiate into the cells with light reflecting subcellular structures[23,24] forming what is clinically referred to as sub-epithelial haze (Figure 1-2D). Minimally, sub-epithelial haze disrupts normal vision by interfering with the transmission of light, causing aberrant halos and starbursts around lights which can severely impair one's ability to drive at night[25,26]. However, if the scarring is severe, the scar can preclude the transmission of light through the cornea leading to corneal blindness. The degree of haze following a stromal penetrating injury has been found to be directly proportional to

the volume of stromal tissue removed[27], the concentration of TGF-β in the tear fluid[28], degree of basement membrane disruption[29], and the degree of correction attempted during laser surgery[30,31].

Current Clinical Interventions

At present, the methods used to decrease corneal haze are topically applied steroids or anti-metabolite drugs which indiscriminately target the cells' capacity to respond to growth factor and cytokine signaling. Given their safety profile, anti-inflammatory steroids have garnered attention as potential anti-fibrotic agents. Steroids have been demonstrated to reduce cell proliferation *in vitro*[32] and stromal collagen synthesis in rabbit refractive surgery models[33]. Initially, a prospective, double-masked clinical trial to test the efficacy of topically applied dexamethasone 0.1% in preventing corneal haze, found no significant effect on scar reduction[34]. However, additional investigations have found that the efficacy of steroids appears to vary with the method[33] and timing[35] of installation, and the magnitude of refractive correction sought[35-37], suggesting that the corneal fibrosis in a sub-set of patients is addressable by the immediate installation of steroids.

The current gold-standard of anti-fibrotic drugs is topically applied mitomycin C (MMC). Mitomycin C becomes a strong alkylating and cross-linking agent after it is biologically reduced by intercellular enzymes, and it is through this activity that it is proposed to have its drug effect[38,39]. At present, it is hypothesized that MMC prevents fibrosis by crosslinking the primary amine moieties on guanosines present in 5'-CpG-3' base pairs and thereby preventing DNA synthesis and subsequent cellular proliferation. While MMC has been found to be effective at reducing corneal haze, there exist conflicting reports about its toxicity to the corneal endothelium[40]. In addition, MMC is

associated with significant toxicity of the ocular surface and narrowing or blocking the tear drainage ducts (a.k.a. punctal stenosis)[41-43]. Given the high function and fragility of the endothelium, lower risk compounds and techniques are actively being sought. A key strategy to mitigating the risk of future anti-fibrotic therapeutics is to have a more targeted approach; nullifying the specific molecular pathways that give rise to the scar. However, increased targeting precision requires more knowledge about the molecular pathways unique to, and necessary for, the generation of fibrotic lesions.

The Molecular Causes of Fibrosis

Knowledge about the molecular biology of fibrosis began with insights from the scarless healing of mammalian fetuses and marsupial pouch young (collectively "fetus")[44,45]. Initially, investigators sought to determine if the womb environment bestowed anti-fibrotic protection upon the fetus by grafting and wounding maternal ovine skin onto fetal lambs. The adult tissue still scarred and immunohistochemistry revealed that the adult tissue, but not the fetal tissue contained transforming growth factor-β (TGF-β) in and around the scar. Further experiments revealed that a fetus could be "forced" to scar by the administration of exogenous TGF-β into a fetal wound. The experiments collectively revealed that the presence of increased levels of TGF-β triggers a fibrotic versus a regenerative wound healing response and that the womb does not provide a protective role against fibrosis. The results from these experiments indicated that the appropriate therapeutic approach to prevent scarring would need to mitigate TGF-β's pro-fibrotic activities.

Transforming Growth Factor – β

The transforming growth factor-β family of cytokines contains three isotypes, two of which (β_1 and β_2) are known to trigger the fibrotic wound healing response, the third

(β_3) is proposed to inhibit the activities of the other two[46]. Transforming growth factor β_1 has been shown to autoinduce its own expression[47] and TGF-β_2 has been shown to induce the expression of all three TGF-β isotypes[48]. Addition of TGF-β_1 to cultures has been demonstrated to be sufficient to induce transdifferentiation of fibroblasts[49] and lens epithelial cells[15] to the myofibroblast phenotype. TGF-β is known to be present in the unwounded mouse epidermis[50], the unwounded corneal epithelium in adult mice[51] and rats[52], and in human tear fluid[28,53,54]. Following photorefractive keratectomy (PRK) of adult rat eyes, whole corneal TGF-β_2 mRNA was found to be 300 fold higher than in untreated corneas[52].

Hypothetically, to prevent corneal haze the myofibroblast differentiation which follows TGF-β stimulation is key. However, given the efficacy of anti-mitotic agents like mitomycin C, targeting its proliferative activity may also have beneficial effects. Initial work to mitigate TGF-β's pro-fibrotic activities *in vivo* via targeting its receptor led to positive effects on the targeted tissue, but with substantial side-effects on epithelial tissues[55]. The key effect that TGF-β has on epithelial cells is to inhibit the hyperphosphorylation of the retinoblastoma protein (pRB) and thereby inhibit G_1/S transition[56]. In the presence of epidermal growth factor (EGF), renal epithelial cells proliferate into hyper-cellular masses (hyperplasia). While these cells exposed simultaneously to EGF ant TGF-β will become enlarged (hypertrophic) but will not proliferate[56]. The TGF-β induced growth inhibition could be reversed by pRB or p53 inactivating proteins[56]. The effects seen with TGF-β inhibition *in vivo* and knowledge of its epithelial growth inhibiting function leads to the conclusion that strong inhibition of TGF-β activity essentially recapitulates a retinoblastoma-like disease state leading to

the generation non-transformed epithelial tumors. Given this observation, therapies targeting downstream effectors of fibroblasts' responses to TGF-β have become the dominant strategy. Connective tissue growth factor (CTGF) is one downstream effector of TGF-β's pro-fibrotic activities which has been identified[57-59]. In fibroblast cultures, CTGF has been demonstrated to be both necessary and sufficient for TGF-β stimulated contraction[60,61], proliferation[58,59], collagen production[58,59], and the differentiation of cells into myofibroblasts[58,59] and is therefore at the forefront of gene targeted anti-fibrotic therapies.

Connective Tissue Growth Factor

Connective tissue growth factor (CTGF) is a 38kDa protein and the founding member of the CTGF/Cyr61/Nov (CCN) family of secreted cytokines which has been demonstrated to mediate TGF-β induced fibrotic activities[58,59,62]. Connective tissue growth factor was first discovered as a mitogen that was co-purified with anti-platelet derived growth factor (PDGF) antibodies[62]. The investigators discovered that CTGF was directly bound to the PDGF antibody, not PDGF itself, and that CTGF itself was directly responsible for the majority of the PDGF-like mitogenic activity. In both skin and corneas, CTGF and CTGF mRNA levels were both low in unwounded tissue, but were both elevated in wounded tissues at time points following TGF-β autoinduction[7,12,57,63,64]. These observations strengthened the relationship between TGF-β and CTGF in animal models and in humans.

Proteolytically processed fragments of CTGF have been found in biological fluids obtained from porcine uterine secretory fluids and in the vitreous of patients with proliferative diabetic retinopathy[65-67]. Connective tissue growth factor has four domains with sequence similarity to other growth factors (Figure 1-3). Experiments with

synthetically bisected CTGF have demonstrated that the individual fragments possess distinct activities[68,69]. The amino-terminal fragment, comprised of the insulin-like growth factor binding (IGFB) and von Willebrand factor binding (VWB) domains, possesses the observed differentiation and collagen synthesis stimulating activities. The carboxyl-terminal half of CTGF, comprised of the thrombospondin-1 (TSP1) and cysteine knot (CT) domains, possesses the observed fibroblast mitogen activity. It has yet to be determined whether the fragmentation has a regulatory role, but the activities found in both halves can result in detrimental clinical outcomes following vision correcting laser surgery. A simple hypothetical molecular model of how the differential activities of CTGF might be regulated through proteolytic processing is presented in Figure 1-4.

The Current Molecular Model of Fibrosis

Building a model of the molecular pathway responsible for the fibrotic wound healing response requires a combination of macroscopic observation of the type of wound necessary for scarring and the known localization and activities of pro-fibrotic molecules. As previously mentioned, a lesion which does not penetrate into the corneal stroma will not scar. For lesions that do penetrate into the stroma, fibrosis is constrained to the location where the stroma is both disrupted and is placed into communication with the tear film and/or epithelium. The restriction of fibrosis solely to the region of epithelium-to-stroma contact is most apparent when comparing scars from transepithelial laser surgery with those from laser-assisted in situ keratomileusis-like (LASIK-like) procedures. In the transepithelial lesion, the entire wound region is capable of scarring, while in lamellar keratectomy surgeries where the removed button of tissue is replaced, or in LASIK procedures, only the margins where the trephine cut or LASIK flap cut through the epithelium form a scar[33,70]. The exact nature of this limitation

is still not understood, but it is also seen in other tissues. In the retina, exogenously added TGF-β could not induce fibrosis in intact retinal detachments, but did if the detachments had an accompanying tear[71]. In the retinal detachments with a tear, the fibrosis was restricted to the region of the tear indicating that tissue disruption is a co-requisite of TGF-β's pro-fibrotic activity. When these facts are integrated together, a more complex cellular and molecular model begins to emerge (Figure 1-5) where TGF-β derived from the tears or the epithelium serves as the initial signal, and the stromal penetration serves to sensitize the corneal cells to TGF-β. Shortly after the stroma-penetrating injury, it has been reported that the underlying keratocytes apoptose, leaving an acellular region below the wound[16,17]. With time, the acellular region can become re-populated by stromal keratocytes which chemotax into the wounded region. It is hypothesized that these cells are the locus of the first wave of the pro-fibrotic TGF-β response (endocrine) and are the loci of subsequent TGF-β and CTGF synthesis and activity (autocrine). Ultimately, these are the cells that are proposed to form the light reflecting haze. Given this model, the residual stromal keratocytes have become the primary target of CTGF targeted mRNA ablation therapeutics.

Nucleic Acid Therapeutics

While nucleic acids are renowned for their capacity to store information, they have also been found to be capable of many of the same functions that proteins possess including catalysis[72-79] and macromolecular recognition[74,80-82]. Many functional nucleic acids were discovered in naturally occurring biochemical pathways (ribozymes, antisense, RNAi)[83], while others were synthetically discovered (deoxyribozymes, aptamers)[79,82], and in the case of aptamers, were found later to occur naturally[74].

Below, these nucleic acids will be discussed in terms of their therapeutic application, not in terms of their natural biochemistry.

There are two general classes of therapeutic nucleic acids, those that can act on their own and those that require endogenous macromolecular complexes. Ribozymes, deoxyribozymes, and RNA or DNA aptamers (Figure 1-6A&B, respectively) are examples of nucleic acids that can, themselves, have therapeutic activity requiring at most a divalent cation (e.g. Mg^{2+})[72,75,79,84]. Antisense oligonucleotides (ASOs) and the various RNAi-based pathways provide "targeting" information to endogenous enzymes and macromolecular complexes which when combined, possess the therapeutic activity[85] (Figure 1-6C).

The general classes are further subdivided based on their mode of action. Most target mRNA for destruction or translational silencing (siRNA, miRNA, ribozymes, deoxyribozymes, and antisense). Others have been demonstrated to guide heterochromatic gene silencing, DNA methylation, or even genomic DNA excision and exclusion (other RNAi-based)[86]. Finally, aptamers have the most disparate function of the therapeutic nucleic acids in that they do not employ Watson-Crick base pairing, but instead behave more like "nucleic acid antibodies" which bind the "antigen" with a specific geometric arrangement of hydrogen bonds, ionic bonds, and ring stacking interactions[87]. The importance of considering the mode of therapeutic action is that any given molecular biological cascade will likely have a "bottleneck" or two which would be the best target(s). If the target is a pre-existing (i.e. already transcribed) protein, employing mRNA targeting therapies would not have any effect on that pre-existing effector. Whereas, if the target is a yet to be transcribed/translated gene, using an

aptamer to neutralize the final product, instead of neutralizing the mRNA transcript would suffer from the target amplification which occurs as a result of a single mRNA molecule being translated multiple times.

The final important distinguishing characteristic is the location where the nucleic acid therapy can have its effect. Simply put, the targeted molecule, its co-requisites, and the drug must be co-located for therapeutic effect. For instance, the mRNA ablating technologies are only active intracellularly, since that is where the target (i.e. mRNA) is located, whereas aptamers can be directed to targets on the cell surface or in the extracellular milieu. Finally, drug delivery is a significant hurdle and therefore the locus of activity constraint can have a significant impact on the efficacy of a candidate therapy if effective concentrations of the drug cannot be delivered when and where it needs to be.

Nucleic acid therapies, as a whole, have the same strategic limits as all pharmacological agents. If the target of interest is a highly stable protein (i.e. a structural protein) with a long half-life, a therapeutic reduction of the target may difficult or impossible even with drastic reductions in mRNA levels. Alternatively, if the target is a highly expressed and highly active enzyme, even a drastic reduction in the total target levels may not have any biological effect. In short, some biological cascades have built-in “buffers” against external perturbations that may be refractory to even highly targeted nucleic acid therapies. The overall sensitivity of the targeted biological response to levels of the targeted macromolecule must be considered very early on in selecting a protein for therapeutic reduction.

To date, one antisense oligonucleotide (ASO) therapy has been approved by the FDA. Fomivirsen (trade name “Vitravene”) is an anti-cytomegalovirus (CMV) antisense oligonucleotide approved for treating CMV retinitis in patients with acquired immune deficiency syndrome (AIDS)[88]. Anti-fibrotic ASOs targeting TGF-β and CTGF have been used to control fibrosis in rat kidneys[89], mouse and rat livers[90-95], and mouse skin[96] in a research setting. More recently, an anti-fibrotic CTGF ASO has been tested in phase II clinical trials for its ability to reduce the visual appearance of scars from acute surgical skin wounds in humans[97].

Methods and Limitations of Macromolecular Delivery

Due to the size and highly negative charge of nucleic acids, delivery and cellular uptake are difficult using traditional means such as systemic delivery or local injections. Additionally, due to the small tissue volume and high function of the cornea, injections are not desirable. Using iontophoresis, which is based on the same principles behind gel electrophoresis, the highly charged nucleic acids can be selectively delivered into the corneal tissue. The factors affecting migration in an electrophoresis gel are the same that can impact the migration of a drug into the tissue; larger, lower charged molecules migrate slower than smaller, higher charged molecules and molecules move slower in a more dense tissue than a less dense one.

Currently, iontophoresis is used clinically for transdermal delivery of small molecule analgesics such as lidocaine. Initial trials using the conditions published for use with small molecules such as lidocaine and epinephrine were unable to deliver ssDNA oligonucleotides into *ex vivo* rabbit corneas[98]. The increased mass of oligonucleotides led to the need of an increased force to “push” the drug into the tissue. The use of a higher electric field (or current density) is needed to impart the force

necessary to surmount the barrier posed by the cornea. Consequentially, there is an accompanying increase in electrolytic alkylization of the delivery reservoir (and acidification of the receiving chamber) which necessitates a robust buffering strategy. Finally, the use of a dual-phase system in which the drug is solubilized in a dense, non-ionic solution (i.e. 15% sucrose) enables the drug to sink closer to the target tissue, reducing the distance that the drug has to "travel" to be "delivered". The dual-phase system also allows the drug, not the buffer ion, to be predominantly delivered. When all of the aforementioned modifications to the standard form of iontophoresis are employed, iontophoresis is capable of delivering a 20 nucleotide single stranded DNA reporter oligonucleotide into the cornea without significant, observable, damage[98-101]. A model of the modified iontophoretic setup is depicted in Figure 1-7A. Schematics of the basic mechanics behind why topical application fails, and why iontophoresis succeeds, as a means of delivery are depicted in (Figure 1-7B&C, respectively)

Projects

Much work has been done to test the role of CTGF in scarring using fibroblast cell cultures with the fibrosis-related activities of proliferation, collagen synthesis, and differentiation as the primary readouts. No work has been reported on the role of CTGF in actually modulating the formation of light scattering entities in corneas following acute mechanical injury. The first attempts with a topically applied CTGF ASO had no observable effect on haze formation, but topical application is not expected to lead to efficient uptake of the oligonucleotide. The first project described herein seeks to deliver a CTGF ASO into acutely wounded rabbit corneas and determine 1) whether CTGF protein is reduced, and 2) whether there is a decrease in haze formation in the same eyes. This project will test whether CTGF is necessary for scar formation and will

test the feasibility of iontophoretically delivered ASOs as an effective therapeutic modality.

The second project seeks to identify the locus or loci of CTGF synthesis and activity within corneas which are healing from acute excimer laser wounds. To date, fibroblasts have been hypothesized to be both the source of synthesis and activity of CTGF indicating an autocrine or regional endocrine signaling mechanism. Initial attempts to measure CTGF protein localization suggested a heavy presence in the epithelium[63], but significant immunohistochemical overexposure of the sections precluded confidence in the finding. What's more, no information about the source of synthesis of the observed CTGF during healing in the cornea is known. A combination of improved immunofluorescent staining and confocal microscopy of healing corneas will reveal the distribution of CTGF protein during healing of acute wounds. In order to reveal the locus or loci of CTGF synthesis, a mouse model with enhanced green fluorescent protein under control of a CTGF promoter will be used. The green fluorescent protein transgene does not possess a secretion signal, leading to an accumulation of green fluorescence in cells with CTGF promoter activity. The results from this reporter mouse were further validated by quantitative real-time reverse transcriptase polymerase chain reaction (qRT-rtPCR) analysis for CTGF transcripts in corneas which were grossly dissected into the three separate cellular layers. The data provided by these experiments are necessary for two key reasons: 1) to provide a better understanding of the role CTGF has in wound healing (protein location) and 2) to ensure that the anti-mRNA therapies are targeted to the correct cells (synthesis location).

The next project sought to investigate the pattern, location, and timing of haze formation and how the distribution of biochemical markers for light reflecting cells were likewise distributed during the formation of the light reflecting scar. A time series of macrophotographic images of the wounded corneas was used to visualize the initiation and change of haze as it developed. Standard immunofluorescent staining and gross histology were used to observe where and when these markers arise and whether their distributions mirror the pattern of the light reflecting scar.

The final project sought to test the growing body of evidence that the epithelium has a greater role in fibrosis than initially appreciated. The two possible roles identified are that the epithelial cells provide a “guidance” role which may be the basis of the observed restriction of fibrosis to only the disrupted tissue, or that the epithelial cells themselves directly contribute cells and/or ECM to the fibrotic mass. For this final project, the hypothesis that the epithelium directly contributes cells to the fibrotic mass by the process of epithelial-to-mesenchymal transition (EMT) was tested. The key experiment used to test the EMT hypothesis was a mouse model with genetically labeled corneal epithelial cells which would determine whether any epithelium-derived cells are present within the stroma after the light reflecting scar has been established. Concurrently, gross histology of wounded rabbit corneas during the time prior to haze formation was used to investigate whether there was any grossly observable evidence of epithelial cells crossing into the stroma or vice-a-versa. Finally, immunofluorescent staining for markers associated with, but not necessarily indicative of, EMT was performed during the time period of haze formation.

In total, the projects seek to provide a better understanding of the role of CTGF in fibrotic would healing and the cellular and molecular biological processes that give rise to pathological scarring. Improvements in understanding the molecules that are believed to communicate and orchestrate the pro-fibrotic wound healing response are necessary to improve design and testing of novel anti-fibrotic therapies. Knowledge of the cellular players and the changes they undergo during fibrosis is key to identifying new potential therapeutic modalities. Only by integrating knowledge about the source and localization of the key molecular effectors and the timing and location of the cellular responses to them, is a comprehensive, well integrated, systemic understanding of fibrosis possible. Only after the fibrotic response is known in such detailed terms will scientists and engineers be able to design highly targeted therapies that can steer a wound away from fibrosis and towards regeneration.

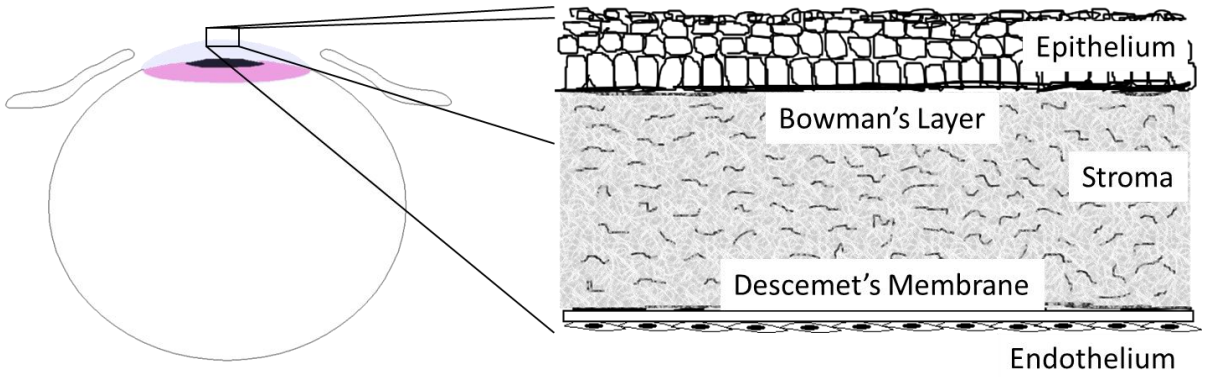

Figure 1-1. A schematic of the corneal cell layers.

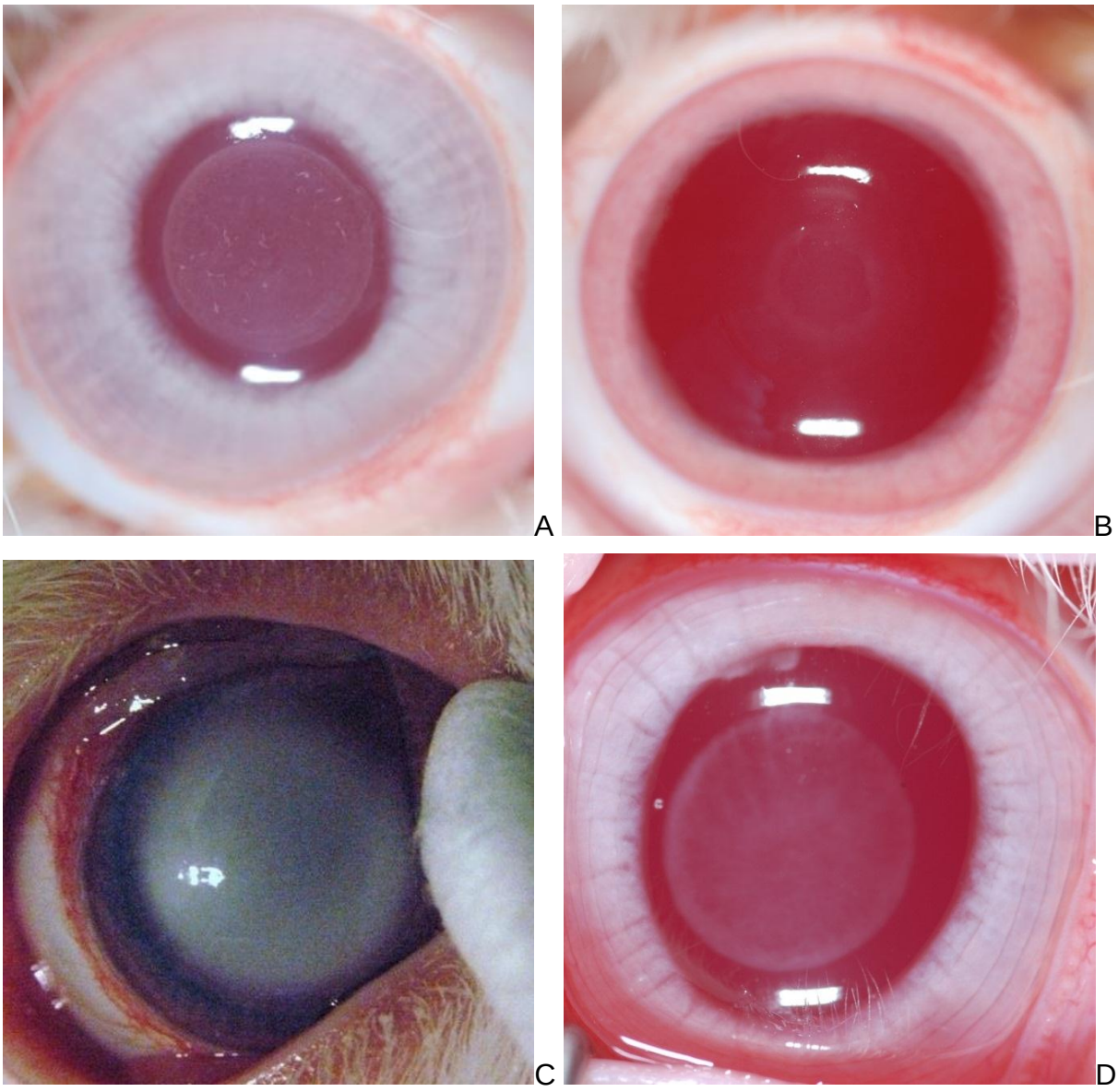

Figure 1-2. Examples of the different classes of corneal opacification. A) Edema 1 day after a wound, B) the same eye as in A), but 2 days after the wound. Note the annular region that has regained clarity after being re-epithelialized while the center remains turbid. C) Coagulation and modification of stromal proteins from an alkali burn, D) cellular haze that takes a week or two to form.

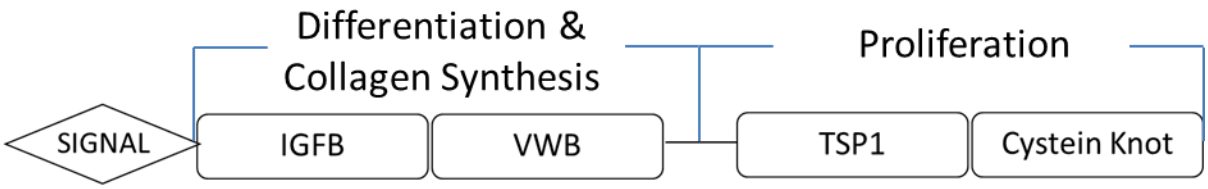

Figure 1-3. A schematic of CTGF's functional domains and the observed activities associated with them.

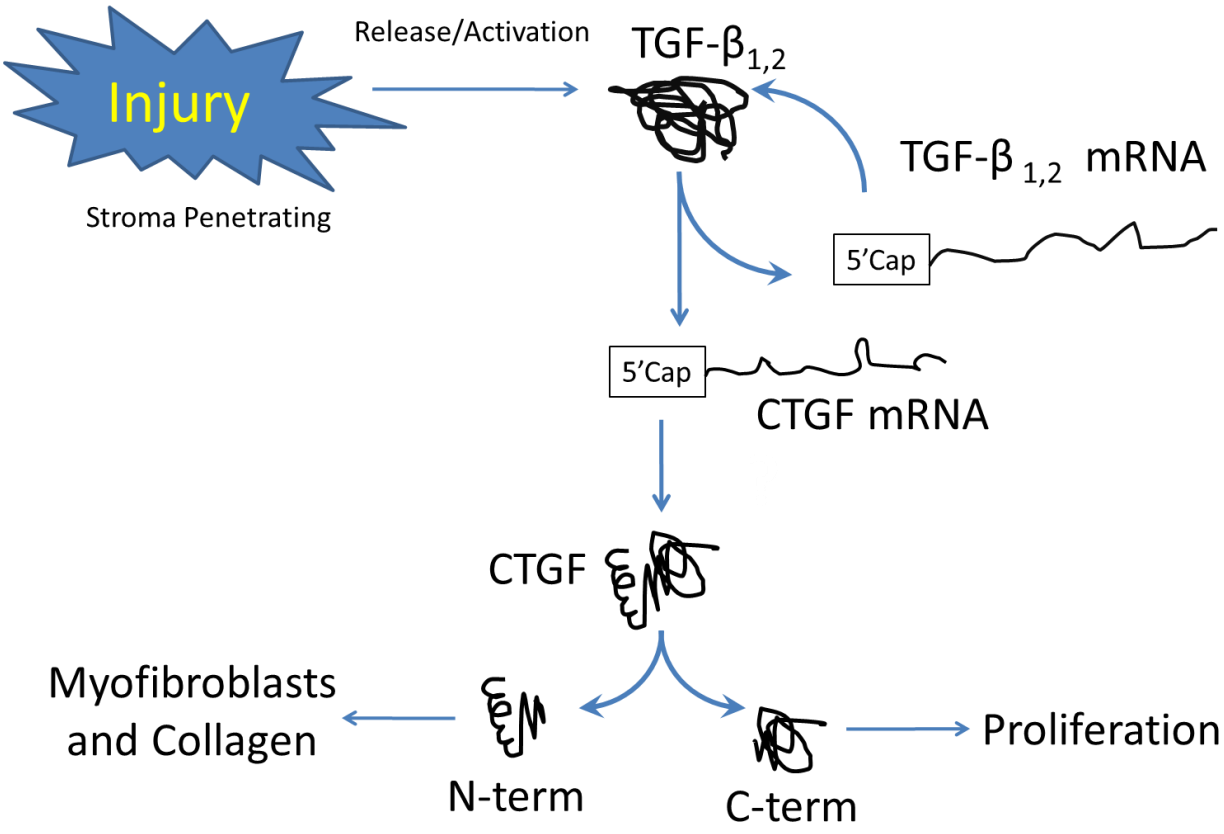

Figure 1-4. The simplified fibrotic cascade.

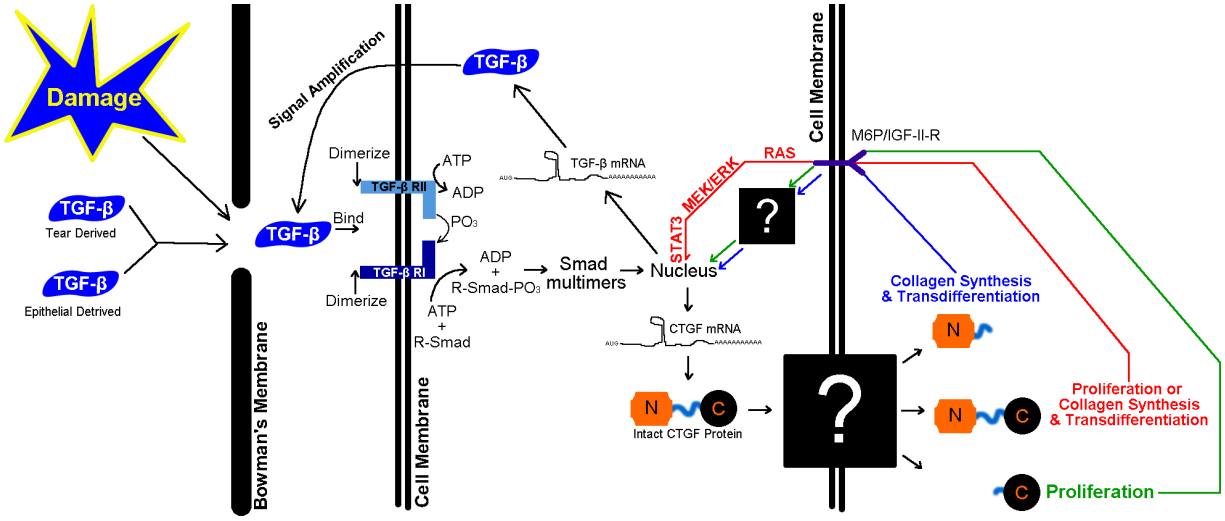

Figure 1-5. A more involved cellular and molecular model of the fibrotic response in the cornea.

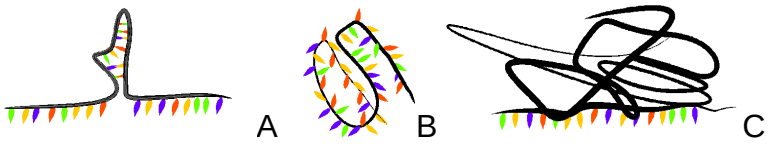

Figure 1-6. A schematic depiction of three general classes of functional nucleic acids. A) Ribozymes and deoxyribozymes possess enzymatic activities themselves. B) DNA or RNA aptamers are capable of selective macromolecular recognition by themselves. A) RNAi and antisense oligonucleotides require macromolecular complexes.

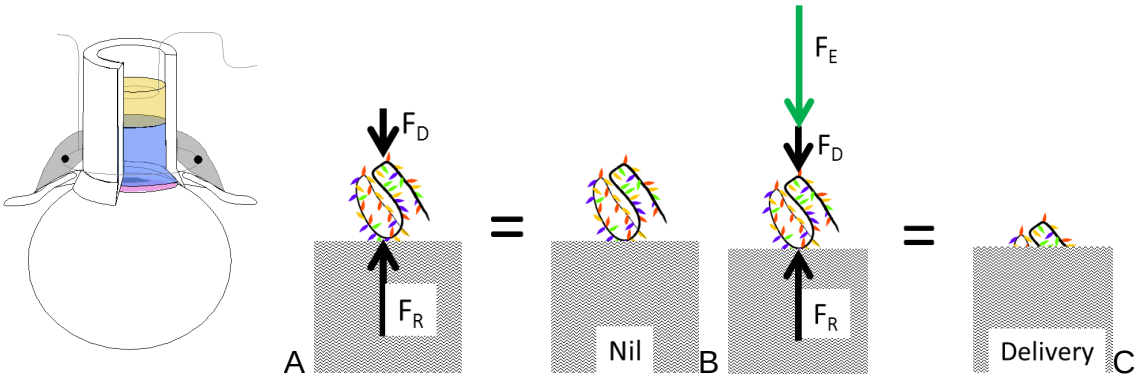

Figure 1-7. General setup and principle behind iontophoresis. A) Schematic of a transepithelial iontophoresis chamber. The blue is the oligonucleotide dissolved in sucrose, the yellow is a suitable buffer, the grey is a buffer soaked gauze in contact with the eyelid. B) The basic mechanics of topical delivery, there are forces resisting delivery (F_R), and forces facilitating delivery (F_D) due to diffusion. C) With iontophoresis, an additional force (F_E) is applied to the drug which enables it to overcome the tissue barrier.

CHAPTER 2
IONTOPHORESIS OF CTGF ANTISENSE OLIOGNUCLEOTIDES INTO EXCIMER WOUNDED CORNEAS

Introduction

Oligonucleotide-based technologies are a relatively new class of drugs capable of highly targeted therapies that are expected to be drastically less toxic than small molecule drugs. If the presence of a protein has been implicated in a particular pathological process, these oligonucleotide technologies can be used to degrade the protein's mRNA and thereby reduce the protein's presence. The discovery that CTGF was necessary for TGF-β stimulated fibroblasts to differentiate into myofibroblasts made it a prime target for a potential anti-fibrotic oligonucleotide therapy. Cell culture experiments further strengthened CTGF as a candidate anti-fibrotic target when the use of CTGF antisense oligonucleotides (ASOs) on TGF-β stimulated fibroblasts was found capable of reducing the resultant contraction[60,61], collagen synthesis[63], and myofibroblast differentiation[60]. The excitement from these early experiments was greatly diminished when unpublished preliminary *in vivo* experiments of topical applied oligonucleotides to excimer wounded rabbit corneas had no therapeutic effect (2004). Translating the CTGF ASO cell culture results into *in vivo* models has been met with the same key obstacle as most other oligonucleotide therapies: delivery.

Given the cornea's size, sensitivity, and high function, a technique classically referred to as iontophoresis has garnered attention as a means of oligonucleotide delivery. Berdugo and others were the first to report successful delivery and short-term bioavailability of fluorescently labeled reporter ASOs into rat corneas[102]. To date, no reports have described pharmacologically or therapeutically efficacious delivery of oligonucleotide therapies into the cornea. However, Kigasawa and others have recently

reported success in both delivering a reporter siRNA into rat epidermis and in reducing IL-10 mRNA levels using an iontophoretically delivered anti-IL-10 siRNA[103]. While they were successful in obtaining the desired biochemical effect of reducing IL-10 mRNA, no mention was made about the therapeutic effect of the observed reduction. We decided to test the ability of an iontophoretically delivered CTGF ASO to reduce CTGF protein and light scattering myofibroblasts in a model which uses a surgical excimer laser to create reproducible acute wounds in rabbit corneas.

Materials And Methods

Optimization of Iontophoretic Delivery of Reporter ASOs

In previous work, it was found that iontophoresis of 5.0 mA for 5 minutes using our 1.1 cm diameter eye-cup was sufficient to deliver a reporter oligonucleotide (ISIS 13920)[104,105] into the deepest layers of intact corneas in the eyes of live rabbits (Figure 2-1). Given that for this wound healing model we will be delivering into an ablated cornea, decreased delivery current and/or time is possible to obtain more optimal results. To this end, a series of iontophoretic deliveries were performed in the corneas of *ex vivo* rabbit eyes acutely injured with an excimer laser. First, frozen whole rabbit globes (Pel-Freez, LLC., Rogers, AR) were thawed and immobilized on a piece of polystyrene foam. A central 6.0 mm diameter by 125 μm deep excimer PTK wound was created on the immobilized globes. Figure 2-2 depictes a representitve PTK wound in an *ex vivo* rabbit eye. Next, using the setup depicted in Figure 2-3, 500 μl of a solution of 15% sucrose and 160 μg of a 5'-carboxyfluorescein (5'-FAM) labeled reverse phase high performance liquid chromatography (rpHPLC) purified ssDNA with the same sequence as ISIS 13920 (Table 2-1, Integrated DNA Technologies, Inc., San Diego, CA) was subjected to iontophoresis for 5 minutes using currents of 0.0, 1.0, 2.0, or 3.0

mA. The corneas were fixed overnight, then cryoprotected, and finally embedded in optimal cutting temperature (OCT) compound for cryosectioning. The sections were mounted with 4',6-diamidino-2-phenylindole (DAPI) counterstain-containing medium and the labeled ssDNA was observed by direct fluorescence microscopy. All micrographs were obtained using the same imaging parameters allowing relative quantitative comparisons amongst the micrographs.

Toxicity of Iontophoresed CTGF ASO

All of the rabbits used herein were treated in a manner consistent with the Association for Research in Vision and Ophthalmology (ARVO) Statement for the Use of Animals in Ophthalmic and Vision Research. In order to establish whether either the iontophoresis or the ASOs themselves were well tolerated we conducted some preliminary experiments measuring the treatments' effects on re-epithelialization and edema. Each rabbit was anesthetized using inhaled isoflurane and each eye was topically anesthetized using one drop of tetracaine (Bausch & Lomb, Tampa, FL). The eye was exposed and the central thickness of the cornea was measured using a clinical grade ultrasonic pachymeter (n = 5 central measurements per eye). Each eye then received a central 6.0 mm diameter, 125 μm deep, excimer laser PTK wound. The thickness of the ablated cornea was measured by ultrasonic pachymetry again, then iontophoretically treated as described below.

A total of 3 rabbits received bi-lateral central corneal wounds and were treated with iontophoretically delivered CTGF ASO^{95} (ISIS 124189) in one eye and a scrambled ASO (ISIS 29848) in the contralateral eye. Details about these ASOs may be found in Table 2-1. Based on preliminary data with unwounded eyes, iontophoresis was performed using a current of 5.0 mA for 5 minutes with the apparatus setup as depicted

in Figure 2-4A. An ASO dose of 0.45 mg in 500 µl of 15% sucrose was used for both treatment and scrambled control ASOs. An additional three rabbits received the same wound in one eye and no further intervention. Re-epithelialization was measured by daily fluorescein staining and macrophotography. Re-epithelialization was analyzed two different ways. First, the day the cornea fully epithelialized was noted (clinical). Second, the daily area that remained wounded was measured using digital photographs of the fluorescein stained corneas (technical). In these same rabbits, corneal edema was quantified via daily pachymetry measurements of the central cornea until re-epithelialization.

In order to understand the source of edema following iontophoresis, 6 additional rabbits received the same bi-lateral wounds as described before. One eye received iontophoresis with only the 15% sucrose vehicle and the other received 1.0 mg of CTGF ASO. The corneal thickness was measured before and after excimer laser PTK and then again immediately following iontophoresis. In all cases, the amount of edema was calculated daily by the difference between the corneal thickness on that day and the immediate post-wounding thickness. The percent difference in thickness was calculated using the formula in Figure 2-5.

Therapeutic and Biochemical Efficacy of Iontophoresed CTGF ASO

In order to determine if iontophoresis of CTGF ASOs could both reduce the target protein and whether there was also a reduction in corneal haze, twelve rabbits were anesthetized and received bilateral excimer wounds to the center of their cornea as described above. Immediately following excimer wounding, 0.125 mg of either CTGF ASO or a scrambled ASO were delivered into the wound by iontophoresis (3.0 mA for 5 min) using the setup depicted in Figure 2-4B. During follow up, the rabbits were grossly

observed with no contact or fluorescein installation due to previous observations of epithelial instability with frequent observation and fluorescein instillation (2009). The rabbits were divided into two groups of 6 each for evaluation at days 7 and 14. At day 7 post-wounding, one rabbit was removed from the study due to an unrelated injury, the remaining 5 rabbits had their eyes photographed for haze quantification, were euthanized, and their corneas were collected for CTGF quantification. Briefly, the cornea with a scleral rim was harvested and placed in a cornea punch block. An 8 mm punch was used to harvest the wound and a 2.0 mm rim of uninjured cornea. The excised tissue was placed in a tube, snap frozen in liquid nitrogen, and stored at -80°C until processed. The remaining 6 rabbits were similarly processed at day 14, thus creating two time points with coordinated haze measurements and CTGF quantification.

Haze Quantification via Macrophotography

At present, a subjective scale of haze density is the accepted method of measuring corneal haze. A value between 0 and 4 is chosen based on qualitative factors such as the amount of detail visible in the iris through the scar. In order to improve the objectivity and to provide a better means of communicating the effect(s) of a given anti-fibrotic therapy, a novel macrophotography-based method for haze imaging and quantification was developed.

Macrophotography

In order to both quantify the amount of light reflecting haze, and to generate a lasting image for complete visualization of the corneal scar, a macrophotography method was developed. Prior to general anesthesia, each eye was topically anesthetized with proparacaine and each pupil was dilated with phenylephrine 2.5% and tropicamide eye drops. Each rabbit was then generally anesthetized with inhaled

isoflurane as described earlier. The eyelids were held open and out of the way with either an eyelid speculum or a pair of cotton swabs. Either a Nikon D40 DSLR, or in later experiments a Nikon D7000, was outfitted with a macro lens capable of native 1:1 reproduction (either a 100mm Tokina or 60mm Nikkor) and the Nikon R1C1 Creative Lighting System (CLS) flash system. The D40 was set to the "Normal" program, ISO 200, manual exposure with a shutter speed of 1/500 second and f/16. The D7000 was set to the "Standard" program, ISO 100, manual exposure with a shutter speed of 1/250 second and f/18. To visualize and measure haze, the flash power was set manually ($1/16^{th}$, D40, $1/6.4^{th}$ D7000) and neither the flash nor lens had a filter. For all images, the lens was set to manual focus and pre-focused to a 1:1 reproduction ratio and the camera was focused by moving the camera closer or further from the subject. Guide lights on the flash heads were used to facilitate haze visualization and focusing.

Haze evaluation and quantification

As with any measurement system, there is noise present in the macrophotographic technique used herein to quantify the amount of light a corneal wound is reflecting. A set of images from normal corneas and from wounded or pseudo-wounded corneas were used to identify the signature of the red reflex of the retina (black level) and the surface report of the macro flash (false positive). First, in order to blacken the retinal red reflex, all of the images were subjected to anti-red grayscale conversion by using only the unmodified data in the blue channel. The overall contrast between the wound and retina was increased by overexposing the image to the point where the sclera became saturated, but the wound was not. The same global exposure correction was applied to every image. A circular region in the center of the cornea which encompassed the wound and/or the flash reports was

selected. The “Record Measurement” button was pressed which generated a histogram of the selected area. Using the recorded histograms, the signal due to the retina reflex and the flash reports were identifiable by comparing the histograms from normal corneas versus the wounded or pseudo-wounded corneas, an example is presented in Figure 2-6. From these comparisons, a band pass filter was generated which excluded pixels with values lower than 80 and greater than 168 to preclude pixels outside of the wound (i.e. reflex, <80) and pixels from the flash reflection (>168) respectively. The pixels within the band were integrated and this band-pass filtered integrated density served as a quantitative measurement of the intensity of corneal haze (haze score).

CTGF Quantification Via Enzyme-Linked Immunosorbant Assay (ELISA)

In order to link the observed effects with changes in our proposed molecular target, the total mass of CTGF was measured by a quantitative sandwich ELISA. The total extracted CTGF mass per biopsy was chosen as the basis of comparison. Since CTGF has been observed to induce both significant cellular proliferation and protein synthesis normalization to the total mass of protein extracted is expected to skew the results.

First, the tissues were removed from deep freeze storage and thawed on ice. Each tissue punch was then diced and then placed in a 1.5 ml tube with 600 µl of extraction buffer (PBS pH 7.4 + 0.1% Triton X100, 5mM EDTA, 2mM PMSF, 0.24 mg/ml levamisole) and ground with a dounce homogenizer. Finally, the base of the tube was submerged in iced saline and the homogenate and remaining tissue were subjected to ultrasonication. The homogenate was cleared by centrifugation and the supernatant was transferred to a fresh tube.

Finally, total extractable CTGF was measured via a sandwich ELISA in a 96 well plate. Briefly, the wells were coated with 50 µl of a polyclonal antibody from US Biological (C7978-25C, 2 µg/ml) in 0.1 M carbonate buffer (pH 9.5) overnight at 4°C. The wells were blocked with 300 µl per well of Pierce SuperBlock TBS as directed. Diluted SuperBlock (1/10th) was used as the reagent dilutent. Three replicate wells per sample (50 µl/well) were applied to the wells. A standard curve was plated in duplicate using recombinant human CTGF (rhCTGF) at concentrations of 400, 200, 100, 50, 25, 12.5, 6.25, and 0.0 ng/ml. The plate was sealed and incubated for 1 hour at 30°C. The plate was then washed three times with 300 µl/well of tris buffered saline with 0.05% (v/v) Tween 20 (TBST). Fifty microliters of 200 ng/ml biotinylated probe antibody from US Biological (C7978-25D) was applied to each well then sealed and incubated at 30°C for 1 hour. The plate was then washed as before. The plate was finally incubated with streptavidin-alkaline phosphatase (Zymed, 1:10,000) at 30°C for 1 hour. The plate was washed four times with 300 µl/well with TBST and the plate was slapped dry. The ELISA was developed with PNPP in basic ethanolamine. The plate was continuously monitored, with the absorbance at 450 nm being measured every 10 minutes for an hour.

Results

Iontophoretic Delivery of Reporter ASOs

In the wounded ex-vivo corneas, topical delivery of the labeled ASO (no current for 5 min) resulted in no detectable delivery (Figure 2-7A). A delivery current of 1.0 mA for 5 min resulted in trace amounts of green fluorescence (Figure 2-7B). For current values of 2.0 and 3.0 mA, the epithelium at the wound margin and the anterior stroma possessed high levels of green fluorescence homogenously distributed in an

electrophoretic-like band (Figure 2-7C-F). The penetration depth and intensity of green fluorescence were both highest in the 3.0 mA treated cornea.

In Vivo Wounding and Iontophoretic Treatment

All of the eyes that received iontophoresis tolerated the procedure well without any observable signs of irritation or damage at the time of surgery. In the days following surgery, some rabbits which received iontophoresis, and some which did not, showed mild signs of inflammation and irritation at levels consistent with corneal wounding. Most wounds were re-epithelialized by day 3, the remainder re-epithelized by day 4 with no clinically significant difference amongst the CTGF ASO or scrambled ASO treated, and the eyes receiving no further intervention (Figure 2-8). Eyes that received the CTGF ASO were significantly thicker immediately after iontophoresis than those receiving the sucrose vehicle (Figure 2-9A, $p = 0.01$). The corneas that received the CTGF ASO had less swelling than the opposing eye that received the scrambled ASO. A paired analysis of the differences in edema revealed a statistical trend for days 1 and 4 (Figure 2-9B, $p = 0.13$ & 0.10, respectively) and significant differences for days 2 and 3 (Figure 2-9B, $p = 0.04$ & 0.03, respectively).

One rabbit from the day 7 set was removed from the study due to a pre-existing wound discovered on the contralateral eye immediately following surgery and treatment of the first eye. Another sample from the day 7 set was lost precluding paired CTGF analysis of that pair. In each pair of corneas, the total extractable CTGF protein contained in the analyzable biopsies was reduced in the treated corneas compared to the mock treated corneas by varying amounts (Figure 2-10). The reduction of CTGF protein was statistically significant for both days 7 ($p = 0.05$) and 14 ($p = 0.002$) with an average reduction of 15.7% and 30.7% respectively.

The images in Figure 2-11 represent paired eyes from two rabbits in two separate experiments. These are examples of the images that are used to quantify the intensity of the scar as measured by the return of light by the scar; Figure 2-11A&B were imaged at day 7 while Figure 2-11C&D were imaged at day 28. The haze is most prominent at the wound's edge and appears to spread from the edge towards the center with time. There is also the appearance of radiating "lines" of haze which are most easily seen in the CTGF ASO treated cornea at day 28 (Figure 2-11C). The total integrated density was not always reduced in each CTGF ASO treated eye compared to the contralateral scrambled control (Figure 2-12). However, in aggregate, the average paired difference indicated a decrease in total integrated density with anti-CTGF treatment. The decreased in haze was not statistically significant at day 7 post-wounding ($p = 0.23$), but was significantly reduced at day 14 ($p = 0.04$).

Discussion

In the work reported here we have demonstrated that iontophoresis is a viable means of delivering oligonucleotides into the cornea. We have also demonstrated that iontophoretically delivered, biologically active, ASOs can both reduce the targeted gene product and have therapeutic effects consistent with that gene's known functions. These findings support the use of iontophoresis both as a therapeutic modality, and as a research tool capable of temporally and spatially controlling a gene product.

The observation of a statistically significant reduction in corneal thickness during re-epithelialization, which is strictly due to reduction in edema, was not expected and potentially reveals a novel role for CTGF in the cornea. In the lung, TGF-β has recently been found to have a role in the modulation of fluid transport where it has been demonstrated to decrease the fluid transport across alveolar epithelia[106]. As CTGF is a

known mediator of TGF-β's fibrotic activities, it is possible that CTGF may also mediate this novel function of TGF-β. In the cornea, the endothelium is responsible for the majority of fluid transport out of the cornea and the epithelium has a minor role. It is conceivable that the presence of CTGF during re-epithelialization decreases the fluid transporting capacity of the migrating epithelial cells. Therefore, a reduction of CTGF may enable these migrating epithelial cells to maintain their capacity to move fluid out of the cornea. While our data here do not rule out other possible explanations, including the possibility that the presence of CTGF could have effects on the barrier function of the migrating epithelial cells, the lack of a significant difference in the re-epithelialization rate between these same groups is evidence against a mechanism based on the re-establishment of the epithelial barrier.

Overall, the amount of edema was elevated in the iontophoretically treated corneas versus wounded corneas receiving no further intervention, though only the increase in the scrambled ASO treated corneas was significant. It is possible that the iontophoretic treatment, or the sucrose vehicle, could stimulate edema above what is normally seen in wounded corneas. The lack of significant difference in the anti-CTGF treated cornea versus the non-intervention control may be explained by our hypothesized improved fluid transport compensating for the treatment induced edema leading to an overall lack of significant increase. While the iontophoresis may have increased the post-operative edema, it appears to be short lived and does not appear to be clinically significant.

The iontophoretically delivered CTGF ASO consistently had the desired biological effect of reducing total CTGF protein present in the healing corneas. Overall, the

amount of CTGF present in the cornea was higher at day 7 than at day 14. There are currently two conflicting reports about the expression levels of CTGF during corneal wound healing. Blalock et al. reported a fairly consistent rise in CTGF levels up through day 21 post-wounding in rat corneas[63], while Yang et al. reported a peak level of CTGF expression at day 3 post-wounding in rabbit corneas[107] which then declines to normal levels by day 21. Our data support the expression profile more in keeping with the observations reported by Yang and others. In this experiment, it is likely that the concentration of intracellular ASO was insufficient at day 7 to handle the increased concentration of CTGF mRNA and generate an equivalent magnitude of effect of that seen in the day 14 corneas. Even with the moderate reduction of CTGF, an observable and statistically significant difference in light scattering haze was measured. Additional *in vivo* work with increased doses must be performed to determine whether greater levels of protein reduction are possible and whether greater reductions in corneal haze will follow.

In these series of experiments, only a few rabbits had a robust scarring response. Similar to humans, the robustness of scarring is not homogenous throughout the population of experimental rabbits. While the quantitative technique employed was sensitive enough to measure differences in the moderate to mild scarring rabbits, the effect was dramatically more profound in those with a robust fibrotic response. Concurrently with the work reported here, Excaliard, Inc., a company which is testing an CTGF ASO as anti-fibrotic drug in skin, has had success in improving the appearance of hypertrophic skin scars in a phase II clinical trial[97]. While these results were obtained in a different tissue and via a different delivery method (injection), they do further

reinforce our findings of the ability for CTGF ASOs to control hypertrophic scarring. In addition to the positive therapeutic effects, the effects observed in the trial followed a pattern similar to what we observed. Subjects with mild scarring had less of a reduction in the appearance of the scar compared to subjects who had robust scarring; suggesting that the reduction of fibrosis may reach some basal level not addressable by anti-CTGF therapy. Experimentally, these observations suggest the presence of a significant heterogeneity in scar formation in experimental populations which needs to be considered during the design of experiments or clinical trials.

The observation that not all treatments reported here resulted in a decrease in haze might be explained by limitations of the measurement system. At present, not enough samples have been generated to determine the variance in measurements made using this photogrammetric technique. Additionally, the current haze measurement only takes into account the reflectivity of the wounded cornea, which may not be the sole measurement to consider. Using the eyes depicted in Figure 2-11A&B as an example, the mock treated eye appears worse due to the more rapid progression of the spread of the haze from the wound margin compared to the anti-CTGF treated right eye. However, the treatment (Figure 2-11A) had an overall higher amount of integrated density than the scrambled, ASO treated eye (Figure 2-11B). The rate of haze generation and rate of spread, not just total reflectivity, may need to be measured at these early time points during formation of corneal haze in order to measure the efficacy of any anti-fibrotic therapy.

The results reported here add to the evidentiary base of that CTGF is necessary for the formation of cornea-opacifying cellular scars. Additionally, the novel observation

of a difference in corneal edema due to treatment with CTGF ASOs implicates a new role for CTGF in the regulation of fluid transport. Here we presented further evidence which demonstrates that iontophoresis has the capacity to deliver biologically active oligonucleotide therapies into the cornea. In addition, for the first time, we provide evidence of combined biochemical and therapeutic effects by reducing the amount of CTGF as well as the amount of clinically relevant, and directly observable, corneal haze following corneal wounding. The results presented here indicate that iontophoresis can be used to surmount the significant barriers currently impeding the translation of oligonucleotide therapies into clinical practice.

Table 2-1. Antisense oligonucleotides used in the anti-fibrotic experiments.

ASO	Target	Molecular Mass	Sequence
ISIS 13920	Reporter/hRAS	7233.21 Da	TCCGTCATCGCTCCTCAGGG
ISIS 124189	CTGF	7235.29 Da	GCCAGAAAGCTCAAACTTGA
ISIS 29848	Scrambled	7233.20 Da	Random

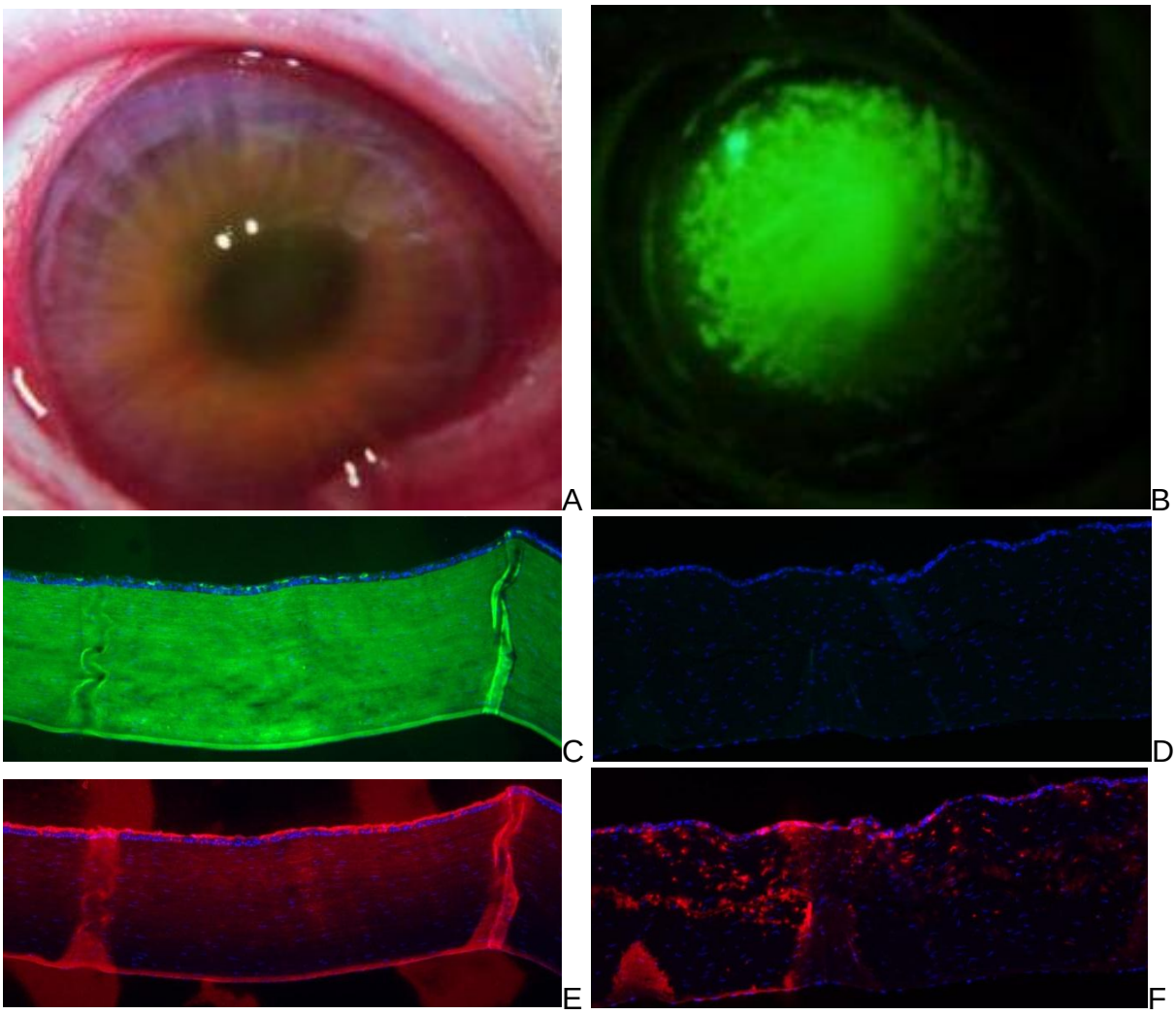

Figure 2-1. Results from iontophoresis into intact rabbit corneas. A macrophotograph of the eye treated with a directly labeled reporter oligonucleotide A) white light illumination and B) blue excited, yellow filtered fluorescent macrophotography of the same eye. Direct fluorescence micrographs C) immediately after delivery and D) 24 hours later. Micrographs of a nuclease resistant oligonucleotide revealed by immunohistochemistry E) immediately after delivery and F) 24 hours later. Approximately 40% of all cells in panel F) are ASO positive by direct counting (216 Red / 547 Blue = 39.4%)

Figure 2-2. A representative excimer PTK wound in an *ex vivo* cornea.

Figure 2-3. The iontophoresis setup used for the *ex vivo* experiments.

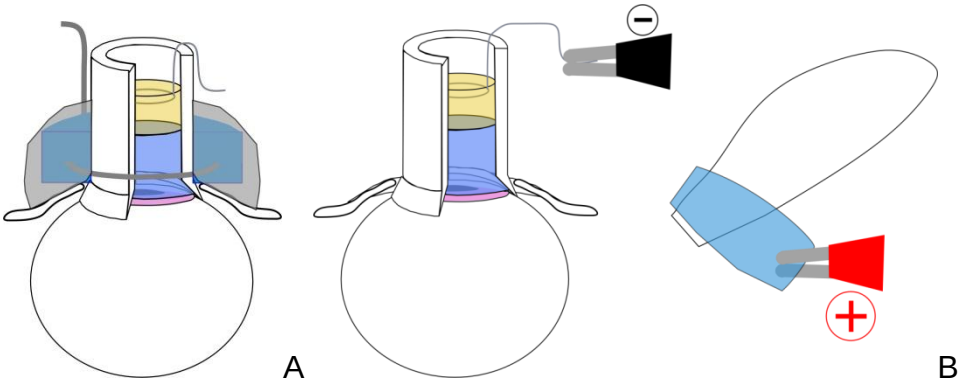

Figure 2-4. Two schematics of the iontophoretic setups used. In the cut-away view, the yellow represents the slightly acidic HEPES, the blue represents the ASO/sucrose solution. In A) the anode is surrounded by a buffer-soaked sponge (blue) and gauze (grey). In B) a schematic of a rabbit ear with slightly basic buffer-soaked gauze (blue) wrapped around it and held in place with the anode. The anode would itself then be wrapped with another buffer-soaked gauze.

$$\left(\frac{T_i - T_0}{T_0}\right) \times 100 = \%\ Thickness$$

Figure 2-5. Calculation of edema or thickness, where, "T_i" is the current thickness and "T_0" is the initial, post-wounding, thickness.

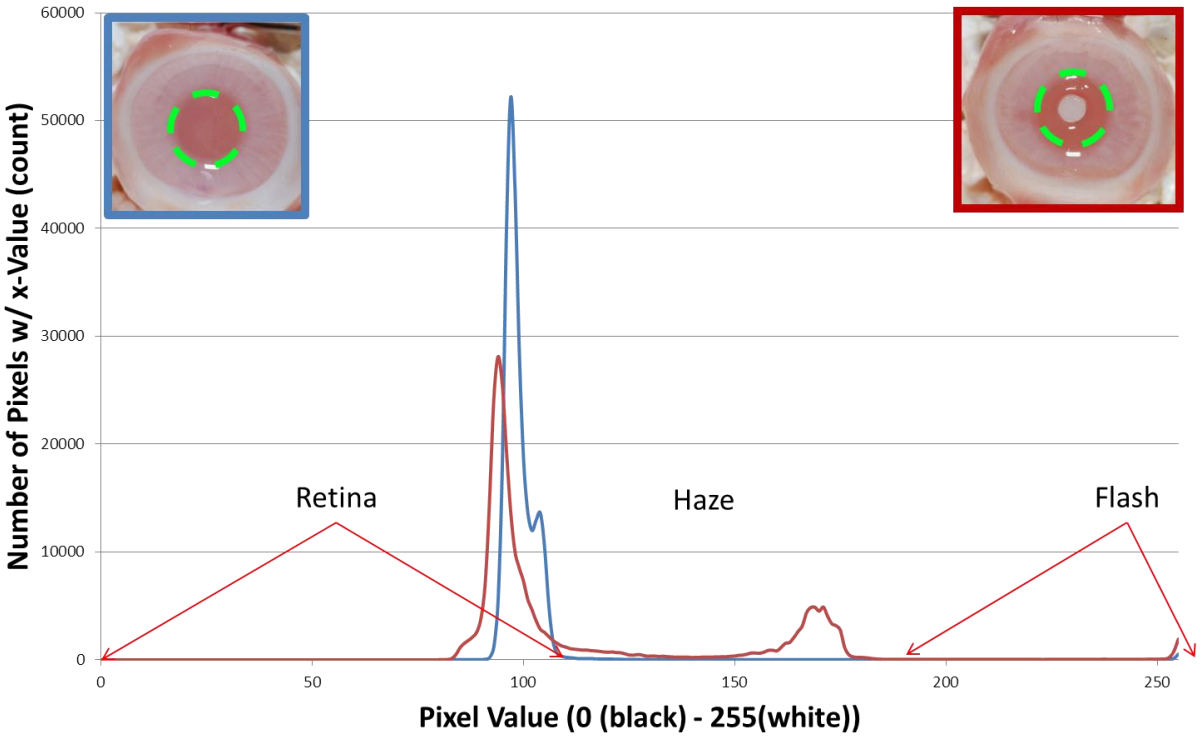

Figure 2-6. An example of a band-pass filter generated with non-viable eyes. A different filter was designed for use on images of viable eyes.

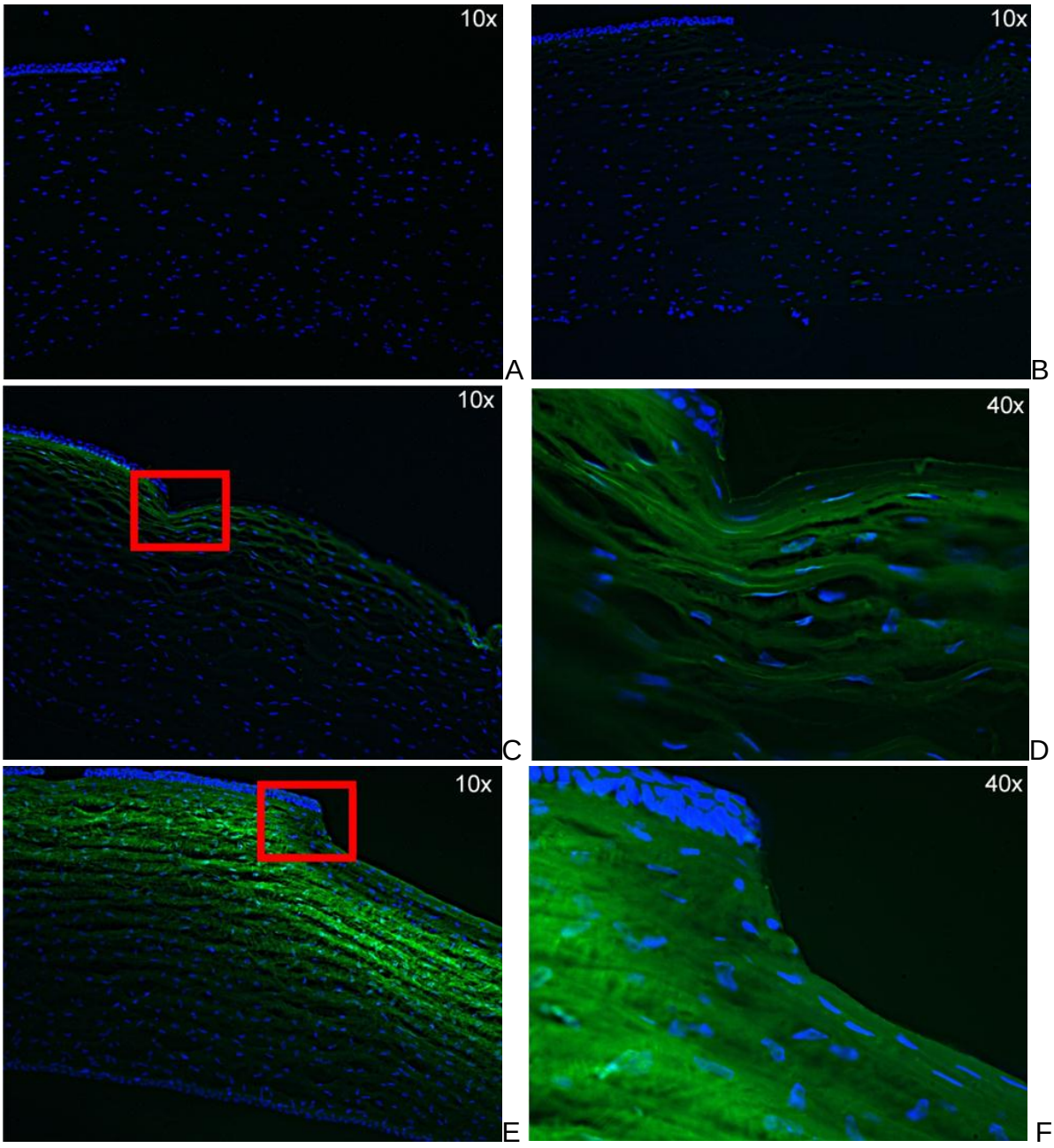

Figure 2-7. Reporter ssDNA delivery into *ex vivo* globes A) 0.0 mA (topical), B) 1.0 mA C,D), 2.0 mA or E,F) 3.0 mA.

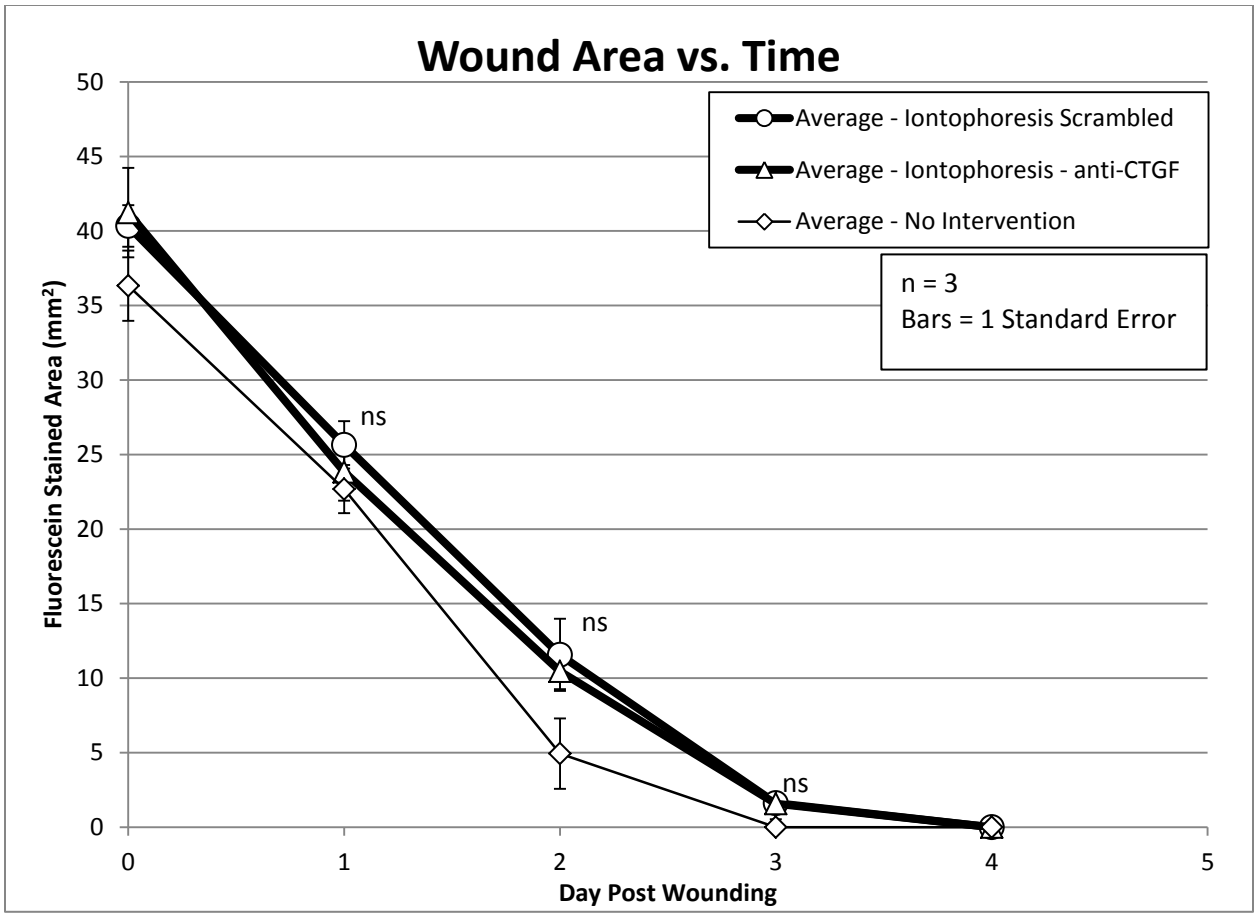

Figure 2-8. The area of fluorescein staining was measured daily following PTK wounding with or without iontophoresis. ANOVA indicates that the differences in wound area during healing amongst the groups were not significantly different.

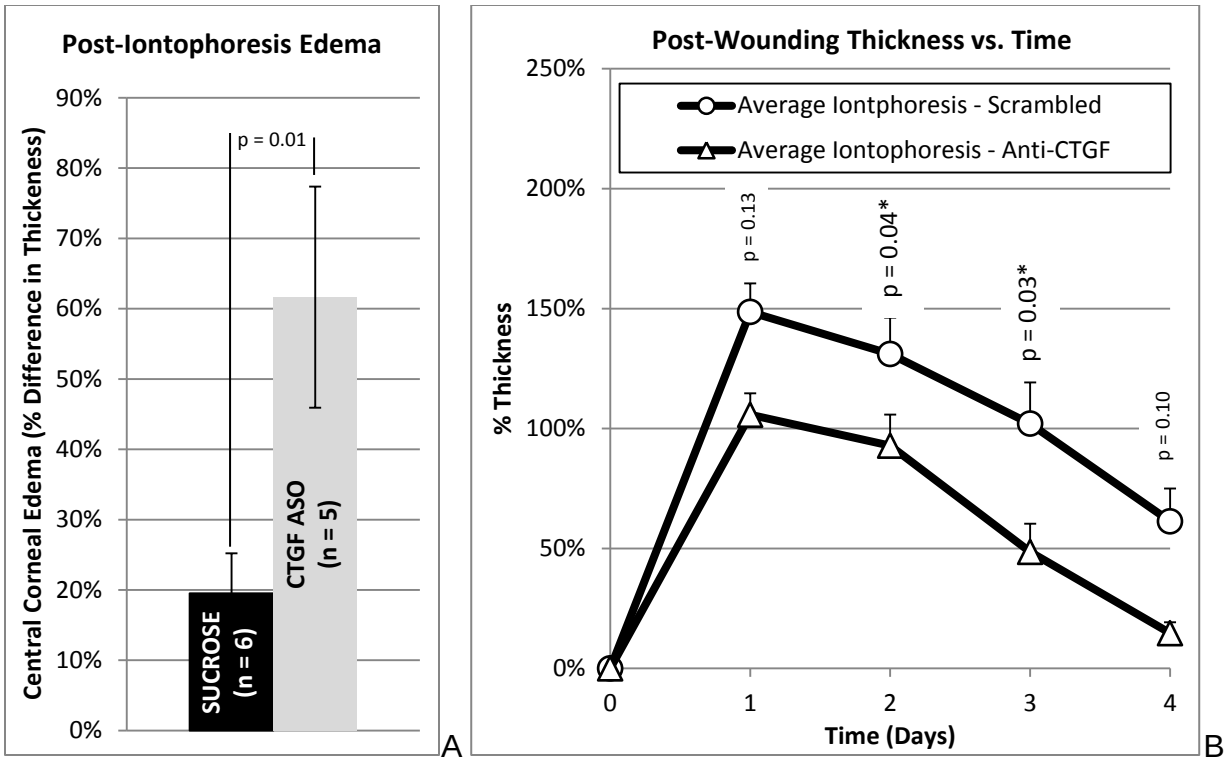

Figure 2-9. Corneal edema following ASO treatment and during healing. A) The difference in corneal edema immediately following iontophoresis of either the sucrose vehicle or the vehicle and CTGF ASO. B) Edema in eyes receiving CTGF ASO or scrambled ASO in the contralateral eye. A statistical trend in edema between the CTGF and scrambled ASO treated corneas was present for days 1 & 4 post wounding (p = 0.13 & 0.10) and statistically significant differences were present for days 2 & 3 (p = 0.04 & 0.03).

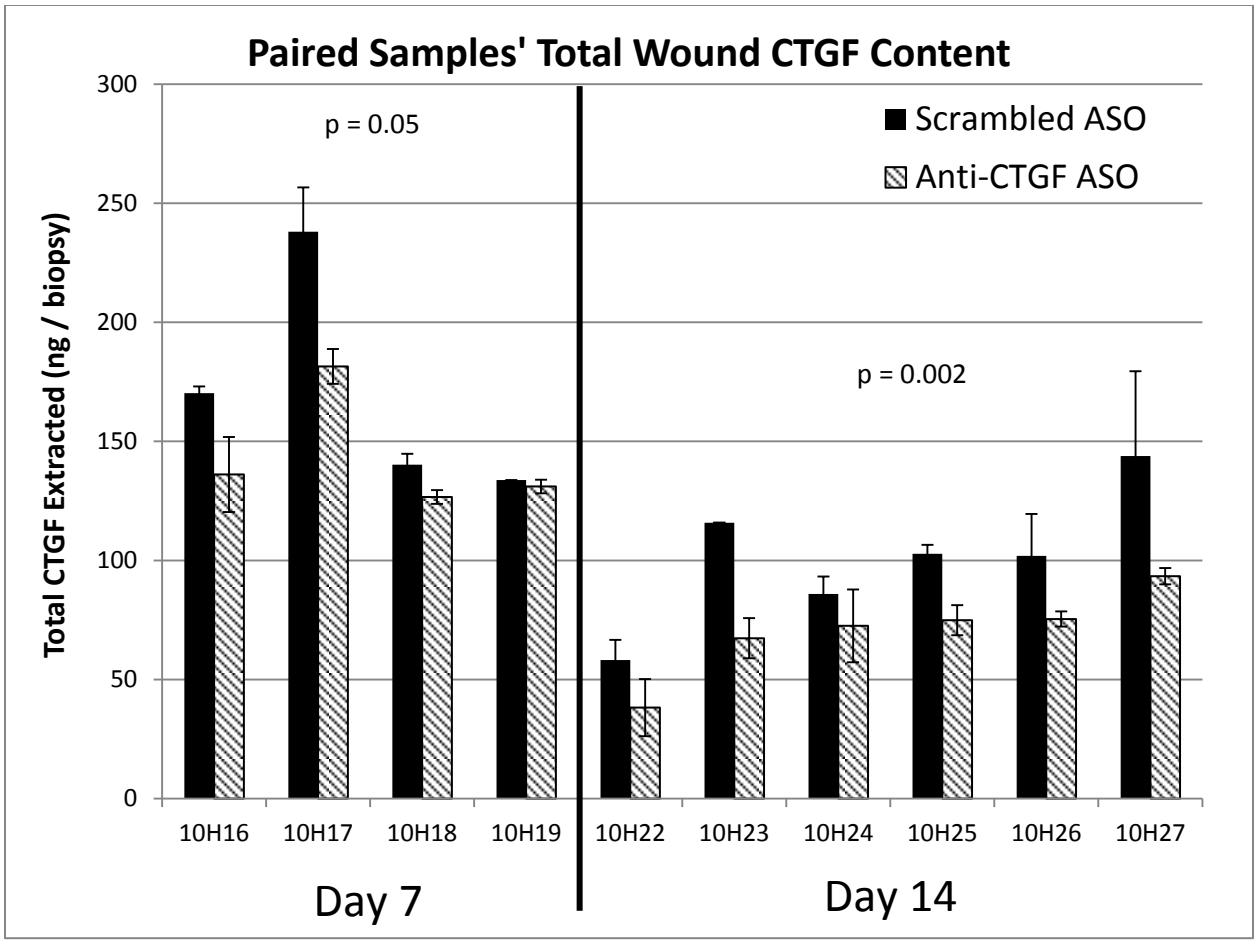

Figure 2-10. The paired quantity of total CTGF mass extracted from each 8.0 mm corneal punch. The samples were plated in duplicate, the error bars represent one standard error. A one-tailed, paired, Student's t-test analysis revealed that the observed paired differences were statistically significant (Day 7, p = 0.05; Day 14 p = 0.002).

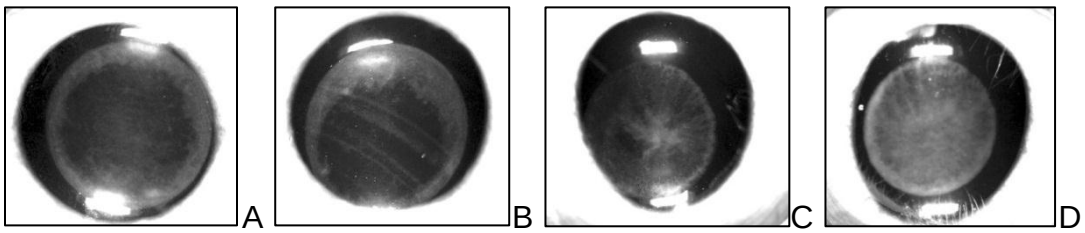

Figure 2-11. Paired examples (A&B, C&D) of CTGF versus scrambled ASO treated corneas. A) Day 7 CTGF ASO treated and B) the opposing eye treated with scrambled ASO. C) Day 28 CTGF ASO treated and D) the opposing eye treated with scrambled ASO from the tolerance experiments.

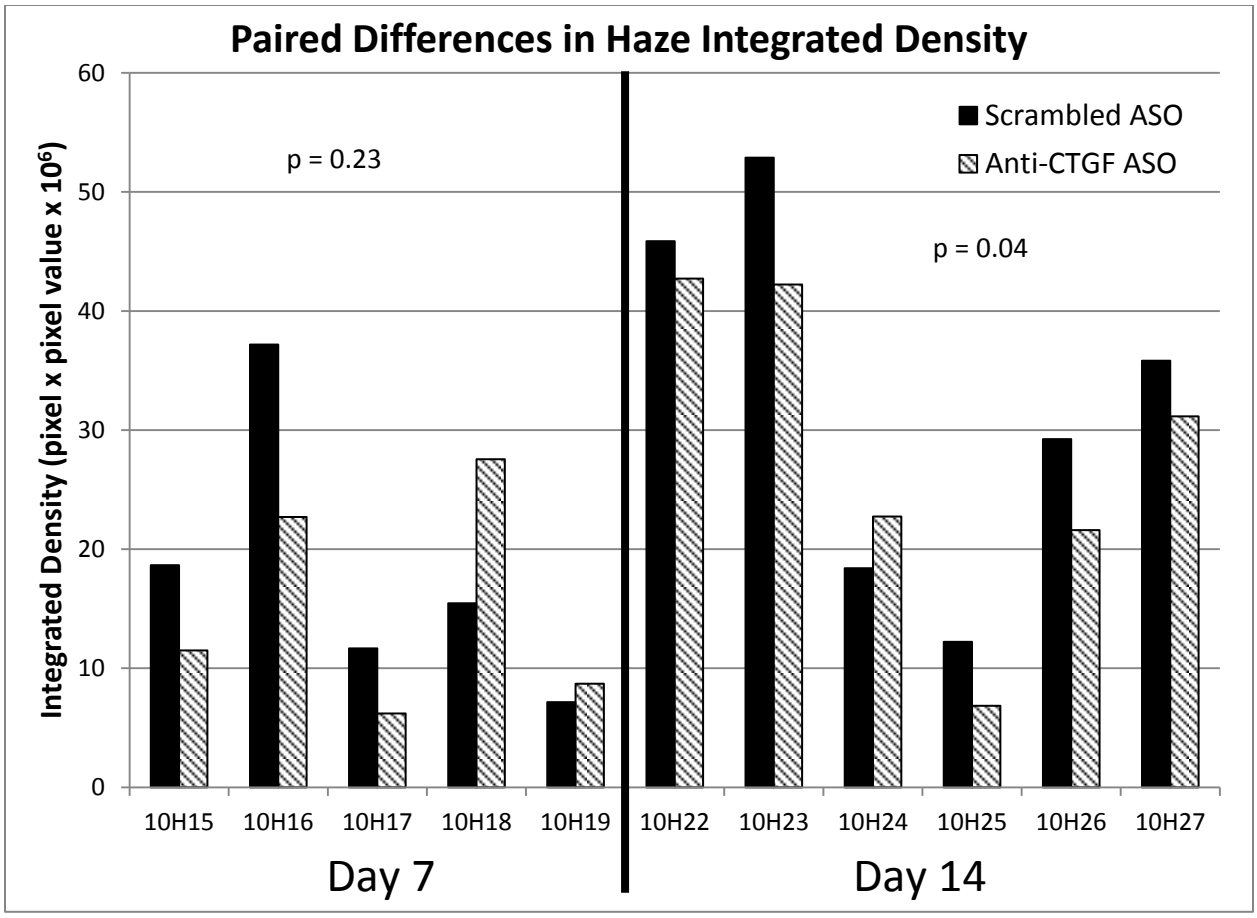

Figure 2-12. Individual paired haze measurements. A one-tailed, paired, Student's t-test analysis revealed that the observed paired differences were not statistically significant on day 7 ($p = 0.23$), but did reach statistical significance on day 14 ($p = 0.04$).

CHAPTER 3
THE LOCATION OF CTGF PRODUCTION AND ACCUMULATION IN HEALING CORNEAS

Introduction

In the preceding chapter, I sought to decrease the presence of CTGF in the wound healing cornea since it had been identified as a key downstream mediator of transforming growth factor-β's fibrotic activities[59]. The results were positive, but both the reduction of CTGF and haze were clinically marginal. The delivery of the ASOs to the region of interest is reproducible (Figure 2-7), which gives rise to the question of whether the right region of the cornea is being treated. Given the mechanism of action of the ASOs, CTGF's site of synthesis is the key piece of information needed to ensure that the ASOs are being dosed to the correct cell layer(s). Additionally, the final locus of activity is necessary both for therapies targeting CTGF protein and/or receptor neutralization, and to further understand the biological role of CTGF in fibrosis. Early investigations have focused on fibroblasts due to fact that they do produce CTGF in response to TGF-β[59]. The first investigations into CTGF localization in healing corneas found that CTGF was present in all cell layers of the cornea, but had higher concentrations in the epithelium[63]. The levels of CTGF were found to continually rise from the time of wounding up through 28 days post wounding[63]. Subsequent reports have observed a peak in CTGF protein at day 2 or 3 post wounding which then returned to basal levels by day 21 post wounding[107]. Given the ELISA results presented in the previous chapter (Figure 2-10), an expression profile with a peak and subsequent reduction during the wound healing process is currently better supported. Herein, I will describe the distribution of CTGF in the time period prior to, and during the early phase of, haze formation in rabbit corneas as measured by immunofluorescent staining. In

order to measure the location of the synthesis of CTGF protein, a CTGF promoter driven eGFP reporter mouse was used to identify the cells with CTGF promoter activity in normal corneas and during wound healing. The promoter activity level found in normal corneas was validated by measuring the amount of CTGF transcripts in grossly dissected normal rabbit corneas. These experiments are expected to reveal where CTGF is synthesized and where the protein is localized within the healing corneas.

Materials And Methods

Excimer Laser Surgery

Each rabbit was anesthetized using inhaled isoflurane and each eye was topically anesthetized using one drop of tetracaine or proparacaine. The eye was exposed using either an eyelid speculum or was proptosed with a pair of cotton swabs. The central thickness of the cornea was measured with a clinical ultrasonic pachymeter (n = 5 central measurements per eye). Each eye then received a central 6.0 mm diameter, 125 μm deep, excimer laser PTK wound. The central thickness was measured again by the ultrasonic pachymeter to verify ablation depth.

Each mouse was placed in a sealed box and anesthetized with 3.5% inhaled isoflurane/oxygen. Once anesthetized, it was removed from the box and placed straddling a 50 ml conical tube and held in place with a semi-adhesive elastic band gently wrapped around both the mouse and tube. The tube was outfitted with a nose cone-fed supply of isoflurane/oxygen. The mouse was laid on its side and supported by a stack of cotton gauze. The eye to be wounded received a drop of proparacain. The whiskers were cut with scissors and the eye lid and lashes were gently pushed out of the way with a cotton swab and held in place with an adhesive strip if needed. The

mouse was then oriented beneath the excimer laser. A 1.0 mm diameter by 40 μm deep PTK excimer wound was created.

Tissue Harvesting, Processing, and Sectioning

At the terminal time point, the rabbits and mice were anesthetized as before and euthanized by intravenous Beuthanasia-D and cervical dislocation, respectively. For rabbits, each globe was immediately enucleated using forceps and sharp scissors to cut the conjunctiva, muscles, and optic nerve. For mice, each eye was proctosed and the posterior portion of the globe was held firmly with fine pointed forceps and the eye was forcibly removed. Both the rabbit and mouse eyes were immediately placed in fresh 10% neutral buffered formalin on ice. The globes were punctured with a 25 gauge needle after 1 hour to improve fixative penetration. The globes were fixed overnight at 4°C. The globes were then grossly prepared by cutting open the posterior retina, removing the lens and any residual air bubbles. The globe and lens were placed in 30% sucrose in PBS overnight at 4°C to cryoprotect the tissues. In order to improve cryosectioning, each globe was injected with embedding medium (OCT) with a blunt-tipped needle and syringe. The lens and globe tissues were then submerged in OCT and rapidly frozen. The frozen blocks were stored at -20°C until cryosectioning. Ten micron sections were cut with a cryotome and mounted on poly-L-lysine coated slides. The slides were air-dried and then stored at -20°C until staining.

Immunohistochemical Staining

Rabbit corneas

In order to visual the localization of CTGF protein in healing rabbit corneas immunohistochemical staining with an anti-CTGF monoclonal antibody (created in a mouse). Briefly, the slides were washed 3 times with wash solution (10 mH HEPES,

150 mM NaCl, 0.02% Na-Azide, and 0.05% Tween-20, pH 7.4). The slides were blocked for 30 min with 10% normal horse serum (Vector Labs). The sections were then washed twice for 2 minutes with wash solution. Half of the sections then received either antibody dilution solution (HEPES Buffer) or the anti-CTGF antibody (50µg/ml, in dilution solution) and were then incubated overnight at 4°C. The antibody solution was then carefully removed and the samples were then washed 3 times for 5 minutes each. The sections were then incubated with affinity purified fluorescein labeled anti-mouse IgG (20 µg/ml, Vector Labs) for 10 min. The samples were then washed 3 times for 5 minutes each. The slides were mounted with 4',6-diamidino-2-phenylindole (DAPI) containing medium and the coverslips sealed with nail hardener. The slides were kept refrigerated in the dark until imaged.

Reporter mouse corneas

In order to determine both the cells producing CTGF and where CTGF is binding, I chose to use immunohistochemical staining with a biotinylated anti-CTGF antibody on the wounded reporter mouse corneas. Briefly, the slides were washed 3 times with wash solution (10 mH HEPES, 150 mM NaCl, 0.02% Na-Azide, and 0.05% Tween-20, pH 7.4). The slides were blocked for 30 min with 10% normal rabbit serum (Vector Labs). The sections were then treated to block endogenous biotin and avidin according to the manufacturer's instructions (Vector Labs). The sections were then washed twice for 2 minutes with wash solution. Half of the sections then received either antibody dilution solution (HEPES Buffer) or the anti-CTGF antibody (50µg/ml, in dilution solution) and were then incubated for 30 min at room temperature. The antibody solution was then carefully removed and the samples were then washed 3 times for 5 minutes each. The sections were then incubated with avidin-Texas Red (25 µg/ml,

Vector Labs) for 10 min. The samples were then washed 3 times for 5 minutes each. The slides were mounted with DAPI containing medium and the coverslips sealed with nail hardener. The slides were kept refrigerated in the dark until imaged.

Transgenic Mice

These mice possess a transgene composed of the promoter from connective tissue growth factor upstream from an enhanced green fluorescent protein (eGFP)[108,109] (Figure 3-1A). This construct results in the accumulation of eGFP in cells that possess activites capable of stimulating transcription from the CTGF promoter. With the additional step of immunostaining for CTGF protein in these mice, the location of production of CTGF (green) and final destination of the protein (red) provides a more detailed picture of the source and locus/loci of activity of CTGF. Mice with the transgene were identified using a cobalt or cyan light source to illuminate the eye, the lenses of transgene-positive mice fluoresce intensely. Using a camera with a dedicated macro flash with a cobalt blue filter on the flash and a deep yellow filter on the lens, the eGFP in the lens was easily observable in the mice with the pCTGF-GFP transgene (Figure 3-1B). The mouse pups were chosen by phenotypic observation of the green fluorescence in the lens in place of standard genotyping.

Whole Mount Confocal Micrography

Enhanced green fluorescent protein positive mice were euthanized and their eyes were immediately enucleated and placed in 10% neutral buffered formalin. Following overnight fixation at 4°C, the eyes were grossly dissected and the tissues were cut into small pieces and placed into a custom made slide with a reservoir. The tissues were immersed in mounting medium containing DAPI counterstain (Vector Labs) and a

coverslip was affixed in place with nail hardener. The pieces of tissue were then imaged with a spinning disc confocal microscope.

Micrography

The sections were imaged on a confocal microscope with either a 10 x objective or a 60 x oil immersion objective. For the whole mount tissues, the entire volume of tissue within the field was imaged. The z-stack was viewed using PerkinElmer's Volocity Acquisition software and the "extended focus" z-stack representation was exported for each image.

For the immunofluorescently stained sections, the brightest field from the brightest section receiving primary antibody was used to determine the exposure to be used for the entire series of rabbit cornea sections. The exposure conditions were chosen by first setting the gain to "0" and the exposure time to 1 second. If the image was overexposed with these conditions, the exposure time was reduced just to the point that the image was no longer overexposed (i.e. that the final overexposed pixels were no longer overexposed). If the initial exposure conditions did not result in an overexposed image, the gain was raised to the point just before overexposure. The gain was never raised above 50% of the maximum gain value, if additional exposure was needed, the exposure time or illumination intensity was adjusted. The signal intensity in the control slides was used as a background correction for the entire series of rabbit cornea sections. The same overall procedure was used for imaging the mouse cornea sections, but given the different staining conditions, a different set of exposure conditions were determined and used.

Gross Corneal Dissection and CTGF Transcript Quantification

Rabbits without observable corneal wounds were anesthetized and euthanized as described before. A scalpel was used to immediately scrape the epithelium off with care taken to ensure that the scraped mass was retained on the blade. The scraped epithelial mass was then transferred to 350 µl of tissue lysis buffer (Qiagen, buffer RLT) and the blade was rinsed with 250 µl of additional lysis buffer. The cornea was then excised from the globe by cutting with a fresh scalpel and scissors at the corneal/scleral boundary. The cornea was placed face down and yet another fresh scalpel was used to scrape off and retain the endothelium as was done with the epithelium. The endothelial mass was transferred to 350 µl of lysis buffer and the blade rinsed with an additional 250 µl of lysis buffer. The residual stroma was cut into approximately 1 mm x 1 mm pieces which were all submerged in 600 µl of lysis buffer. Each grossly isolated cellular layer was then subjected to ultrasonication on ice for further tissue disruption. The probe was rigorously washed, rinsed and dried in between each sample. The homogenates were then immediately loaded onto Qiagen gDNA removal columns and the RNA was purified in accordance with the manufacturer's provided protocol (Qiagen RNAeasy, Qiagen, Inc., Cat. #74104).

The purified RNA was quantified via ultra-violet absorbance using a Nanodrop ND-1000 spectrophotometer set for RNA quantification. Equal masses of RNA were loaded for each sample and 2-fold concentrated TAQMan™ Universal PCR Master Mix in a 96-well PCR reaction plate. Real-Time PCR (RT-PCR) was performed on an Applied Biosystems 7900HT Fast Real Time PCR System utilizing the manufacturer's recommended thermal cycling conditions. The relative gene expression of CTGF versus GAPDH was calculated for each tissue using the primers and probes listed in Table 3-1.

This relative metric was used to compare the relative enrichment of CTGF mRNA in each tissue. A few samples were run without reverse transcriptase to measure the quantity of genomic DNA (gDNA) present in the sample.

Results

Excimer Wounding

The excimer wounding was well tolerated by both the rabbits and mice with no complications. An example mouse corneal wound is depicted in Figure 3-1C. The wounds were consistently circular and the rough appearance of the ablated surface evidences that the wound penetrated into the stroma.

The Location of CTGF Protein Accumulation

Within 30 minutes after wounding, a green fluorescent signal was present in the migrating in the epithelial front (Figure 3-2A,C,E), but not in the 1° antibody withheld control (Figure 3-2B&D). One day after wounding, there is an increased presence of green fluorescence in the healing epithelium, stroma, and endothelium (Figure 3-3A,C,E). The green fluorescence in the stroma is also present in the 1° antibody withheld control indicating that it is either non-specific binding of the 2° antibody or autofluorescence (Figure 3-3B). Given the hue and homogeneity of the cytoplasmic staining, the stromal signal in these fields is most likely autofluorescence. Day two after wounding the intensity of the green fluorescence peaks, and is found in both the epithelium and stroma (Figure 3-4). This time, however, the majority of the green fluorescence is not present in the control and has the “splotchy” extracellular distribution more indicative of a positive signal. Again, the corneal endothelium also has a positive green fluorescent signal. In the remaining days, the total intensity of staining diminishes

and the major locus of binding is primarily confined to the basal epithelium (Figure 3-5 through Figure 3-9).

The Location of CTGF Promoter Activity

For this model, the presence of green fluorescence within the cytoplasm of cells is evidence of CTGF promoter activity. In the unwounded cornea, the endothelium is the only cell layer in the cornea with a detectable signal (Figure 3-10). Fluorescent confocal micrographs of the cryosectioned eyes revealed that within the cornea, the endothelium was still the site of highest CTGF promoter activity as was seen in the unwounded corneas. However, in the wounded cornea some sub-epithelial cells in the stroma possessed detectable green fluorescence (Figure 3-11A, red arrows). But the presence of red fluorescence in these cells in the immunofluorescent control (Figure 3-12A) suggests that this signal is a result of autofluorescence. Furthermore, the location and appearance of the fluorescence is reminiscent of the autofluorescence seen earlier in the rabbit samples (Figure 3-3B).

The high red fluorescent background prevented interpretation of the presence or absence of CTGF protein in the mouse endothelium in these samples. Despite the high background signal in the control sections, a key difference was noted between the sections receiving the primary antibody and those that did not. As was seen in the rabbits, the basal epithelium of the cornea was the primary location of CTGF antigenicity (Figure 3-12C). The CTGF protein is predominantly located on the basal portion of the basal epithelium and appears to have an extracellular, punctate, distribution as was seen in the rabbit samples.

Gross Corneal Dissection and CTGF Transcript Quantification

In the unwounded rabbit eyes, the grossly dissected epithelium was the tissue with the greatest RNA mass recovered (Figure 3-13A). All three layers possessed CTGF transcript with a cycle threshold value indicative of a good level of confidence. Of the three layers, the endothelium had more CTGF transcripts per GAPDH transcript (Figure 3-13B), mirroring the data that the pCTGF-eGFP reporter mouse provided.

Discussion

Given that our primary theory behind the formation of haze centers on the activity of connective tissue growth factor, and that CTGF is primarily located in the basal epithelium, new questions arise about which cells we should be targeting for therapies. The observation that in the cornea, CTGF promoter activity and mRNA quantity are both highest in the endothelium is novel. During wound healing, any change in promoter activity in the epithelium or stroma does not appear to reach a level sufficient for detection under the conditions used. However, additional work is currently planned to repeat the gross dissection qRT-rtPCR quantification of CTGF mRNA during the wound healing process to observe where in the cornea the previously observed cornea-wide upregulation occurs. These data is key to refining future delivery methods for anti-CTGF mRNA therapies that are in continued development.

Given that the basal epithelium is both the location of high CTGF protein accumulation and it is where the scar will eventually be, significant conflicts have now been introduced to the initially proposed cellular and molecular model for scar formation (Figure 1-5). Connective tissue growth factor is present in abundance in the unwounded lens (Figure 3-1B) and is constitutively expressed in the corneal endothelium in unwounded corneas. These facts indicate that CTGF presence is not

sufficient to generate a scar, it also suggests that CTGF may have a basal function that is present in these tissues that is also necessary for the generation of a scar. These observations raise the specter of potential off-target effects given that they are present in unwounded tissues. The function of CTGF in these tissues is currently unknown thereby precluding a prediction of potential side-effects.

The presence of CTGF in the cornea increases during wound healing. While increased transcription and translation is the most commonly attributed mechanism for increases in protein levels in a tissue, other mechanisms are possible. One such mechanism is increased accumulation due to a change in a cell's capacity to bind the protein in question. Given the evidence that CTGF begins to accumulate in the basal epithelium as soon as 30 minutes after wounding, it may very well be that one of the first stages in the CTGF response pathway is that contact de-inhibited epithelial cells become rapidly sensitized to CTGF, thus enabling a rapid response to the basal levels that exist in the intact cornea. Further evidence supporting a differential cellular sensitization are the facts that fewer suprabasal epithelial cells bind CTGF than the basal epithelium do not accumulate CTGF. During re-epithelialization, the epithelium has yet to begin re-stratification and the CTGF staining is present throughout the epithelium (up to day 2 post wounding). Once the epithelium begins to re-stratify, staining for CTGF is predominantly located in the basal epithelium, not the differentiated cells that form the more apical surface of the epithelium (day 3 and beyond). This observed differential sensitization may be another, better, therapeutic target given both that the epithelium is accessible to topically applied agents and that sensitization would be "higher" in the CTGF response cascade.

By far, the most interesting finding was that the primary source of CTGF synthesis and protein binding were in separate cell layers on the extremities of the cornea. The effects of strongly iontophoresed CTGF ASO (5.0 mA) on corneal edema (Figure 2-9B) and haze (Figure 2-11C) indicate that the observation warrants further investigation. At first consideration, a mechanism of synthesis in the endothelium, diffusion through the stroma, and subsequent binding to the epithelium is difficult to accept. The difficulty arises due to the fact that the bulk flow of water is out of the cornea across the endothelium and that the stroma is a significant barrier to ionic macromolecule diffusion. However, during wound healing the next flux of fluid is into the cornea, as is evidenced by the edema during the first several days of healing. It has been reported that an edematous stroma is not as effective of a barrier as the normally dehydrated one[110]. In diffusion chamber experiments with excised rabbit corneas under differing degrees of hydration, it was found that neither Descemet's layer nor the stroma posed a significant barrier to the diffusion of insulin under highly hydrated (i.e. edematous) conditions[110] (Figure 3-14A). This reduction in stromal barrier function provides a reasonable mechanism to enable endothelial derived CTGF to diffuse to and bind to the corneal epithelium (Figure 3-14B). This proposed hypothesis is further supported by the observation that the peak of CTGF binding of the epithelium occurs during the edematous phase and tapers off in concert with the restoration of the normal corneal hydration state. While these observations and proposed mechanisms do not definitively prove that the endothelium is the source of pro-fibrotic CTGF during wound healing, they do form the basis of a new consistent and testable theory.

Table 3-1. TAQMAN™ RT PCR Primers and probe sequences

Growth Factor	Species	Accession Number
CTGF	Forward	AGGAGTGGGTGTGTGATGAG
	Reverse	CCAAATGTGTCTTCCAGTCG
	Probe	ACCACACCGTGGTTGGCCCT
GAPDH	Forward	GAGACACGATGGTGAAGGTC
	Reverse	ACAACATCCACTTTGCCAGA
	Probe	CCAATGCGGCCAAATCCGTT

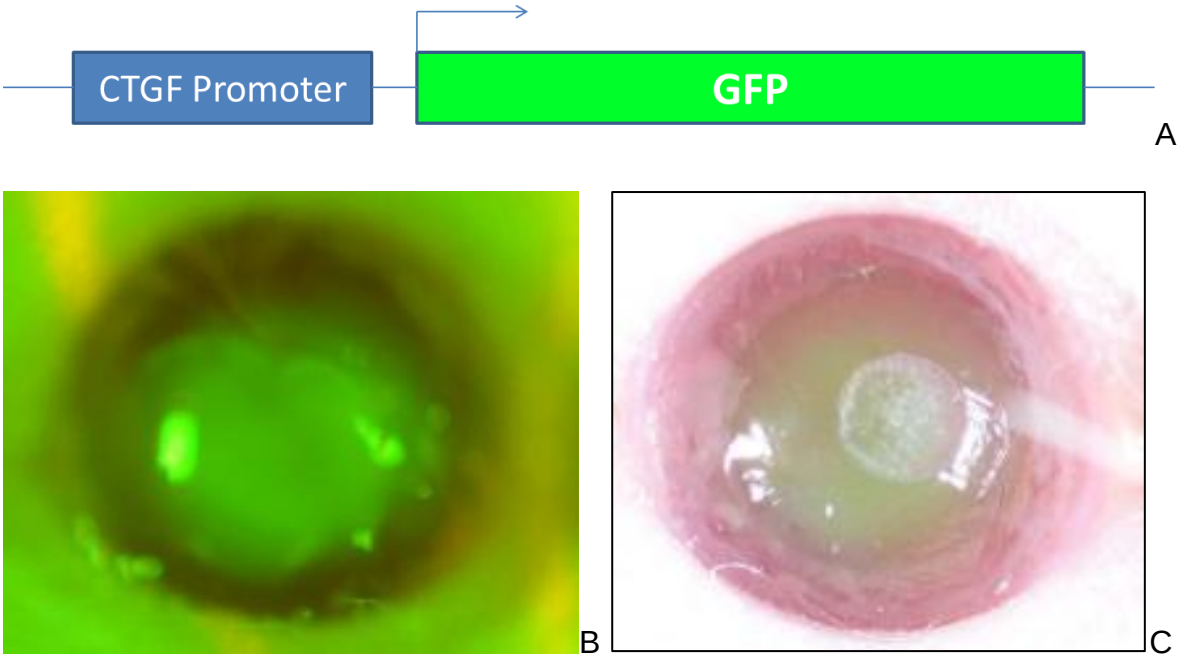

Figure 3-1. The CTGF synthesis reporter mouse. A) A schematic representation of the reporter transgene. B) The lenses pCTGF-eGFP mice have a green fluorescent phenotype enabling easy sorting of reporter mice from their liter-mates. C) A representative PTK wound on a pCTGF-eGFP mouse cornea.

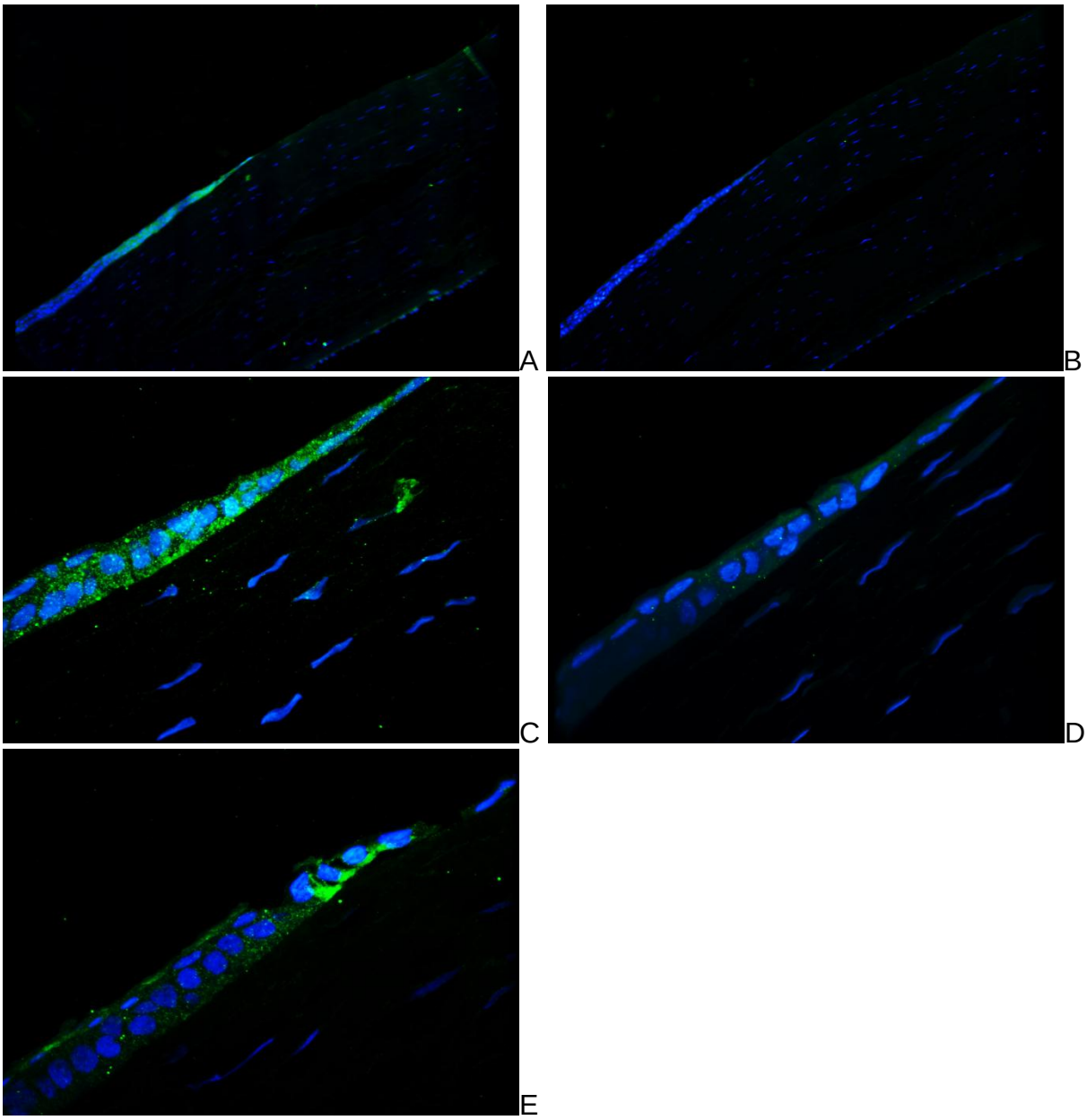

Figure 3-2. Confocal micrographs of anti-CTGF (green) immunofluorescent stained wounds 30 minutes post-wounding. A) A wide field (10 x) image of the wound margin. C) & E) Higher power (60 x) micrographs of the migrating epithelial edge. B) & D) are controls in which the primary antibody was withheld.

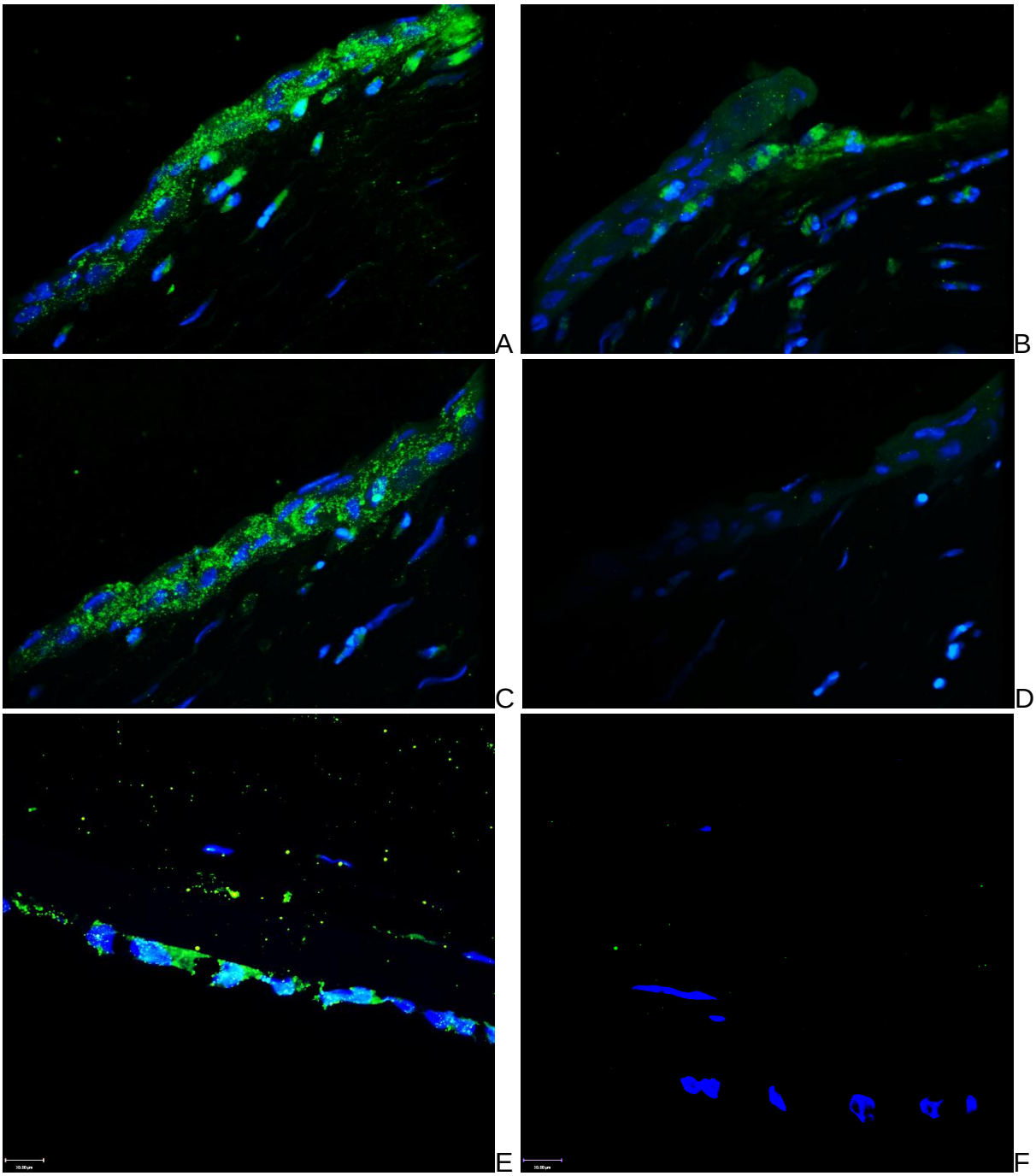

Figure 3-3. Confocal micrographs of anti-CTGF (green) immunofluorescent stained wounds 1 day post-wounding. A) & C) represent portions of the epithelium while E) is the endothelium. B), D), & F) are controls in which the primary antibody was withheld.

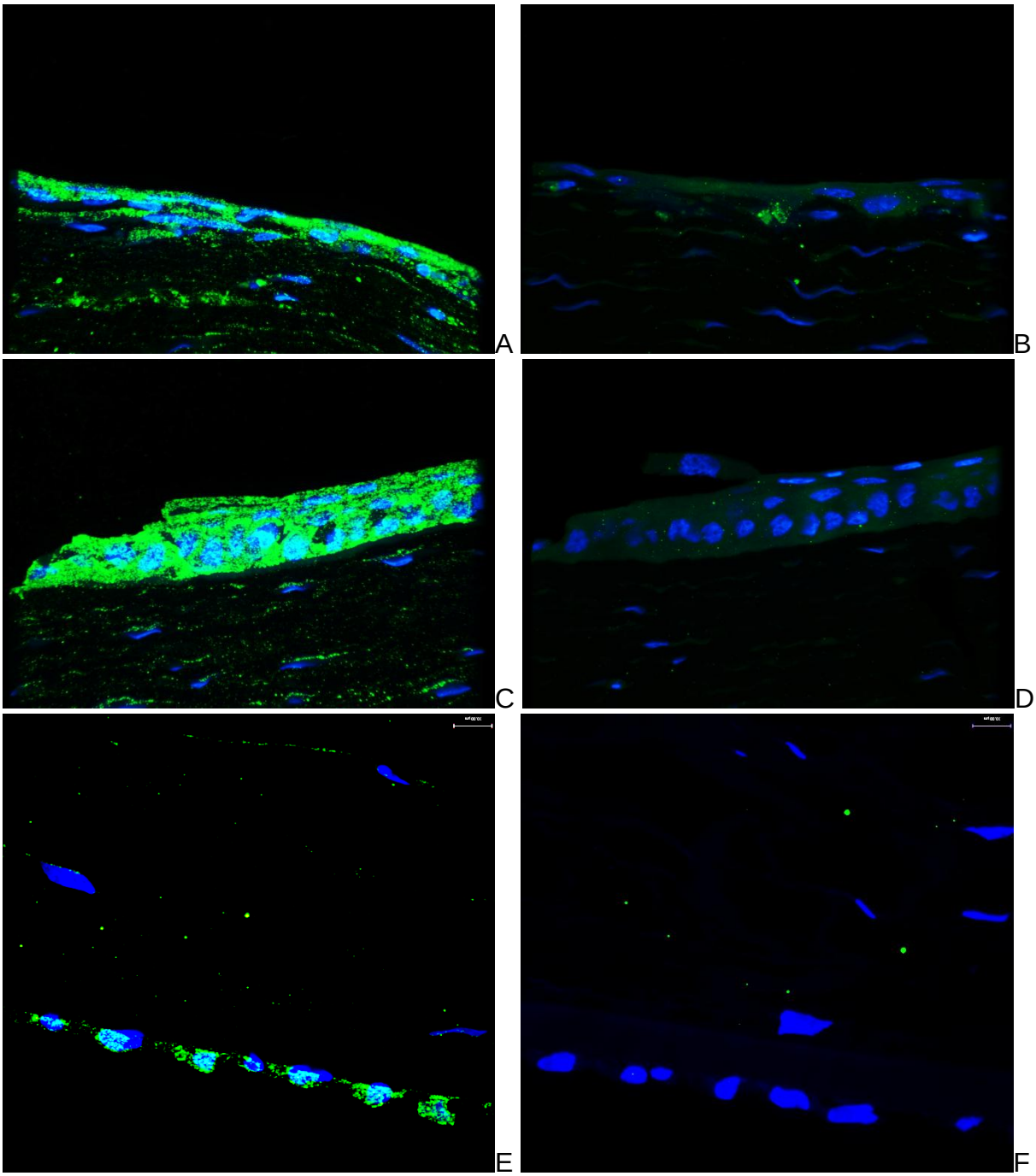

Figure 3-4. Two days post-Wounding: Wound Margin. Most likely surface effects magnified by a not very flat tissue. A) & C) represent portions of the epithelium while E) is the endothelium. B), D), & F) are controls in which the primary antibody was withheld.

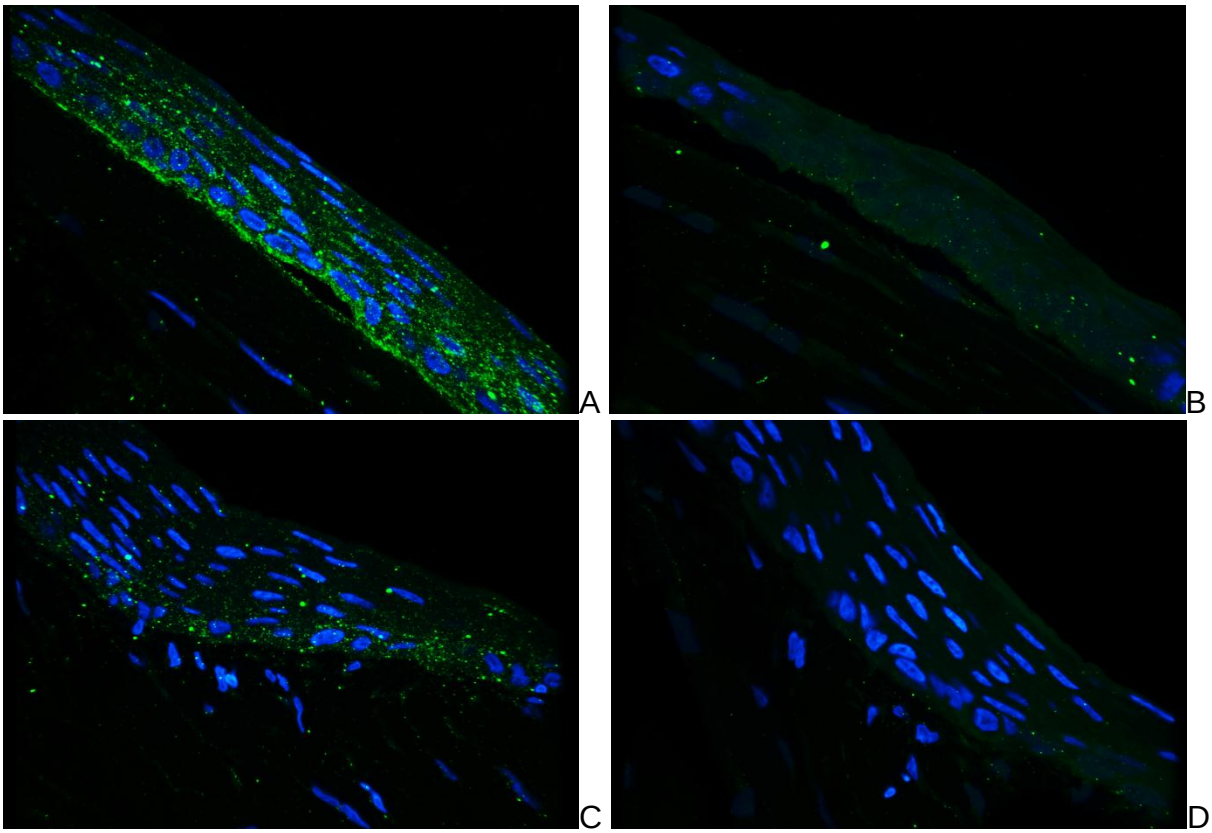

Figure 3-5. Day 3 Post-Wounding: A) & B) Wound body. C) & D) wound margin. B) & D) are controls in which the primary antibody was withheld.

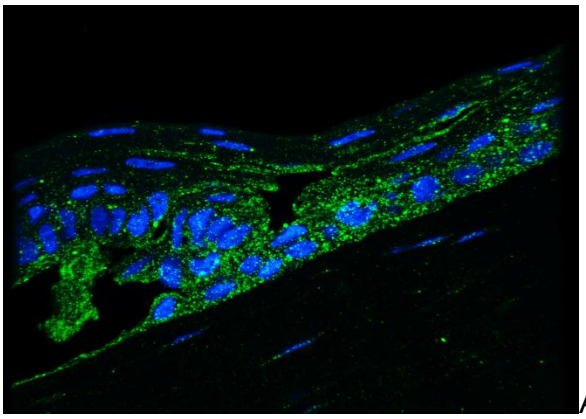
A
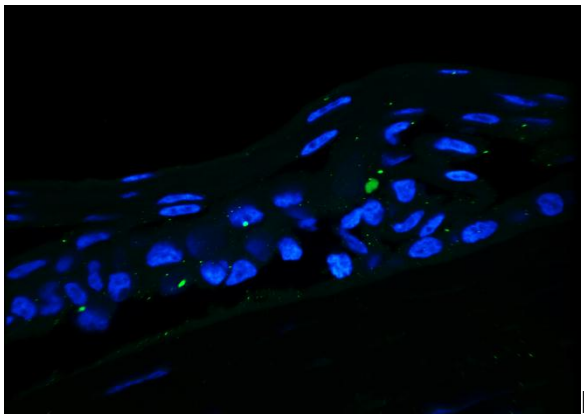
B
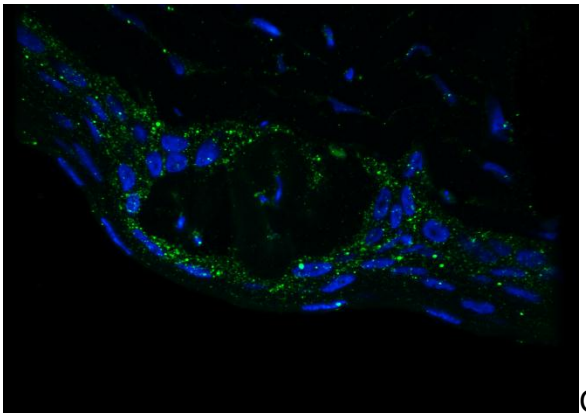
C

Figure 3-6. Day 4 Post-Wounding. A) & B) Edge of hyperproliferation. C) a piece of undermined stroma in the body of the wound included as a mass surrounded by epithelial cells. B) is a control in which the primary antibody was withheld.

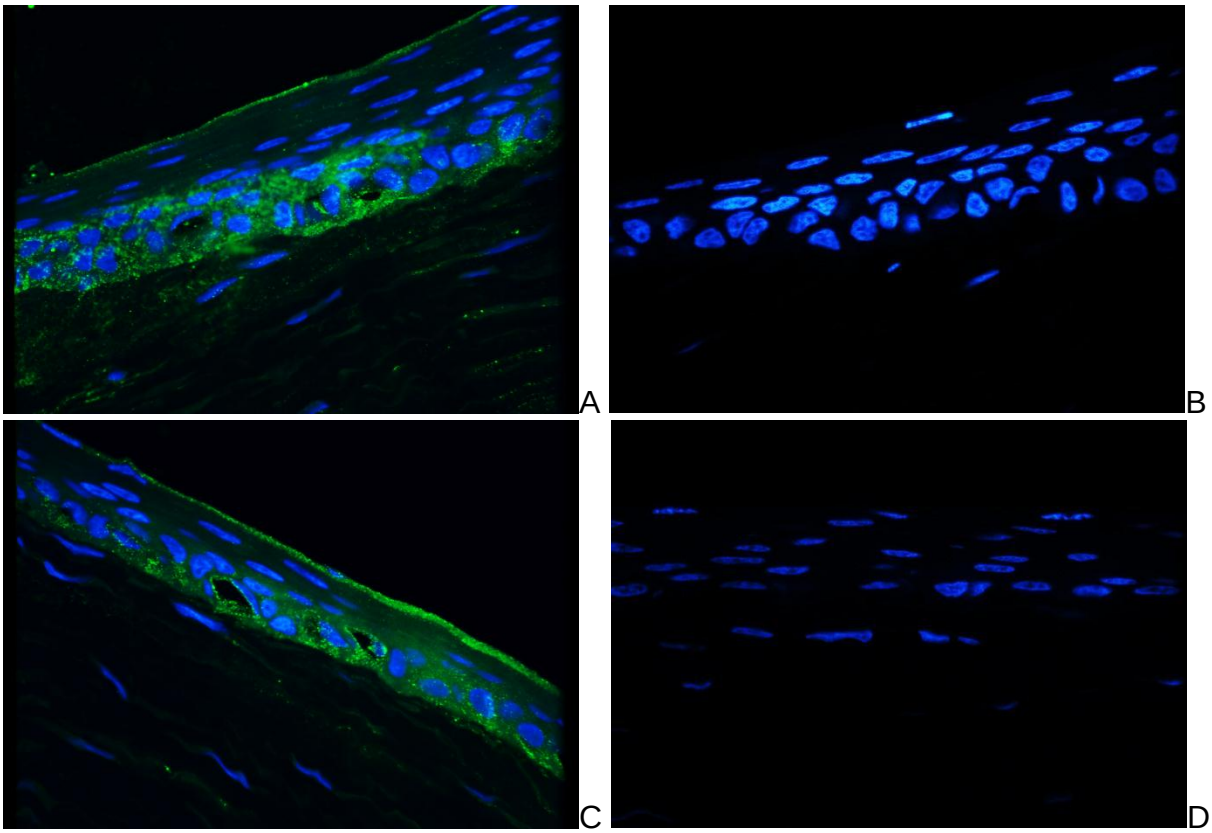

Figure 3-7. Day 5 post wounding. A) & B) the wound margin C) & D) the wound body. B) & D) are controls in which the primary antibody was withheld.

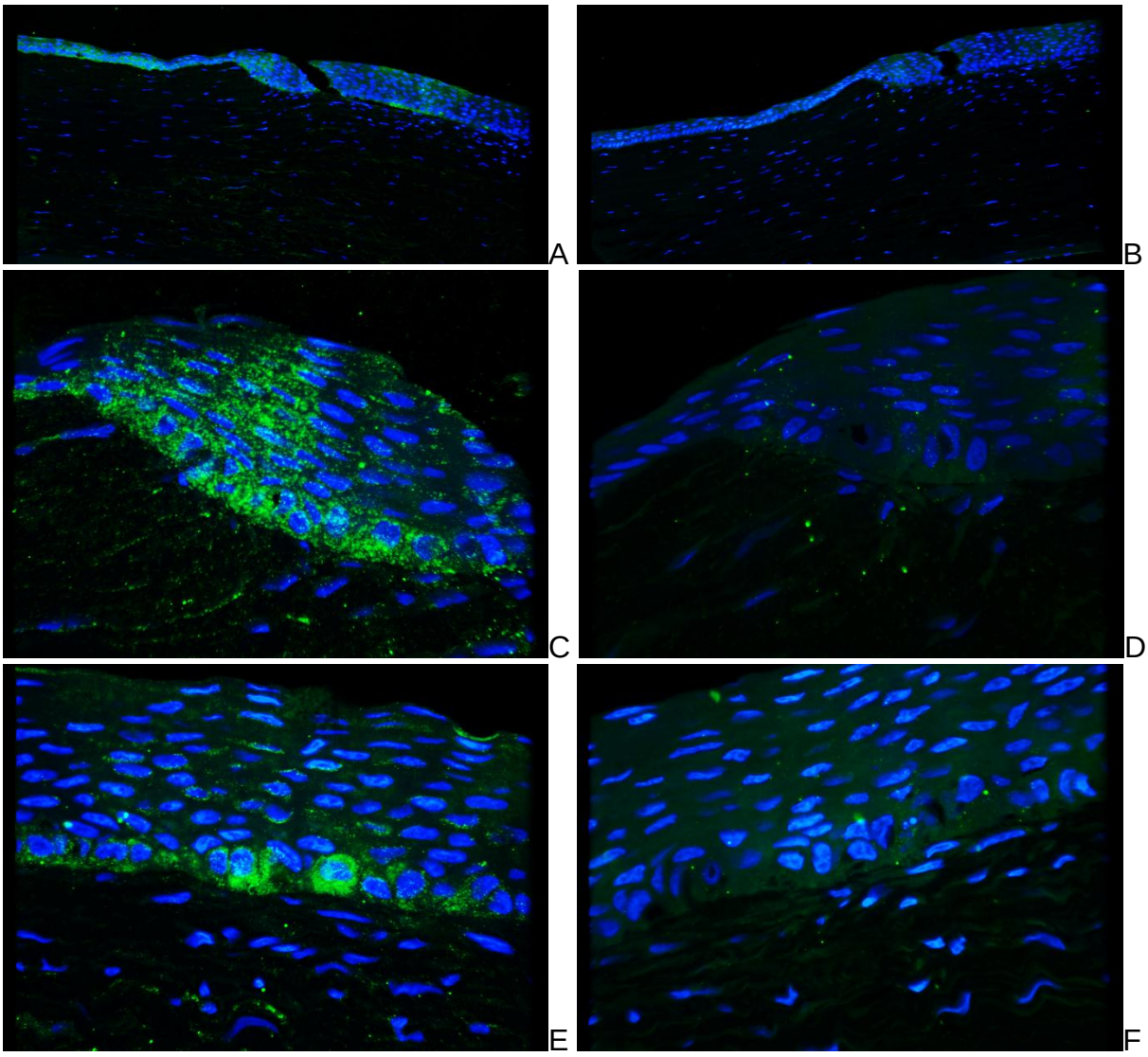

Figure 3-8. Day 7 post wounding. A) & B) 10x mag of the margin and surrounding area. C) & D) the wound margin E) & F) the wound body. B), D), & F) are controls in which the primary antibody was withheld.

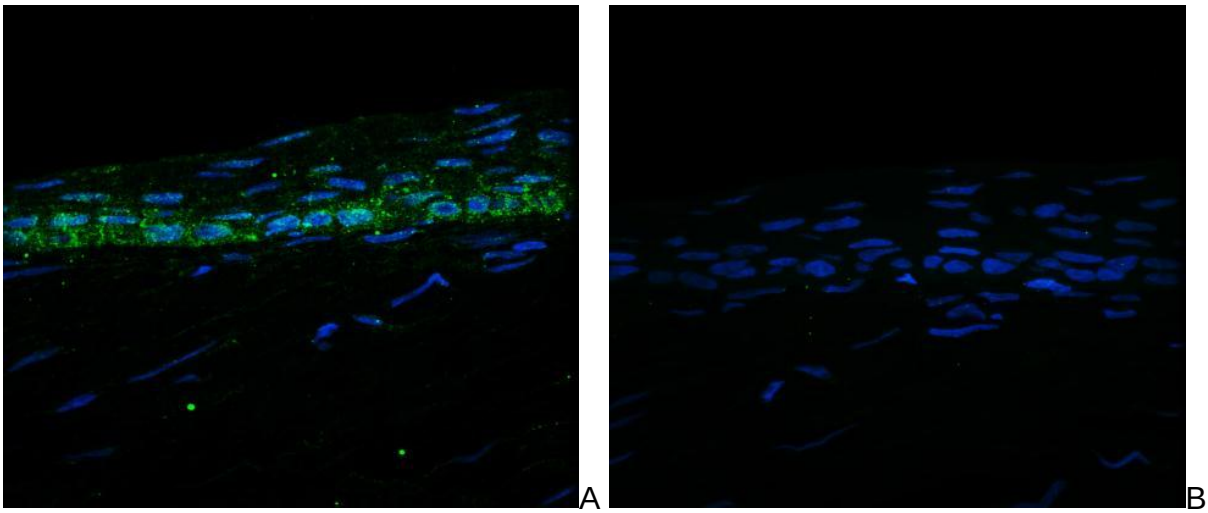

Figure 3-9. Day 10 post wounding at the wound margin. A) CTGF in the wound margin, and B) is a control in which the primary antibody was withheld.

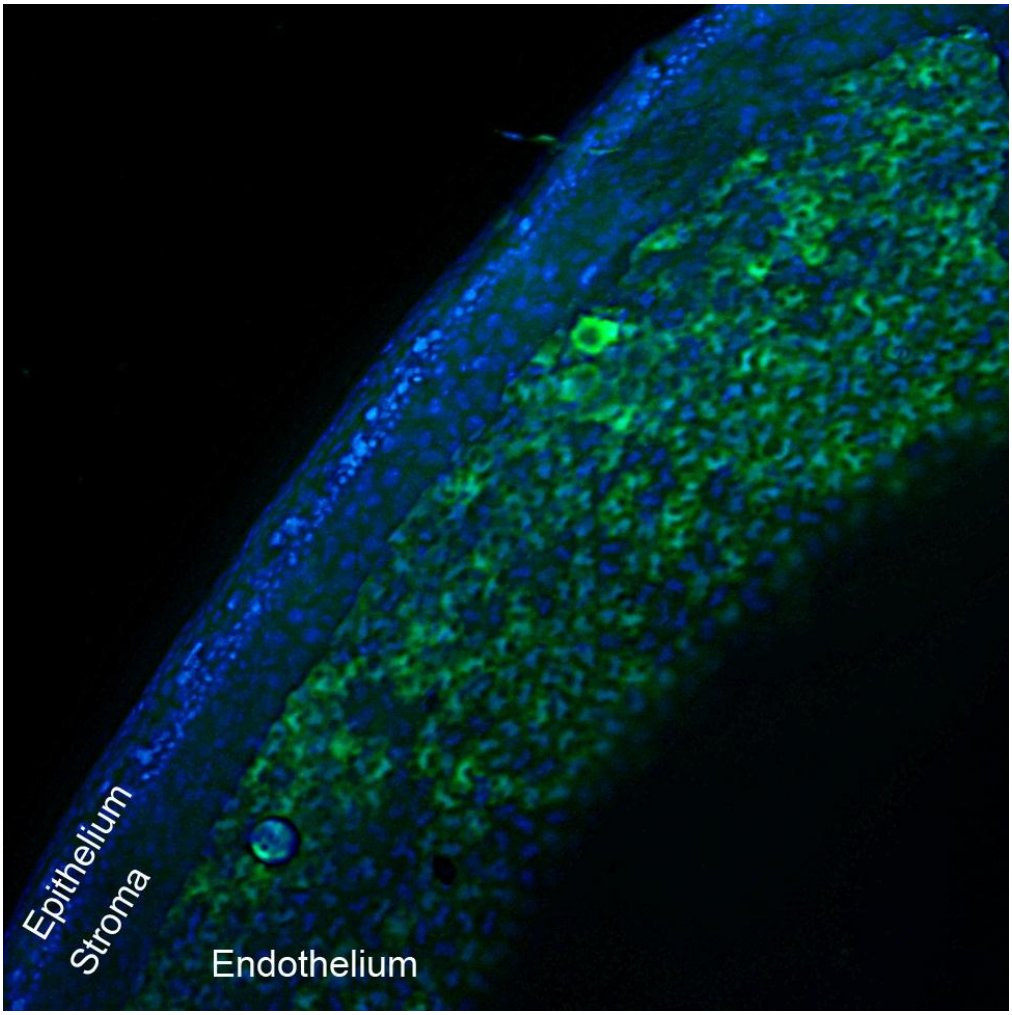

Figure 3-10. CTGF promoter activity in an unwounded mouse cornea. This z-stack merged confocal micrograph is a whole tissue mount of a cut cornea. The epithelium and stroma are visible at the cut face, while the posterior surface of the cornea (endothelium) is visible as viewed *en face*.

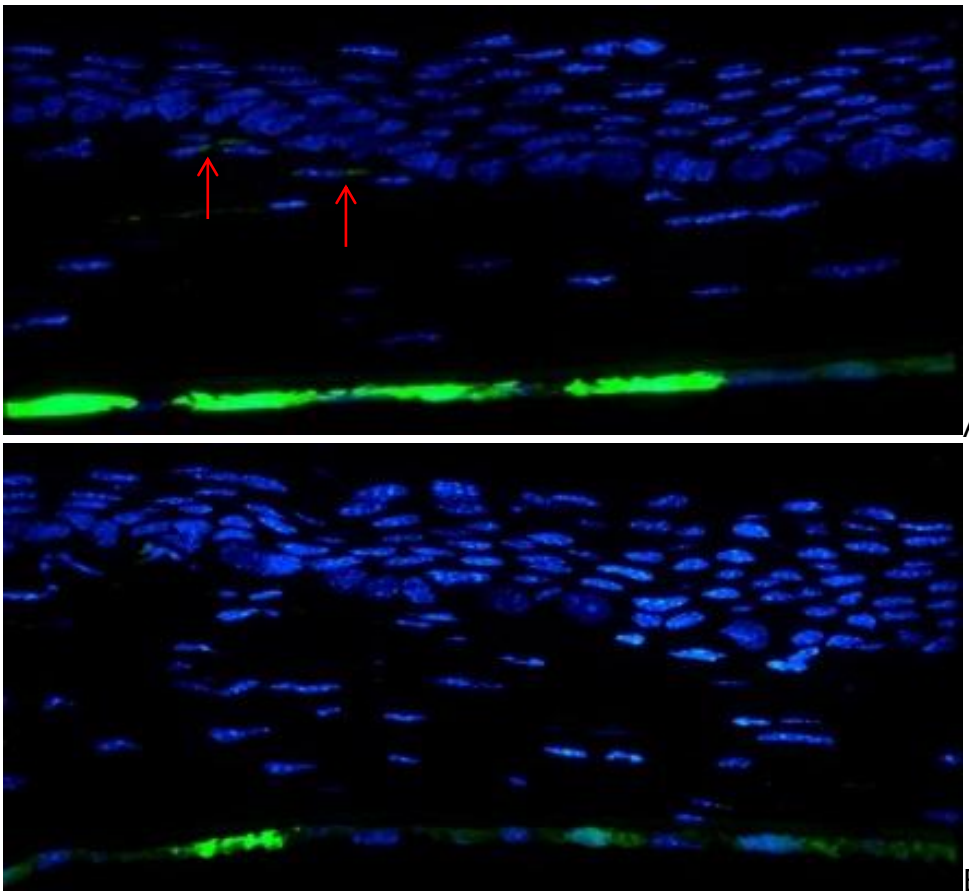

Figure 3-11. The corneal endothelium is the primary location of CTGF promoter activity (green). A) The field that did not receive the primary antibody and B) primary antibody present. A) There is some green fluorescence in the anterior stromal cells (red arrows).

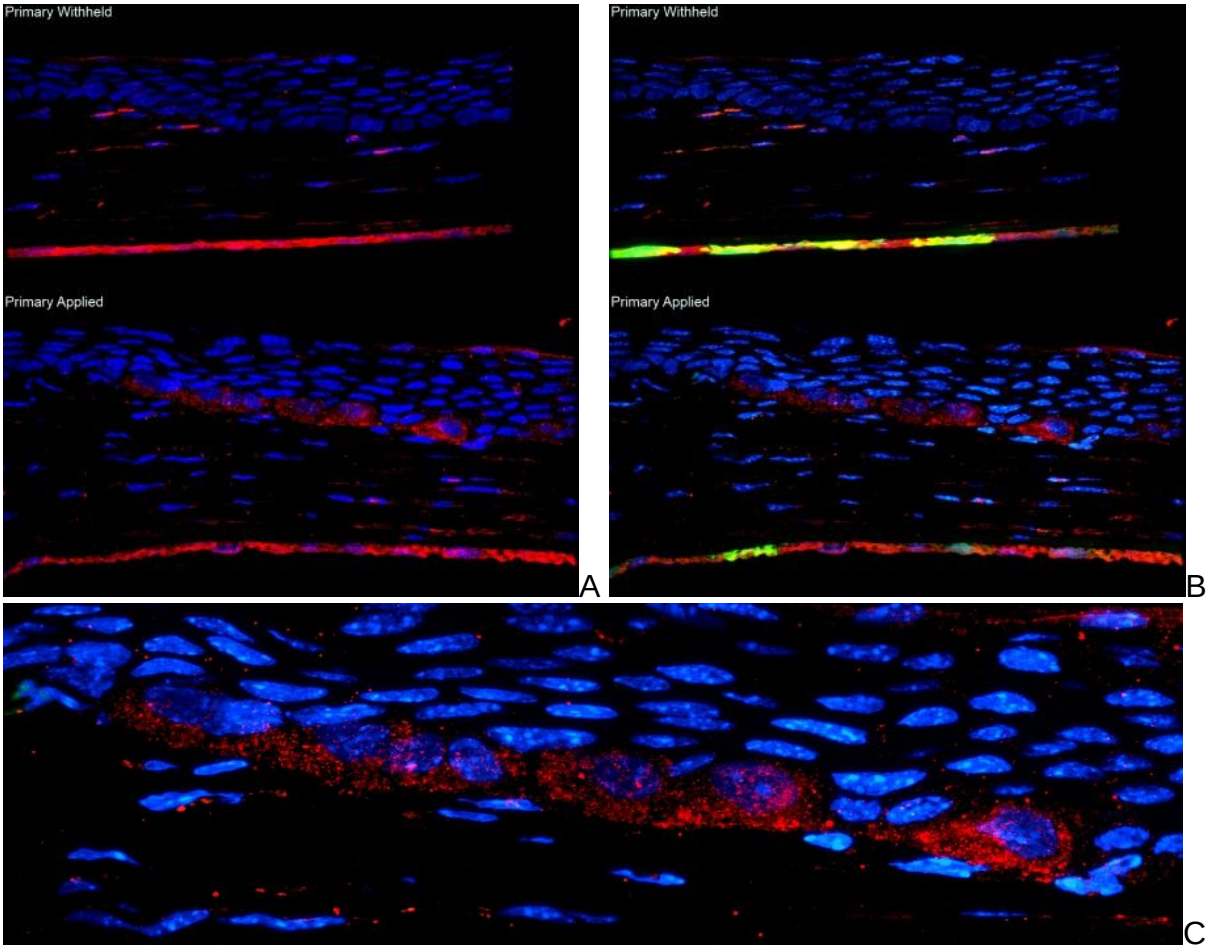

Figure 3-12. The localization of CTGF protein in healing mouse corneas. A) Comparison of the red channel data representing the presence of CTGF (lower panel) or background noise (upper panel). B) The merged layers of promoter activity and protein accumulation. C) Detail of the merged layers at the basal epithelium.

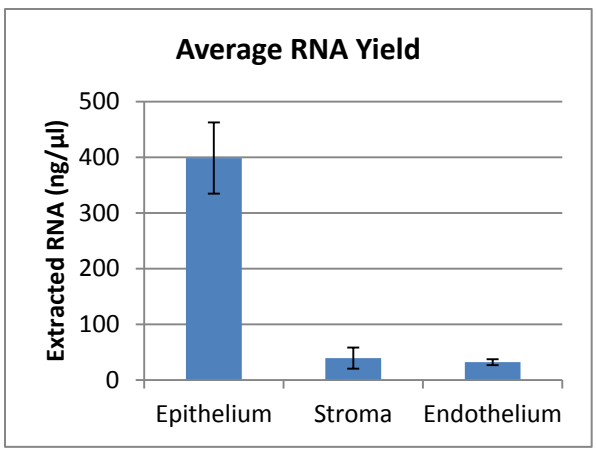

A
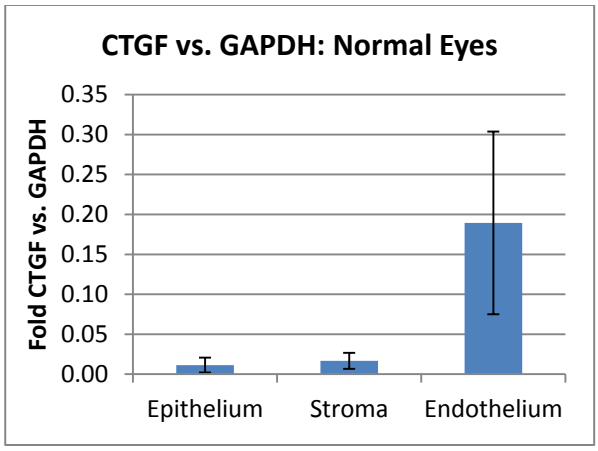

B

Figure 3-13. Comparison of RNA mass yields and CTGF levels from grossly dissected rabbit corneas. Equivalent volume of lysis buffer was used for each layer. A) RNA mass extracted and B) GAPDH normalized CTGF levels in each grossly dissected corneal layer.

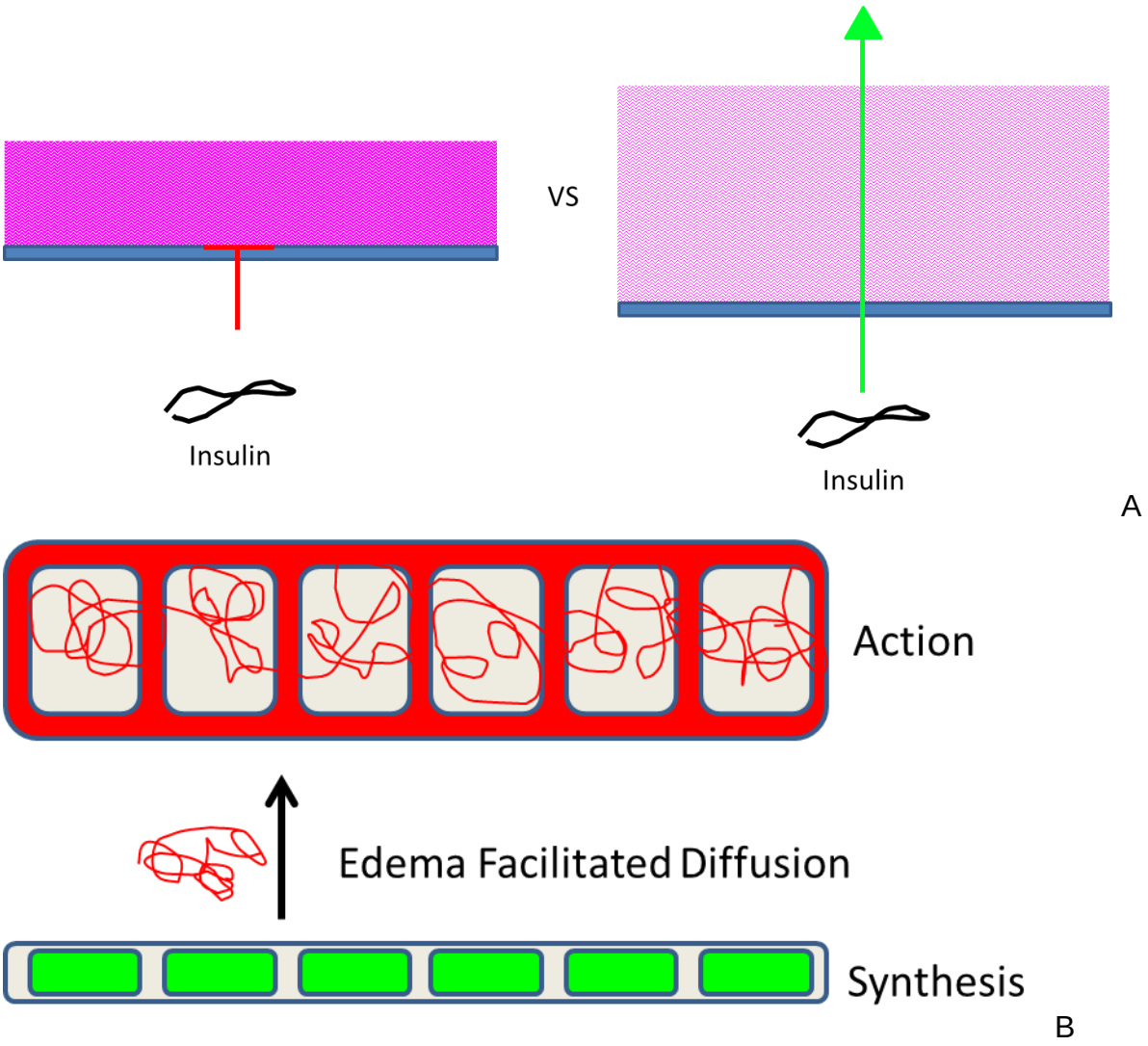

Figure 3-14. A new theory to explain the different loci of CTGF synthesis versus accumulation and action. A) A schematic of the observation that a normal (dehydrated) stroma is a barrier to insulin, but an edematous stroma permits the entry of insulin. B) A new theory which integrates the new findings about CTGF synthesis and localization, its timing with respect to edema, and the observed permissiveness of the edematous stroma.

CHAPTER 4
HAZE FORMATION TIMELINE

Introduction

To date, studies of light scattering haze have focused on the magnitude of haze that forms in mature scars, while there is currently little to no information published about the establishment of haze. Studying the final stable scar can enable one to ascertain what modulates the amount of haze that forms, but it does not provide much insight about the process of haze formation. Because the formation of haze is the therapeutic target, this process deserves greater scrutiny. It is well established that cell migration, proliferation, and differentiation are key processes in the development of haze, but little is known of *when and where* these processes occur. More detailed information about the when and where of haze formation will not only provide insight into the basic science of tissue repair, it will also provide a more refined target for highly targeted therapies.

Materials and Methods

Excimer Wounding

Each rabbit was restrained in a PLAS Lab rabbit restraint and each eye was topically anesthetized using a single drop of tetracaine. Each rabbit was generally anesthetized using inhaled isoflurane and oxygen. Once sedated, the central thickness of the cornea was measured by an ultrasonic pachymeter (n = 5 central measurements per eye). The eye being operated on was proctosed using a pair of cotton swabs. The cornea was then centrally ablated using a Nidek EC-5000 in narrow beam mode PTK with a beam 6.0 mm in diameter to a programmed depth of 125 μm and no transition zone.

Follow Up

Three time points were chosen prior to epithelial closure, while the other three were during the time period of haze formation (5 to 10 days). Prior to euthanasia, the pupil was dilated with topical tropicamide and phenylephrine then the wound was photographed. Two rabbits were euthanized at each time point by injection of Beuthanasia-D into the lateral ear vein while generally anesthetized with inhaled isoflurane and oxygen.

Macrophotography

Corneal haze was documented using a Nikon D40 digital single lens reflex (DSLR) camera was outfitted with a Nikkor AF-D 60 mm macro lens and a Nikon R1C1 Creative Lighting System (CLS) flash system. The camera was set to the “Normal” program, “JPG Fine” image types, ISO 200, manual exposure with a shutter speed of 1/500 second and f/18. For all images, the lens was set to manual focus and pre-focused to a 1:1 reproduction ratio and the camera was focused by moving the camera closer or further from the subject. The built-in guide lights were used to facilitate haze visualization and focusing. Pictures were taken until an image with adequate focus and framing of the wound was achieved and the reflection of the flash heads were not within the wound.

Two SB-R200 remote flash heads were mounted on the front of the lens and were positioned at 12 and 6 o’clock respectively. The flash power was manually set to 1/32nd power for each flash. Each flash was rotated to the most inward facing angle to provide the most oblique lighting possible.

Evaluation of Haze Development

The day-to-day change in haze was observed using macro photographs. The color images were converted to grayscale using Adobe Photoshop CS3 Extended with a custom black and white conversion filter that used only the data in the blue channel of the image followed by an adjustment of the "Curves" such that the portion of the cornea just outside of the wound bed was to be considered "black" and that the flash report was to be considered "white". The grayscale image was overexposed by a consistent amount *in silico* in order to better visualize the detail within the scar. The wound area was selected using a circular selection region with a diameter of 850 pixels and a gradient color map was applied to the selected region (Table 4-1). These pseudocolored images were assembled in a time line sequence and the progression of haze development was followed.

Molecular and Histological Analysis

Following euthanization, each cornea was briefly irrigated with 10% neutral buffered formalin (10% NBF) and then each globe was enucleated. In order to preserve the shape of the cornea, each globe was placed cornea down into a 12-well tissue culture dish well that was filled with 10% NBF for one hour. The cornea was then excised and placed in another well with fresh 10% NBF and was fixed for 4 to 18 hours at 4°C.

Frozen sections

Following fixation, the corneas chosen for cryosectioning were bisected and then cryoprotected in 30% sucrose in PBS overnight at 4°C. The cornea halves were then oriented in OCT and quickly frozen on dry ice. The OCT blocks were stored at -20°C until sectioning. The corneas were sectioned between 10 to 20 μm depending on the

cornea's integrity. The sections were mounted onto poly-L-lysine coated glass slides and then air dried overnight. The sections were stored at -20°C until staining.

Paraffin sections

Corneas chosen for paraffin embedding and sectioning were bisected and then transferred into 70% ethanol and kept at 4°C until submission for processing at the McKnight Brain Institute's Cell and Tissue Analysis Center's Histology Core (MBI-CTAC Histology Core). The corneas were sectioned between 4 to 5 μm depending on the cornea's integrity. The sections were mounted onto poly-L-lysine coated glass slides. One slide per cornea was stained with hematoxylin & eosin (H&E) for gross histological analysis.

Immunohistochemistry

Paraffin sections were de-paraffinized with xylenes and rehydrated though a graded series of ethanol though tap water. Frozen sections were rehydrated with PBS. The rehydrated sections were then rinsed with wash buffer (phosphate buffered saline with 0.05% Tween 20, PBST). The sections were blocked with 10% normal horse serum (NHS) for 30 minutes at room temperature. The blocking solutions were carefully removed from one section group per slide by aspiration and blotting. The primary α-smooth muscle actin (α-SMA) antibody was diluted (1:500) in 1% NHS in PBST and was incubated for 1 hour at room temperature on the one section while the negative control remained in blocking solution. Following this incubation, the slides were washed three times for 5 minutes with wash buffer. The sections were then incubated with a fluoresceinated secondary horse anti-mouse IgG for 30 min at room temperature. Following the final washes, the slides were mounted with DAPI containing medium and the slide cover was fixed in place with nail hardener.

Results

Wound Macrophotography

The first sign of haze was typically present at day 5 post wounding. The first site of haze formation was invariably a ring shaped region of haze at the wound margin. At the same time, there was usually, but not always, a spot of haze in the body of the wound, but its shape and location varied wound to wound. Once initiated, the haze spread from the loci and intensified with time (Figures 4-1A&B).

Immunohistochemistry

The presence of α-SMA was co-incident with the beginning of haze formation. The localization of α-SMA within the tissue also mirrored the initiation and spread of haze (Figure 4-2A,C,&E); beginning with a distinct region at the wound margin (Figure 4-2B), and spreading laterally (Figure 4-2D&F) with time. Also, the intensification of haze was mirrored by an increase in the number of α-SMA positive lamellae (Figure 4-2D&F) with time. Unexpectedly, α-SMA was present in significant quantities in the basal epithelium (Figure 4-3), but its intracellular distribution was significantly different (diffuse) from that of the distribution in the stromal cells (sharp, fibrous).

Discussion

There appear to be two distinct regions of haze initiation (Figure 4-4). The formation of a ring of haze at the wound margin was invariant, while both the formation of islands of haze in the body of the wound, and the location of these islands, varied. Once initiated, the haze appears to first spread laterally and secondly to become more intense with time. The distribution of α-smooth muscle actin, a putative marker of light reflecting cells, mirrored the spread and intensification of haze with an increase of cells along stromal lamellae increasing with time (spread) and the number of affected

lamellae increasing as well (density/intensity). These observations are the first to describe when and where haze first begins to form, and to describe how it covers the rest of the wound region by “radiating” from these distinct regions of nucleation.

The formation of haze occurs only after re-epithelialization and the spread of haze from the wound margin is a pattern similar to the migrating epithelial front. While the presence of α-SMA staining in the epithelium was not expected, it was fairly consistent and has been seen in cell cultures with the key difference being how the α-SMA is distributed. Following TGF-β stimulation, both epithelial cells and fibroblasts will synthesize α-SMA, but the α-SMA will be arranged in fiber-like structures in the fibroblasts while it remains globular and diffuse in the epithelial cells[111]. The presence of CTGF on the surface of basal epithelial cells (Figure 3-7A), and α-SMA present inside the basal epithelial cells (Figure 4-3) supports a new hypothesis that the epithelium may have a more central role in the formation of haze following acute injury to the cornea. The observations reported here all served as a “tipping point”, which gave rise to the final project presented in the next chapter.

.

Table 4-1. Color map used in Photoshop to generate the pseudocolored images.

Color	% Full Scale
Black	2%
Blue	5%
Green	8%
Yellow	11%
Orange	14%
Red	17%
Magenta	20%
White	22%

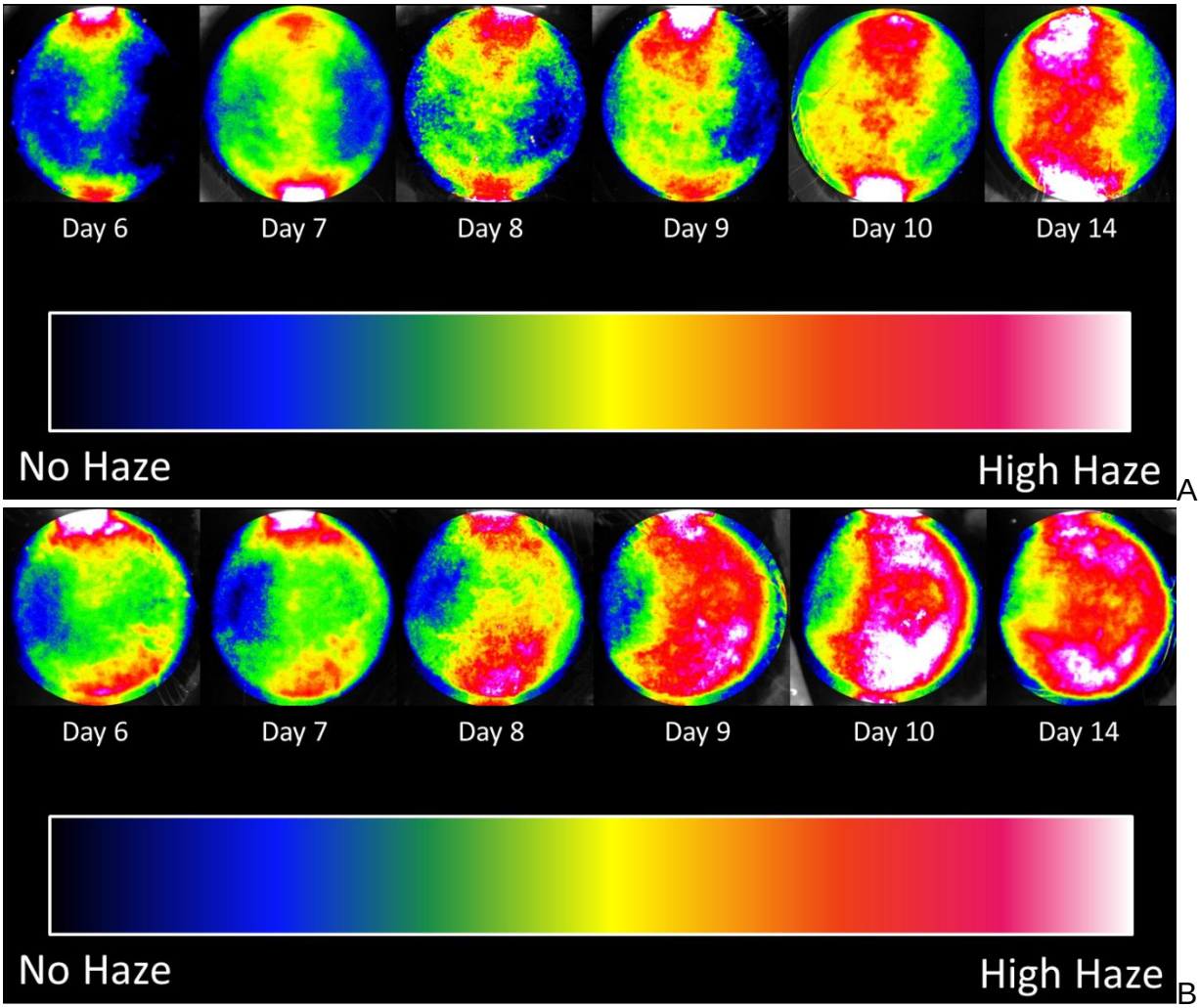

Figure 4-1. Pseudocolored images of day-to-day haze formation.

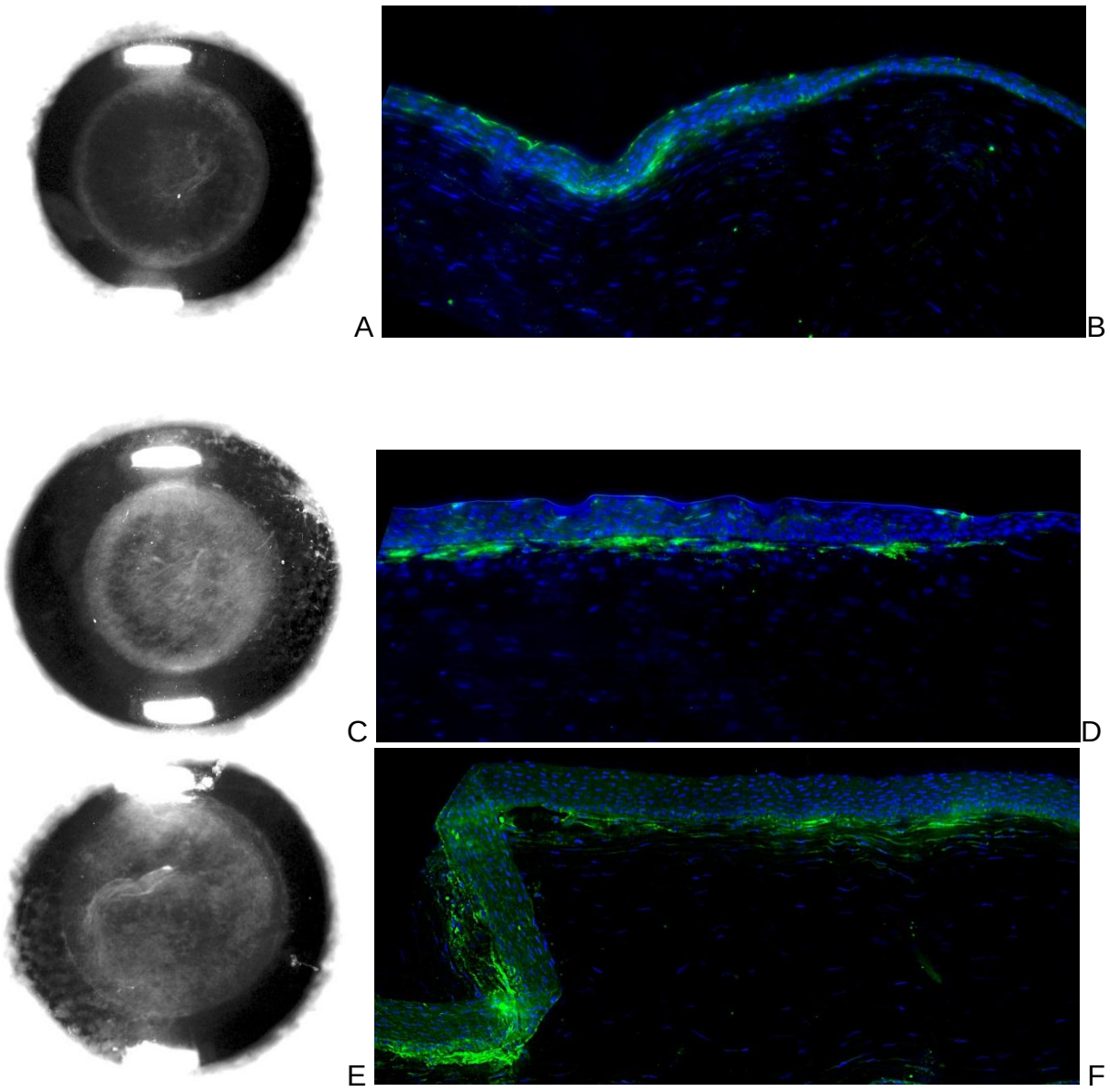

Figure 4-2. Haze and α-SMA localization. A,C,E) are macrophotographs of the healing cornea and B,D,F) are micrographs of α-SMA localization. A&B) Day 5 post, C&D) day 7 post, and E&F) day 10 post.

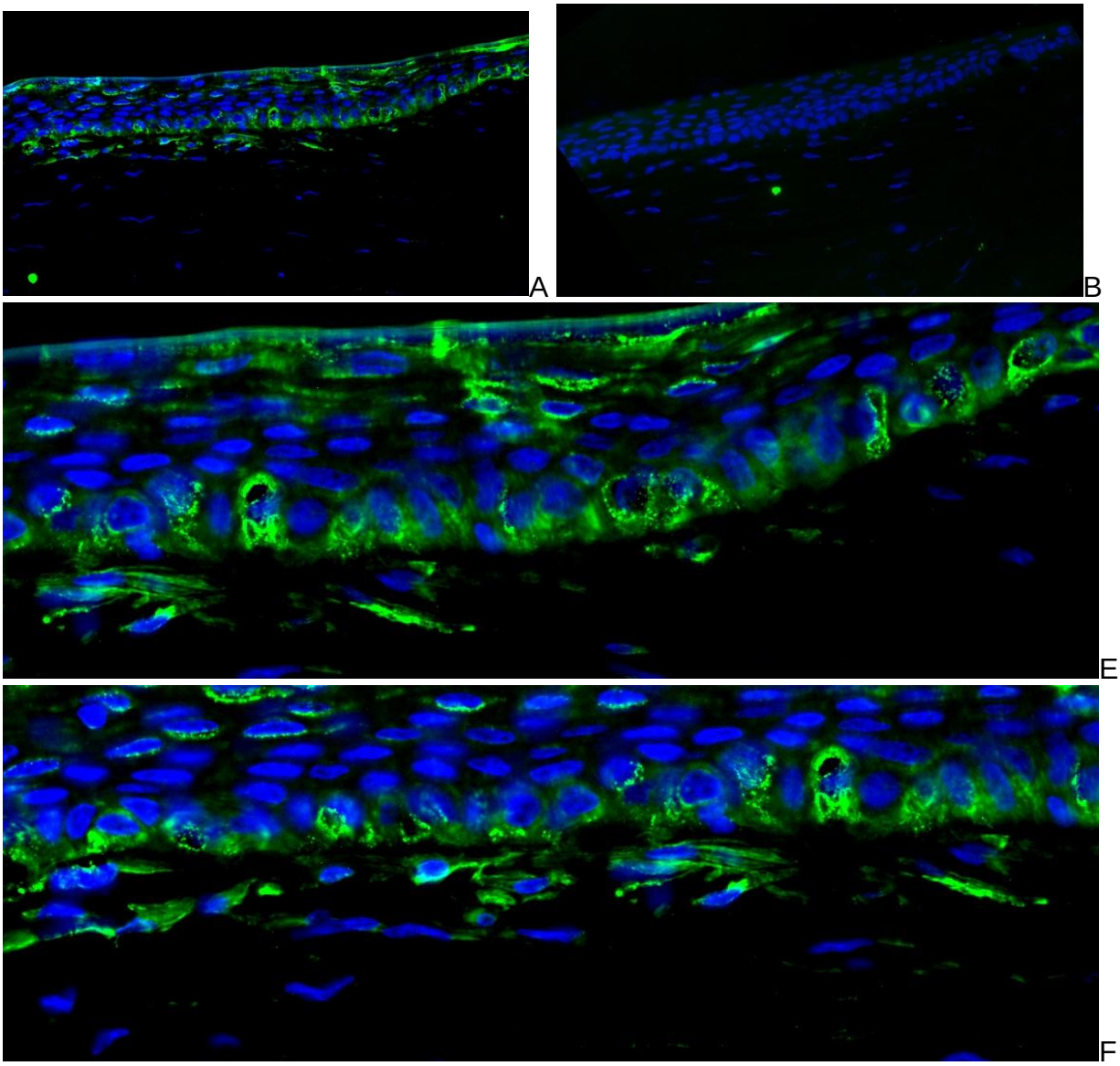

Figure 4-3. Higher power micrograph of the day 5 wound. A) original micrograph and B) the primary antibody withheld control. E&F) are zoomed in regions of A) to better show the detail of the staining in the epithelium and stroma.

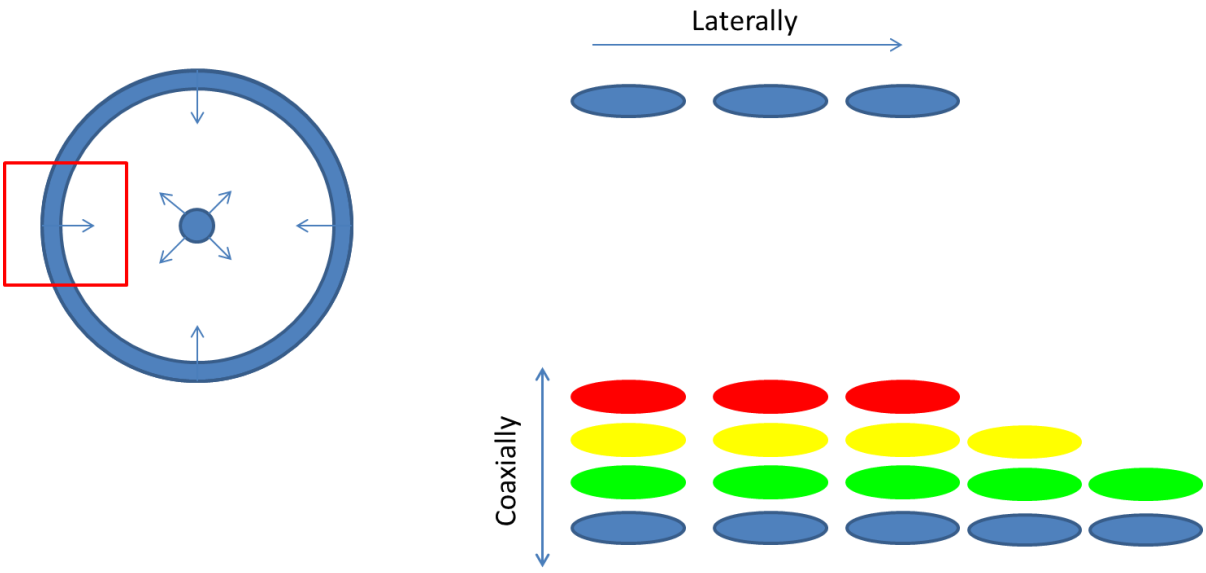

Figure 4-4. A schematic of where haze begins, how it spreads, and how it becomes more dense. The colors used to represent the coaxial spread of haze are related to the intensification as represented in the pseudocolored images in Figure 4-1 while the layering is related to the build-up of α-SMA positive cell layers seen in Figure 4-2F.

CHAPTER 5
THE EMERGENCE OF A NEW THEORY FOR HAZE FIBROGENESIS

Introduction

To date, it is believed that the fibroblasts underlying the wound are the source of light reflecting cells that comprise corneal haze based scars. The observations presented in the preceding chapters cast doubt on this theory of haze fibrogenesis. The observed timing and localization of CTGF synthesis and accumulation severely undercut the hypothesis that the underlying fibroblasts were the site of CTGF activity. The emergence of haze at two distinct regions of the cornea following acute injury is difficult to reconcile with the idea that the underlying fibroblasts migrate by spiraling up. How can this theory explain the gap between the haze encircling the wound at the wound margin and the variable “island” of haze in the center of the wound? In addition to the new data reported here, other information adds to cast further doubt on the current theory. First, it is generally known in the field of ophthalmology that the cells in the epithelium are the first cells to come into contact with the surface of the unwounded stroma as they migrate to cover the wound within the first few of days following acute injury. By day 5 following wounding in rabbit corneas, the wound volume is filled with dark eosin staining epithelial cells. However, over the next 9 days, the wound volume becomes filled with a light eosin staining, collagenous matrix which is filled with fibroblastic cells. This first became apparent when examining gross histological sections of mature scars where the shape of the scar tissue, and the staining for α-smooth muscle actin, were both precisely the shape of the excimer laser wound (Figure 5-1A&B). This same pattern was repeated in the worst wound scar observed during the experiments reported herein (Figure 5-1C&D). While these observations were

independently discovered, a search of the literature found that the next, more conclusive, experiment had already been done[33]. Tuft and others covalently labeled the unwounded stroma with a fluorescent dye and found that "[the non-fluorescently labeled fibrotic mass] first appeared in the periphery of wounds after reepithelialization, and had usually extended over the entire wound bed between the 7th and 14th postoperative days", demonstrating that the location once occupied by the epithelium had be replaced by new stromal scar tissue. In addition to validating the observation that the fibrotic mass fills the wound volume, the pattern of tissue deposition reported mirrors the onset and spread of haze reported in the previous chapter. Given these facts, the following conundrum arises: "What happens to the epithelial cells that are the first cells in contact with the unwounded stroma?" The conundrum can be conceptualized in two separate ways, in terms of the cells present ("Where do the epithelial cells go?", Figure 5-2), or in crude terms of the major structural proteins present ("Where do the keratins go?", Figure 5-3).

Given the observed timeline and location of haze emergence, and the localization of the key effectors of haze formation, two new hypotheses emerge. The first is centered on the fact that the epithelium is the first cell layer to come into contact with the unwounded stroma, and that it is the first cell layer to fill the wound volume. During the time period of prior to and during haze formation, CTGF is predominantly localized to the basal epithelium, and α-SMA is present there as well. These observations led to the hypothesis that these epithelial cells transdifferentiate in place into mesenchymal-like cells to form the new scarred stroma. The second hypothesis is that while the epithelium is the first on the scene, cells from the peripheral stroma can migrate in

between the epithelium and unwounded stroma in a manner reminiscent of the *de novo* formation of the stroma during embryonic development[112,113] (Figure 5-4). Briefly, the cornea begins as a bilayer with cells from two different sources, one of which gives rise to the epithelium, the other the endothelium. Cells from the neural crest then migrate from the periphery and split the bilayer, effectively *displacing* the epithelial layer from the endothelium. Interestingly, the epithelium also begins stratifying in this same period; a process which is also present during corneal wound healing just prior to scar formation. It is important to note, that these might not be mutually exclusive mechanisms. Cell tracing experiments in the scarring of internal organs found that cells from multiple sources were present in the scar[114,115]. In order to elucidate which cells are ultimately responsible for forming the light reflecting scar, an epithelial cell tracing experiment was conducted. Concurrently, a series of experiments using excimer wounded rabbit eyes sought out evidence of grossly observable cellular interchange in between the epithelium and stroma (or vice-a-versa), and the presence of tenascin-C during haze formation since it has been proposed to be a marker for the epithelial-to-mesenchymal transition[116] (EMT).

Materials and Methods

Cell Tracing Experiment Reporter Mice

In order to test whether the epithelium contribute cells to the final scar, a genetically labeled reporter mouse model was used. The reporter mice employ the Cre-recombinase system[117] to de-inhibit a β-galactosidase reporter enzyme[118]. Briefly, these mice have two transgenes, one of which is a β-galactosidase gene (LacZ) which ultimately will provide the “signal”, the other is Cre-recombinase which provides the cell layer specificity. The LacZ gene possess a premature translation “stop” codon which

prevents the reporter enzyme from being translated. The stop codon is flanked on either side by a *cis* acting sequence (loxp) which serves to mark the stop condon for Cre-mediated removal by DNA recombination (Figure 5-5A). For this project, the Cre-recombinase is under the transcriptional control of the PAX6 promoter (Figure 5-5B). This promoter is active in various tissues in the eye, but in the cornea it is solely active in the corneal epithelium[119]. In the corneas of the reporter mice, cells derived from the epithelium will possess β-galactosidase activity, while cells from the stroma will not.

The pups were genotyped and marked by ear punch prior to weaning (postnatal day 21). Tail biopsies were collected with sharp, bead-sterilized, surgical scissors. Silver nitrate was applied to the cut tail for hemostasis. Genomic DNA was isolated from the tail biopsies using a Sigma REDExtract-N-Amp kit. The primers listed in Table 5-1 were used to detect the presence of both necessary transgenes. The polymerase chain reaction (PCR) reactions were always run with a negative control comprised solely of 20ul of master mix. The PCR amplified samples were resolved on a 1.5% agarose gel with 100 base pair ladder. The β-galactosidase transgene has a 220 base pair amplicon, while the PAX6-Cre has a 270 base pair amplicon.

Excimer Laser Wounding

Slides from rabbit samples generated for the CTGF localization experiment described in Chapter 3 were used for the H&E analysis, while slides from the previous chapter on haze formation were used to measure tenascin-C for use in this chapter. No further rabbits were needed for this experiments described in this chapter. Mice were placed in a sealed box and anesthetized with 3.5% isoflurane/oxygen. Once a mouse was anesthetized, it was removed from the box and placed straddling a 50 ml conical tube and held in place with a semi-adhesive elastic band gently wrapped around both

the mouse and tube. The tube was outfitted with a nose cone-fed supply of isoflurane/oxygen. The mouse was laid on its side and supported by a stack of cotton gauze. The eye to be wounded received a drop of proparacain. The whiskers were cut with scissors and the eye lid and lashes were gently pushed out of the way with a cotton swab. The mouse was then oriented beneath the excimer laser. A 1.0 mm diameter by 24 μm deep PTK excimer wound was created. The mouse was periodically observed in the following weeks to determine whether and to what extent the wound scarred.

Reporter Mouse Tissue Harvesting, Processing, and Sectioning

At the terminal time point, the mice were anesthetized as before and euthanized by cervical dislocation. Each globe was immediately enucleated via blunt dissection with fine-tipped forceps and placed in fresh 10% neutral buffered formalin on ice. The globes were punctured with a 25 gauge needle after 30 min to improve fixative penetration. The globes were intentionally under-fixed for 1 hour at 4°C to preserve the enzymatic activity of the β-galactosidase reporter. The globes were then placed in 30% sucrose in PBS overnight at 4°C to cryoprotect the tissue. In order to improve cryosectioning, each globe was grossly prepared by cutting open the posterior retina, removing the lens, and injecting embedding medium (OCT) into the globe with a blunt-tipped needle and syringe. The tissue was then submerged in OCT and rapidly frozen. The frozen blocks were stored at -20°C until cryosectioning. Ten micron section were cut and mounted on poly-**L**-lysine coated slides. The slides were air-dried and then stored at -20°C until staining.

β-Galactosidase Detection

The sections were rehydrated and washed in PBS 3 times in PBS. The slides were then incubated in 5-bromo-4-chloro-3-indolyl-beta-D-galactopyranoside (XGal)

staining solution (2 mM $MgCl_2$ (Sigma), 5 mM $K_4(CN)_6$-$3H_2O$ (Sigma), 5 mM $K_3(CN)_6$ (Sigma), 1 mg/ml XGal (Promega), in PBS pH 7.4) at 37°C in a humidified chamber overnight. The slides were then washed 3 times with PBS, counter stained with nuclear fast red (Vector Labs, CA). The sections were dehydrated and permanently mounted with Permount (Fisher Scientific). The slides were imaged with a light microscope and mounted Nikon D7000 dSLR.

Molecular and Histological Analysis

Following euthanization, each cornea was briefly irrigated with 10% neutral buffered formalin (10% NBF) and then each globe was enucleated. In order to preserve the shape of the cornea, each globe was placed cornea down into a 12-well tissue culture dish well that was filled with 10% NBF for one hour. The cornea was then excised and placed in another well with fresh 10% NBF and was fixed for 4 to 18 hours at 4°C.

Frozen sections

Following fixation, the corneas chosen for cryosectioning were bisected and then cryoprotected in 30% sucrose in PBS overnight at 4°C. The cornea halves were then oriented in OCT and quickly frozen on dry ice. The OCT blocks were stored at -20°C until sectioning. The corneas were sectioned between 10 to 20 μm depending on the cornea's integrity. The sections were mounted onto poly-L-lysine coated glass slides and then air dried overnight. The sections were stored at -20°C until staining.

Paraffin sections

Corneas chosen for paraffin embedding and sectioning were bisected and then transferred into 70% ethanol and kept at 4°C until submission for processing at the McKnight Brain Institute's Cell and Tissue Analysis Center's Histology Core (MBI-CTAC

Histology Core). The corneas were sectioned between 4 to 5 μm depending on the cornea's integrity. The sections were mounted onto poly-L-lysine coated glass slides. One slide per cornea was stained with hematoxylin & eosin (H&E) for gross histological analysis.

Immunohistochemistry

Paraffin sections were de-paraffinized with xylenes and rehydrated though a graded series of ethanol though tap water. Frozen sections were rehydrated with PBS. The rehydrated sections were then rinsed with wash buffer (phosphate buffered saline with 0.05% Tween 20, PBST). The sections were blocked with 10% normal horse serum (NHS) for 30 minutes at room temperature. The blocking solutions were carefully removed from one section group per slide by aspiration and blotting. The tissue was then blocked for endogenous avidin and biotin. The slides were then washed three times for 5 times with wash buffer. The primary tenascin-C (TNC) antibody was diluted (1:500) in 1% NHS in PBST and was incubated for 1 hour at room temperature on the one section while the negative control remained in blocking solution. Following this incubation, the slides were washed three times for 5 minutes with wash buffer. The sections were then incubated with a biotinylated secondary horse anti-mouse antibody for 30 min at room temperature. The sections were then washed 3 times for 5 minutes with wash buffer. Finally, the sections were incubated with avidin-Texas Red (25 μg/ml, Vector Labs) for 10 min. The samples were then washed 3 times for 5 minutes each. The slides were mounted with DAPI containing medium and the coverslips sealed with nail hardener. The slides were kept refrigerated in the dark until imaged.

Results

Corneal Wounding

The reporter mice appear to have thinner and/or weaker than normal corneas since 3 out of 4 eyes burst during laser wounding with wounds less than 30 μm deep. The one eye that didn't burst was ablated only 24 μm deep. A visible opacification was present in this one cornea by day 7 (Figure 5-6). Even though the scar appeared to be mature by day 7, the eyes were not harvested until day 32 to ensure that a mature scar had formed.

Cell Tracing

Overall the fixation was insufficient for good tissue integrity, and it did not quench the transgenic β-galactosidase activity in the epithelium (Figure 5-7A). Only one region in the wound possessed a strong positive signal, and upon closer inspection the β-galactosidase positive region appears to be two cells in close juxtaposition (Figure 5-7B). The majority of the cells in the wound surrounding the two positive cells are β-galactosidase negative, Nuclear Fast Red positive, cells indicating that they were not epithelial-derived cells.

Gross Histology

Within 24 hours following wounding, there is evidence of a significant number of neutrophils and epithelial invasion of incompletely ablated stromal lamellae (Figure 5-8A&B). One day later, there is evidence of continued migration of epithelial cells between stromal lamellae, and evidence of additional regions of stromal invasion (Figure 5-8C). On day 4 post-wounding, one eye had evidence of the epithelium effectively "bulldozing" several stromal lamellae and creating a stromal-mass inclusion within the central epithelium (Figure 5-8D). Three days after wounding, the basal

epithelium is mostly intact with evidence of peripheral stromal cells migrating towards the wound margin and possibly proliferating there as well (Figure 5-9). While the epithelium in the day 3 sample was mostly intact, there is a single blister-like structure which appears to be surrounded by nuclear staining. By day 5, the blister-like structures have become significantly more numerous and are at this time point the predominant feature at the wound interface (Figure 5-10).

Immunohistochemistry

At day 5 following wounding, tenascin-C was present in a distinct region within the wound margin and appears to be limited to a single layer of stromal cells (Figure 5-11A). Two days later, tenascin-C staining had spread towards the center of the wound and now appears to cover two layers of stromal cells (Figure 5-11C). By day 10, tenascin-C staining is present throughout the wound and encompasses about 4 to 5 cells layers in the stroma (Figure 5-11E). The initiation and spread of tenascin-C mirrors the spread of haze as was seen earlier (Figures 5-11B, D, & F).

Discussion

The data provided by the cell tracing experiment does not support the hypothesis that the newly synthesized stromal tissue is derived from the epithelium. But, the combination of the cell tracing experiment and the gross histology indicate that epithelial cells can penetrate into the stroma, adopt a low fibroblastic profile, and remain embedded in the stroma up to 32 days after wounding. A study conducted on post-mortem corneas from individuals who had undergone laser-assisted in-situ keratomileusis (LASIK) at various times prior to death, found that portions of the reflective scars in the center of the LASIK-treated corneas were “implanted” epithelial cells in various states of necrosis[23]. In LASIK, a microkeratome or laser is used to

make an incomplete cut along the stromal lamellae with a hinge-like portion left in place which keeps the tissue “flap” attached to the cornea. The laser is then used to reshape the exposed stroma, and the “flap” is then laid back down on the ablated surface. If the “flap” does not align correctly, or it does not re-adhere well, the cut provides an easy conduit for epithelial cells to migrate into the stroma. With the laser surgery techniques which ablate directly through the epithelium, such as phototherapeutic (PTK) and photorefractive (PRK) keratectomies, there isn’t an immediately obvious avenue for invasion into the stroma. However, examination of a cornea one day after PTK surgery (Figure 5-12A) presents a potential mechanism. The migrating epithelial front is clearly visible (white arrows) as is the presence of a proteinaceous slough (green arrows). While lasers might make highly reproducible wounds, the cut cannot account for the heterogeneity of the interwoven structure of the stroma; even a very clean cut will have residual “tags” of incompletely removed stromal lamellae. If the migrating epithelial front migrates into one of these disrupted stromal lamellae at a certain angle, the stromal lamellae will direct the migrating epithelial cells into the stroma Figure 5-12B. While epithelial cells do enter and remain in the stroma and become light reflecting entities[23], the total area covered by the sole β-galactosidase positive cluster observed in the reporter mouse (Figure 5-7B) cannot account for the entire area of opacity that was observed (Figure 5-6C).

The first hypothesis proposed a mechanism which entailed epithelial cells turning into myofibroblasts via epithelial-to-mesenchymal transition (EMT). Connective tissue growth factor α-smooth muscle actin, and tenascin-C were all present within the scarring corneas, and they have been implicated as either effectors (CTGF) or markers

of EMT[116,120,121]. But the facts presented herein, especially the cell tracing experiment, indicate that the preponderance of cells in the scarring tissue come from the stroma, not the epithelium. The key problem with the use of these "markers" is they are, by and large, the result from studies in systems where EMT is known to occur due to the complete lack of fibroblasts (such as the lens), or where there is a paucity of fibroblasts (like the heart and brain). In effect, these proteins are markers *within a highly specific context*, they are not *universal*. What does appear to be the case given the evidence presented here is that these proteins are markers of wound healing and that in tissues without fibroblasts, epithelial cells can provide the wound healing activities and factors represented by these markers. Within the EMT literature, there are some who are backing away from protein markers of EMT and from the premise that epithelial cells are turning into fibroblasts[111]. Instead, the emerging idea is that epithelial cells which take on mesenchymal-like characteristics, such as loss of tight cell-cell contact, flattening of the cellular profile, and migration and/or invasion into surrounding tissue, have effectively undergone EMT. On this basis, the invasion and implantation of epithelial cells into the stroma demonstrated here would classify as EMT. Overall, this shift in EMT paradigm appears to be a mere re-labeling of metastasis, and calls into question whether EMT as a separate research focus has any merit. Without question, understanding the process and mechanisms of invasive epithelial cells is important for understanding diseases (particularly in cancer), but to generate a new, redundant, concept just serves to dilute the attention of those studying these processes.

The evidence presented in this chapter greatly supports a mechanism of scar formation which is very similar to the *de novo* formation of the stroma during

development. In the days preceding the emergence of the first signs of visible haze, stromal fibroblasts are concentrated along the stromal lamellae at the wound margin. Concurrent with the first appearance of haze, the basal epithelium begins losing contact with the unwounded surface of the stroma by a mechanism which most closely resembles blistering. These two observations provide two additional hypothetical targets for anti-fibrotic therapy in the cornea. Given that the fibroblasts are migrating to the epithelial-stromal interface, there is likely a chemotactic molecule being secreted by the basal epithelium. Identification and neutralization of the chemotactic factor(s) would prevent the fibroblasts from being "beckoned" to migrate into the wound and would thereby prevent the haze cells from ever arising. Alternatively, a therapeutic strategy which prevents the epithelium from "blistering-off" would enable the clear epithelium to remain in place, thus preventing the opaque myofibroblasts from migrating into and accumulating in the wound.

Going back to consider the structural protein-based conceptualization of the wound healing conundrum, there is a hypothetical proteinase activity responsible for remove the "keratinous" plug from the wound volume which could possibly give rise to the observed blister-like structures. Interestingly enough, this concept is the proverbial "other side of the coin" for the haze formation hypothesis that preceded the current cellular theory of haze formation. The initial theory was that the immature collagen bundles were the source of haze and that preventing the synthesis of collagen was the key to preventing haze. In order for there to be room for the collagen producing cells to enter into the wound region, the "keratinous" material must first be removed. Given its temporal precedence, one would expect that inhibiting the removal of keratins would

also prevent the accumulation of collagen, but not vice-a-versa; making the hypothetical keratinolytic activities a better therapeutic target than those giving rise to collagen synthesis.

All together, the data support a mechanism of scar formation that is similar to the process by which the corneal stroma is first generated. A new model which integrates all of the evidence presented herein is presented in Figure 5-13. Following a transepithelial stroma penetrating wound (Figure 5-13A), the epithelial cells migrate into the wound volume covering the stromal surface (Figure 5-13B). A portion of the migrating epithelial front occasionally migrates into the stroma along incompletely removed stromal lamellae (Figure 5-13C). The basal epithelium where CTGF was predominantly found, appears to be the destination for stroma-derived cells migrating from the periphery of the wound (Figure 5-13D). Around the time that the stroma-derived cells arrive at the basal epithelium, a blister-like process displaces the epithelium from the wound surface thereby making room for the stroma-derived cells to populate the wound interface and subsequently form the light reflecting scar (Figure 5-13E). With time, these cells proliferate into multiple layers and form a scar which can fill the entire wound void (Figure 5-13F).

With this new model in hand, one issue is still not clear. If the process is similar to *de novo* stromagenesis, then why are the cells opaque? Clearly, these cells share a common lineage, but something either happens to them in the time following development, or as was seen in the fetal fibrosis experiments, a factor is present in the adult tissue which causes them to change their phenotype. Work to identify the key difference(s) between the neural crest cells in development and the resident fibroblasts

in adult tissues, and between the factors present during stromagenesis versus fibrosis must be identified if a truly regenerative response is to ever be obtained.

Table 5-1. Primers for the mice with genetically labeled corneal epithelium

Name	Sequence
R26R-F	5'-TTT CCA CAG CTC GCG GTT GAG GAC-3'
R26R-R	5'-CTA AAG CGC ATG CTC CAG ACT GCC-3'
Cre-F	5'-GCC GTA AAT CAA TCG ATG AGT-3'
Cre-R	5'-TGA CGG TGG GAG AAT GTT AAT-3’

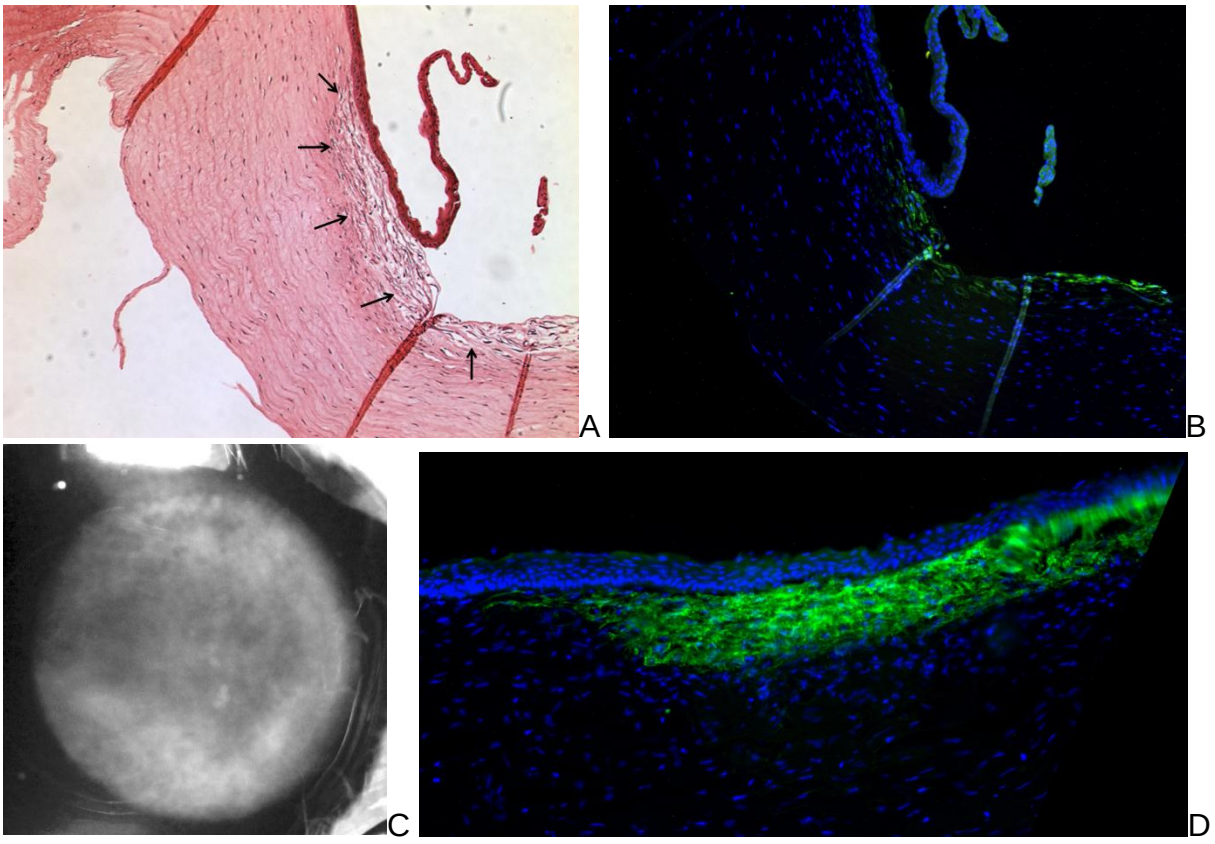

Figure 5-1. Evidence that the scar is formed in *de novo* synthesized tissue. A) & B) Gross histology and immunofluorescent staining for α-SMA, respectively, in a day 28 post-wounding scar. The arrows indicate the border between scar and non-wounded tissue, not that the scar is in the shape of the wound volume. C) & D) A photograph and immunofluorescent staining for α-SMA, respectively, in a day 14 wound. It is the worst scar observed in this project to date. Note also, that the α-SMA staining is within the sharply delimited wound boundaries.

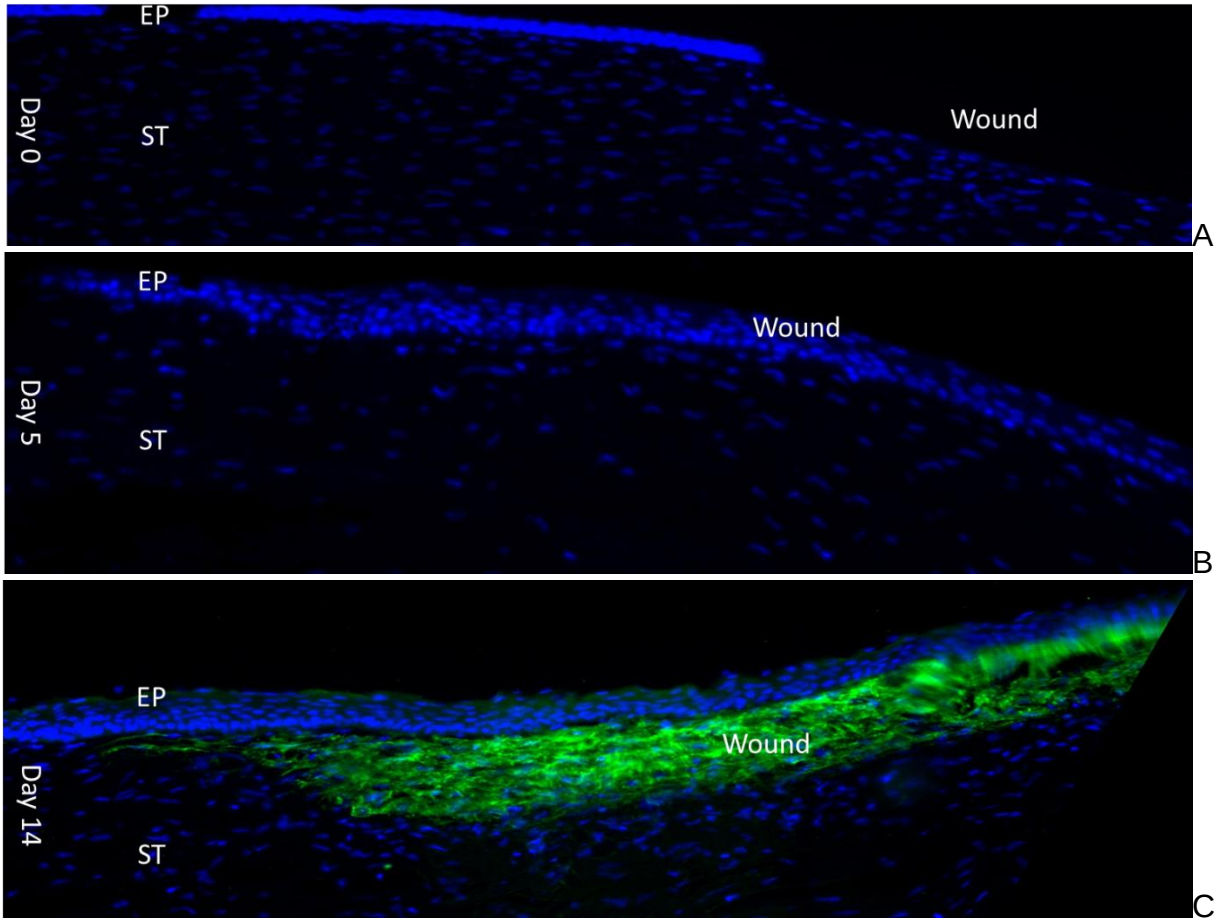

Figure 5-2. The cellular representation of the haze generation conundrum. A) The initial wound viewed at the wound margin. B) By day 5, the wound is filled with epithelial cells. C) But, by day 14 the epithelial cells have been replaced or displaced by myofibroblasts.

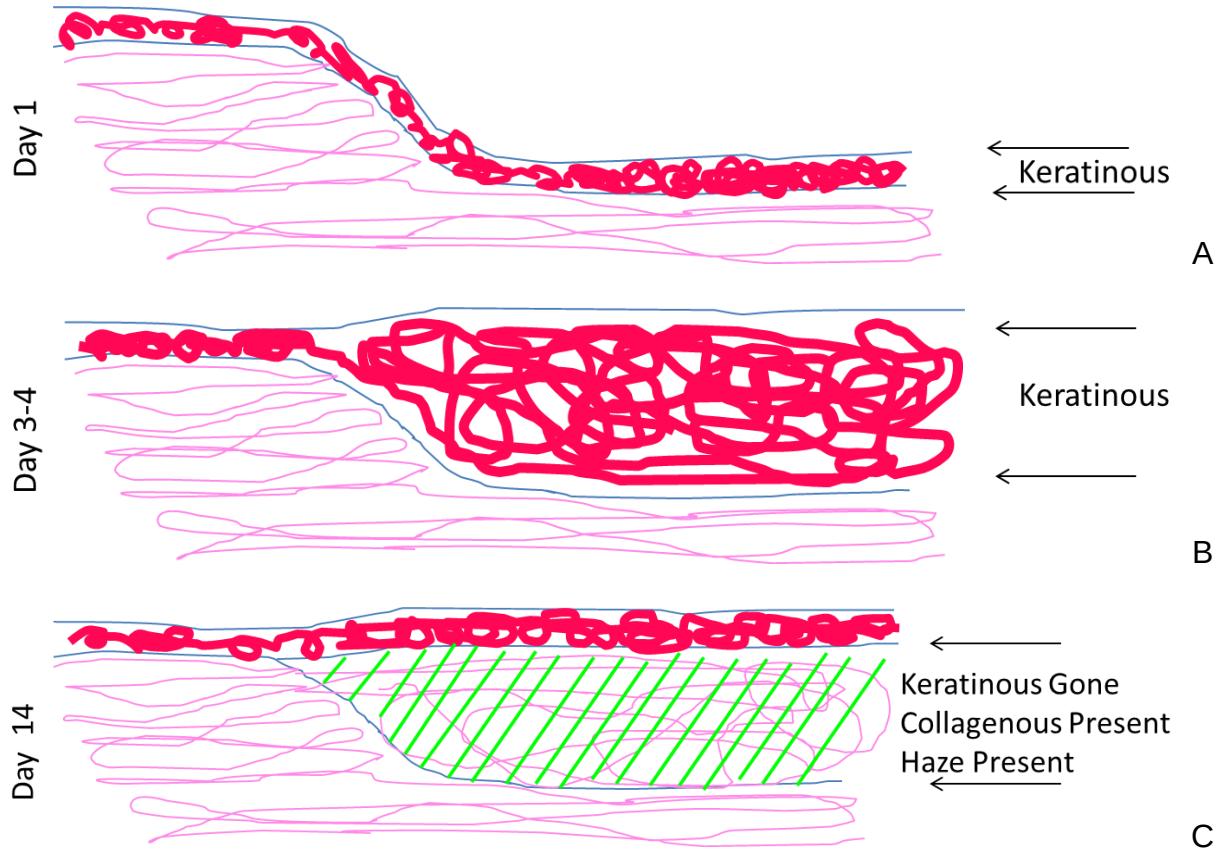

Figure 5-3. An unresolved conundrum with the current prevailing theory. The conundrum is represented in the context of the major structural proteins present in the healing wound.

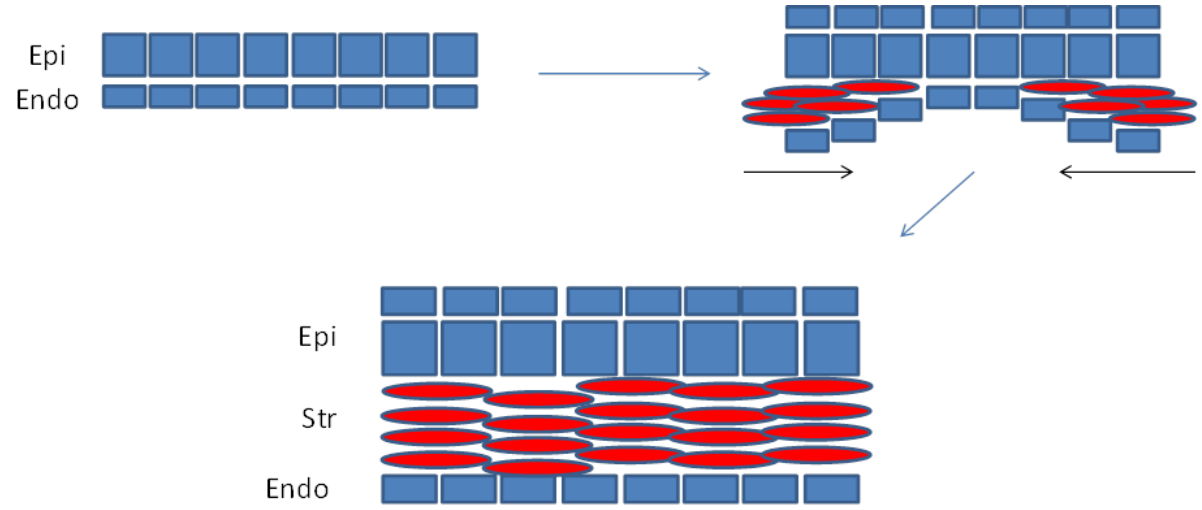

Figure 5-4. A schematic representation of *de novo* stromagenesis that occurs during development. A similar mechanism might be behind the corneal wound healing process.

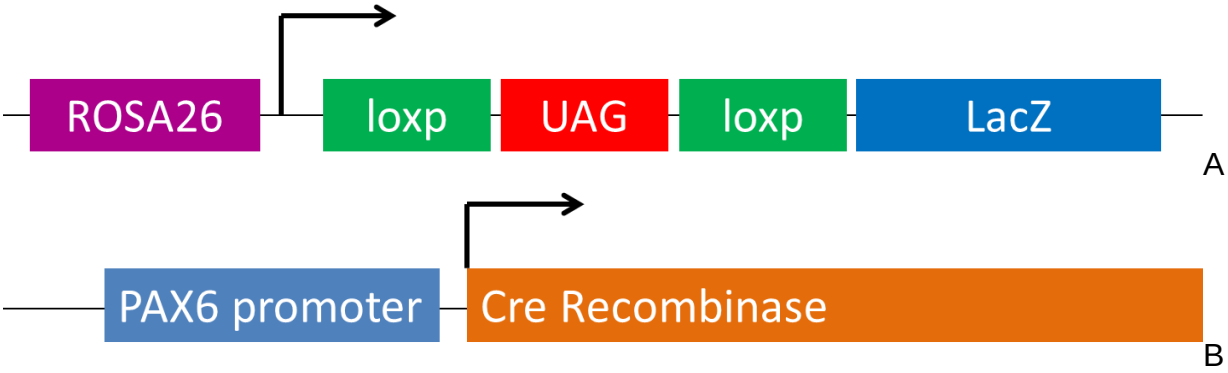

Figure 5-5. The two transgenes which lead to an irreversible genetically labeled corneal epithelium. A) The conditional reporter enzyme transgene. In the presence of Cre-recombinase, the premature stop codon "UAG" is removed, thereby enabling translation of the full-length active β-galactosidase encoded by the LacZ gene. B) Is a scematic of the corneal epithelium specific promoter driving Cre-recombinase expression.

Figure 5-6. Normal and scarred mouse eyes. A) A normal non-scared mouse cornea. B) A representative PTK scar at day 7 post wounding in a ROSA26R/PAX6-Cre mouse eye. C) The same eye in B) one week later and emphasized by grayscale conversion.

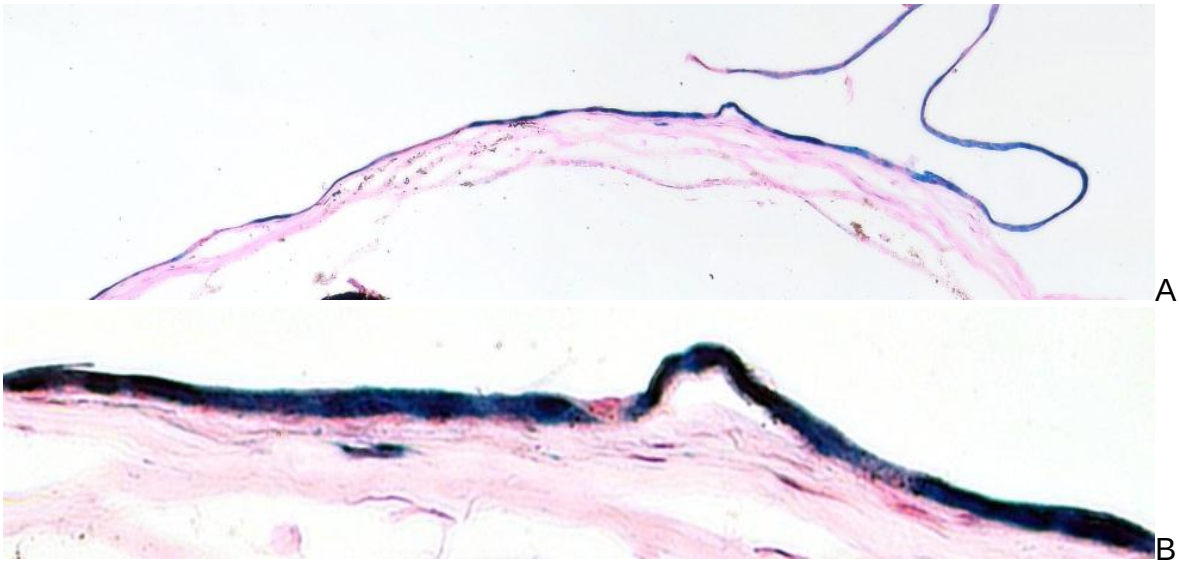

Figure 5-7. A single strong positive blue mass comprised of at most two cells in the anterior-center of the stroma. A) Low power and B) higher power image with detail from the center of the cornea. There are surrounding cells without β-galactosidase activity indicating that they're not epithelial derived.

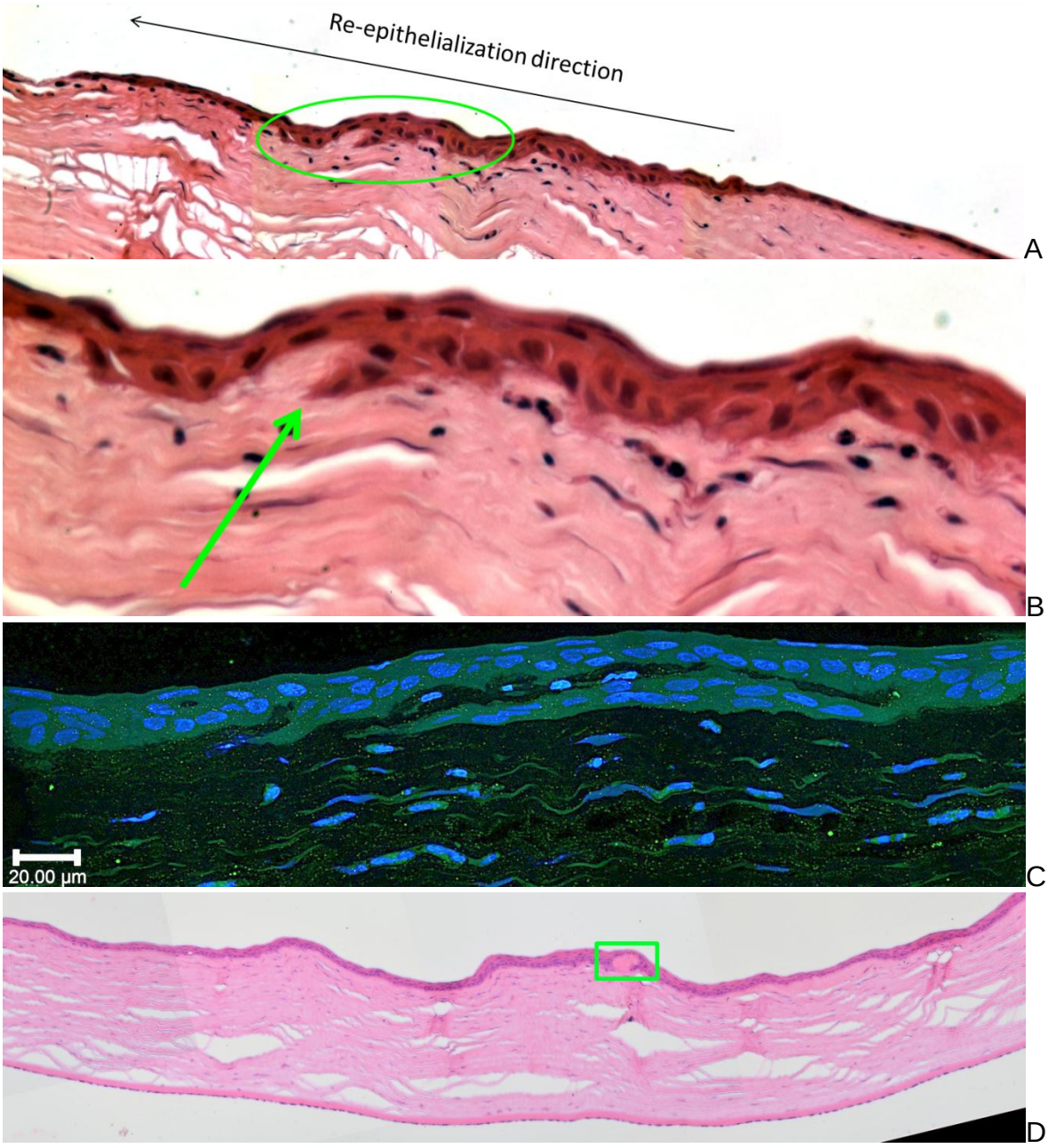

Figure 5-8. Epithelial invasion of the stroma during re-epithelialization. A) An H&E wide-field mosaic of a day 1 post-wounding cornea. B) A higher power image of the region highlighted region. C) An autofluorescence and DAPI images of a day 2 post-wounding cornea where the initial invasion has progressed significantly. D) An H&E low power mosaic of a day 4 post-wounding cornea. The invading epithelial front has effective delaminated several lamellae and generated an included mass.

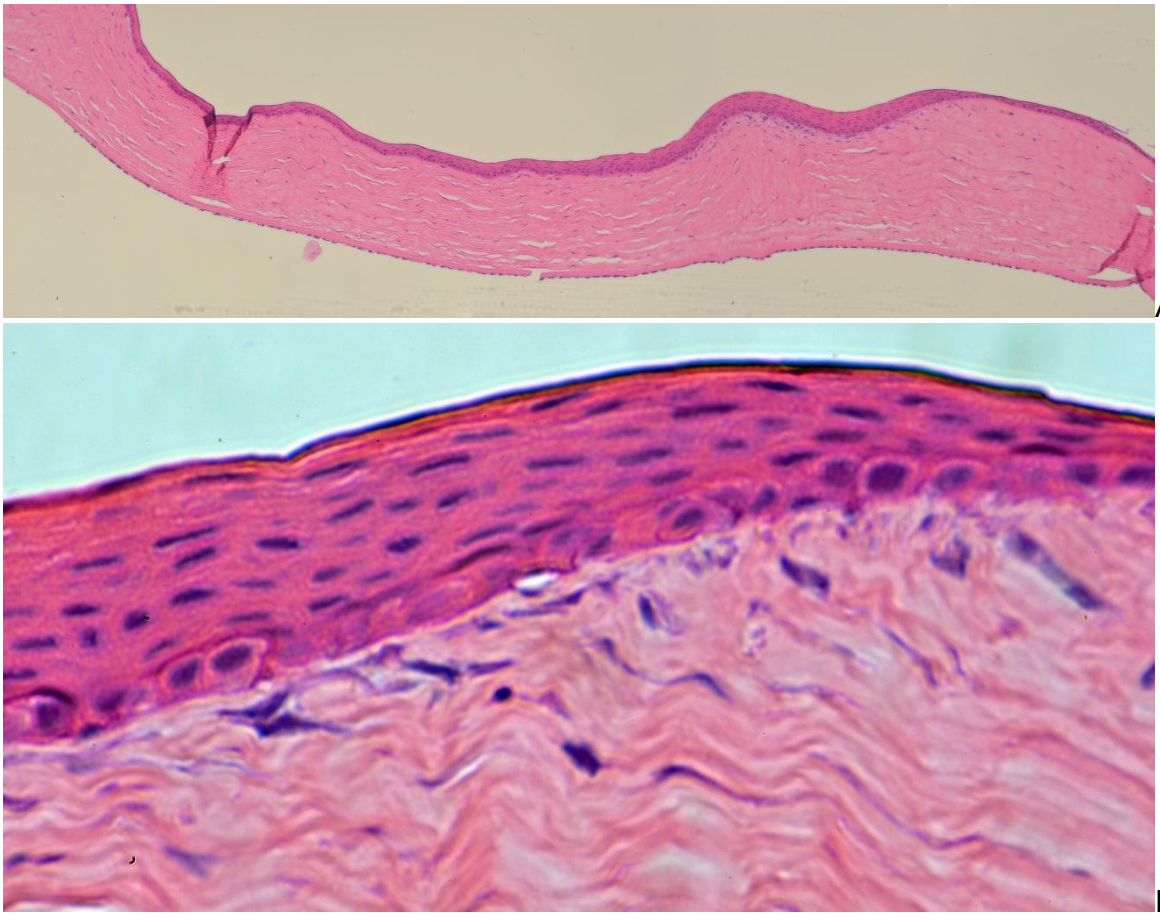

Figure 5-9. Epithelial hyperplasia at the wound margin and migration of stroma-derived cells into the wound interface. A) A low power H&E image and B) a higher power image from the wound margin in the same section.

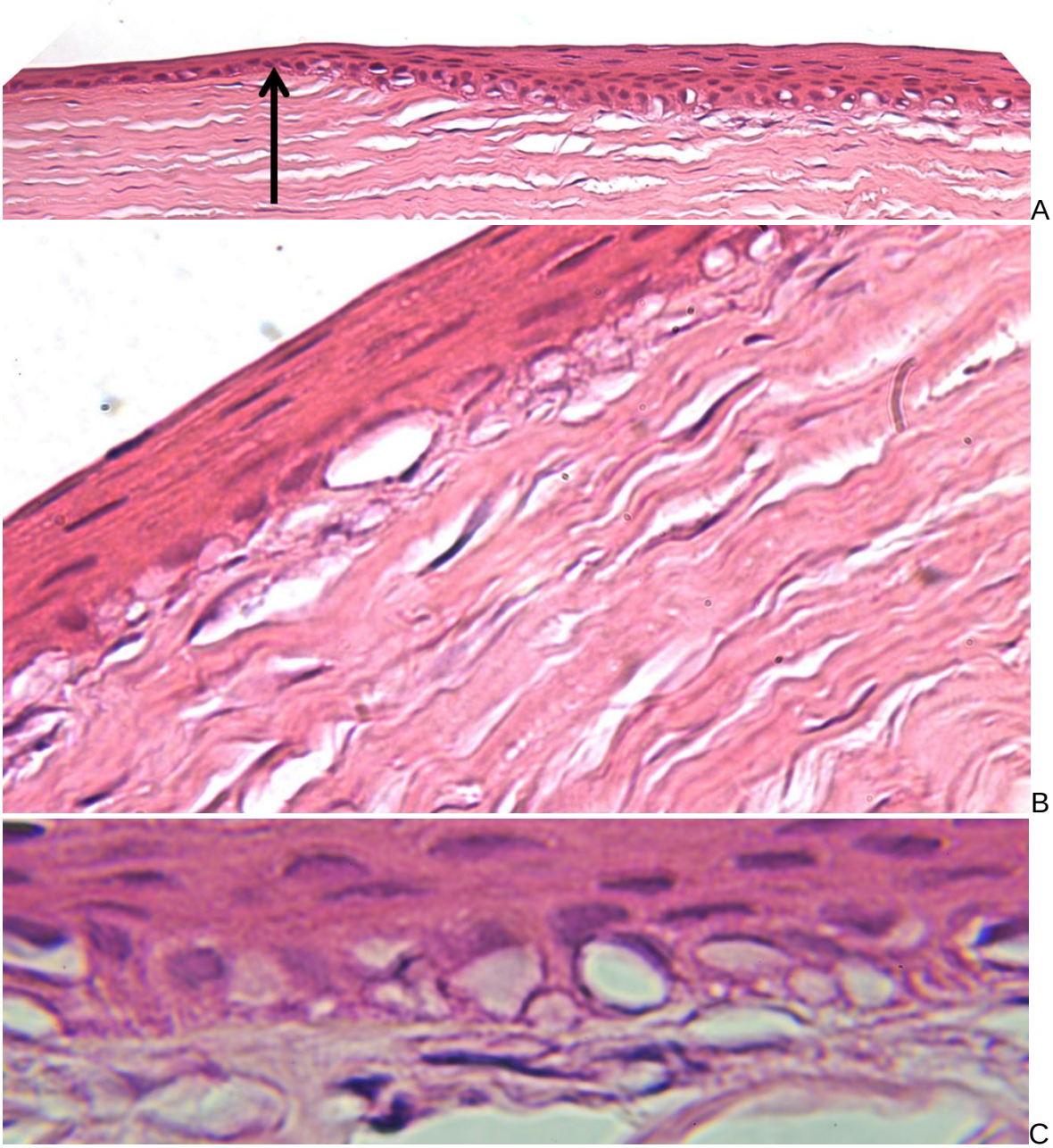

Figure 5-10. The loss of epithelial attachment via a blistering-like mechanism. A) Five days after wounding, a region of blistering between the basal epithelium and wounded stroma (right of the arrow) begins to appear while the epithelium outside of the wound (left of the arrow) appears fine. B&C) Detail of the blister-like structures.

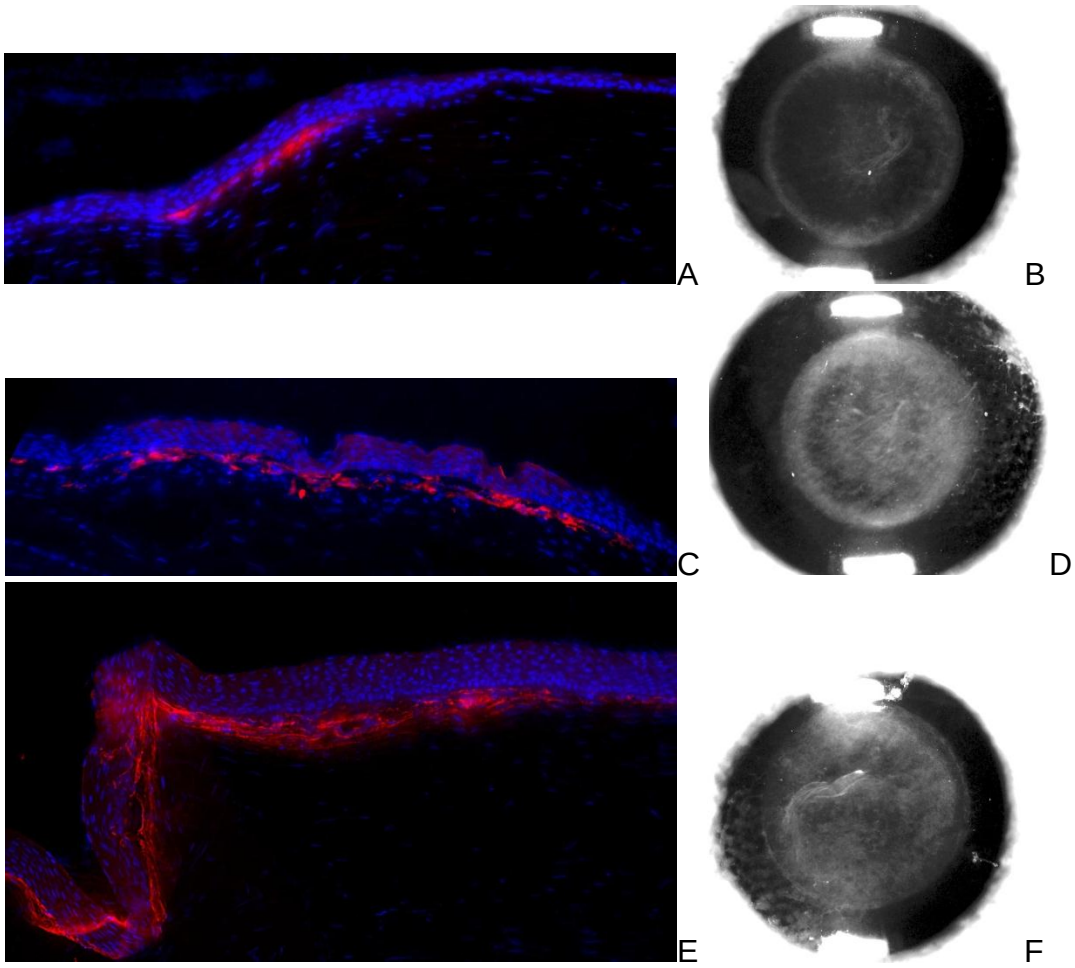

Figure 5-11. The distribution of tenascin-C during haze formation. A), C), & E) are immunofluorescent micrographs from days 5, 7, & 10, respectively. B), D), & F) Macrophotographs of the haze present in the corneas just prior to tissue harvesting. These are separate sections from the same corneas that were used to measure α-SMA (Figure 4-2). Note, that the pattern of staining for tenascin-C has is highly correlated with the staining seen for α-SMA.

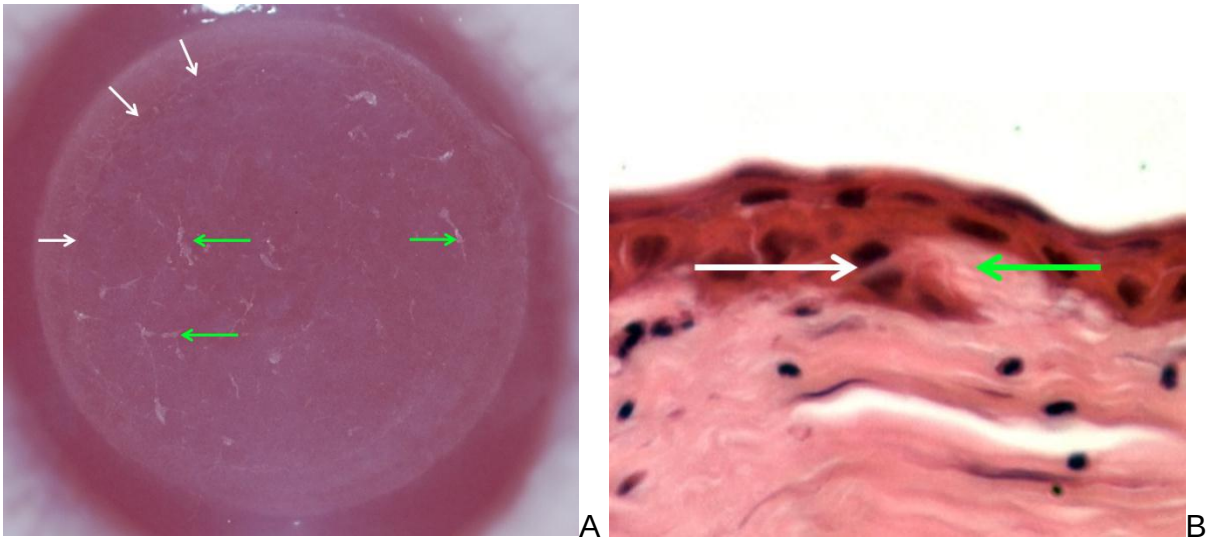

Figure 5-12. A potential mechanism for the observed epithelial invasion of the stroma. A) A cornea one day after PTK surgery. The white arrows indicate the migrating epithelial front while the green arrows indicate peeling residual stromal lamellae. B) If the migrating epithelial front aligns with the peeling stromal lamellae, then the epithelial cells can enter and become embedded in the stroma.

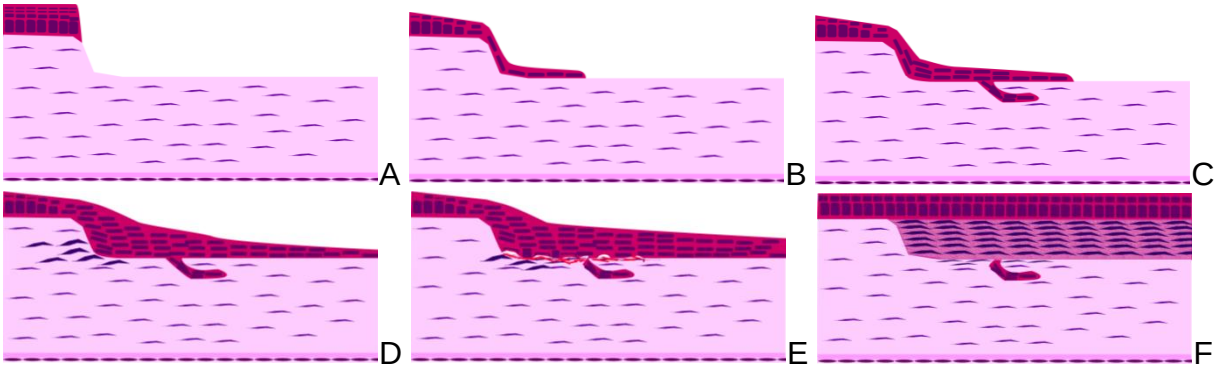

Figure 5-13. A new cellular model for the generation of corneal haze. A) The initial wound. B) The migrating epithelial front (day 1). C) Occasional epithelial invasion of the stroma (days 2-3). D) Epithelial hyperplasia at the wound margin and keratocytes migration into the wound (days 3-4). E) Stacking of αSMA+ cells in the sub-epithelial stroma and loss of epithelial adhesion via a blistering-like mechanism. E) The epithelial implant is surmounted by stromal-cell derived scar cells and matrix which form the preponderance of light reflecting material.

CHAPTER 6
CONCLUSIONS AND FUTURE DIRECTIONS

A New Therapeutic Modality Validated

Iontophoresis of small molecules has been a viable technology for decades, but there are substantive barriers to adapting the process for the delivery of larger macromolecular therapies like mRNA ablating oligonucleotides. A few groups have been working on using iontophoresis to deliver oligonucleotides into skin[103] and corneas[102,122]. Both have reported success in delivery, but only the group treating skin had any measurable biochemical effect. Here, I have demonstrated a change in a physiological process as a consequence of iontophoretically delivered, gene targeted, therapy in the cornea. This success justifies continued attention to refining the method and device in for use in subsequent studies of other gene products within the cornea.

A New Standard in Visualizing and Reporting Corneal Haze

The current standard in measuring and reporting corneal haze essentially represents a qualitative assessment of the observed scar. The approach reduces a complex geometric distribution across the wounded area into a single scalar number on a scale from 0 to 4. It is currently impossible to objectively compare results from other investigations within this field of study, or even from one article to another written by the same group. The new method of recording and quantifying corneal scars presented here, has the ability to improve both the communication of, and comparison of, results amongst groups which can drastically improve the rate of progress in research targeted at preventing corneal fibrosis. That said, there are still aspects of the method described here that need refinement and standardization. Future work will focus on ensuring that the method is amenable to variations in the choice of imaging platform, sensor size, and

camera placement as well as operator to operator variations. Most of these issues will be greatly remedied with the use of external standards, placed next to the wound, which can be included within the image and thereby enable corrections for differences in exposure (intensity) and camera placement (distortion).

Connective Tissue Growth Factor in Healing Corneas

The success in reducing connective tissue growth factor (CTGF) with an ASO and the observed reduction in haze that followed served to greatly support the hypothetical role of CTGF in corneal haze formation. The additional evidence that CTGF protein was primarily localized to the basal epithelium, where the scar will eventually be, further supported its hypothetical role in scarring, owing to it being in the right place at the right time. Had CTGF not been highly concentrated in the wound prior to the formation of haze, and more importantly in the location of where the scar tissue was growing, then its role in scarring would have been difficult to support. While the evidence does support a role for CTGF in scarring, the fact that it was predominantly found on the epithelium calls into question what, precisely, that role is. The evidence provided here demonstrate that the location of CTGF binding, epithelial blistering, and the destination of the migrating fibroblasts are coincident. Whether CTGF stimulates the blistering, or the secretion of chemotactic signals for the fibroblasts remains unclear.

The initial hypotheses about the source of CTGF in the cornea was also undercut by the data presented here. The data revealed unexpectedly that CTGF is predominantly produced in the corneal endothelium, not the stromal fibroblasts. That the locations of maximal synthesis and maximal binding were on opposing sides of the cornea was interesting, but difficult to understand at first. Typically, the net flow of fluid is out of the cornea across the endothelium, giving the appearance that the endothelial

derived CTGF would have to diffuse “upstream” against the current. However, during healing the net flow of fluid is into the cornea as is evidenced by the corneal swelling during the first few days. Additionally, the fact that the peak of CTGF binding and its decline coincide with the peak and tapering off of edema provides a plausible mechanism for the proposed trans-corneal diffusion. The stoma is a significant barrier to diffusion of ionic macromolecules until it becomes edematous[110]. The sum of these observations is the new theory that CTGF synthesized by the endothelium is permitted by the edematous stroma to diffuse and bind to the basal epithelium. Given the proposed mechanism of edema-permitted diffusion of CTGF from the endothelium to the epithelium, preventing edema might be a viable anti-fibrotic target in that it would preclude the introduction of CTGF to the epithelium.

While the endothelium was the predominant site of CTGF synthesis, it was not the only site. Both the stroma and epithelium had CTGF synthesis that was measurable by highly sensitive real-time PCR analysis. An alternative theory to the edema-permitted diffusion theory is that the epithelium undergoes a change during healing which permits it to accumulate the low levels of CTGF synthesis present in the epithelium and stroma. Resolving which cell layer the “effector” CTGF arises from more conclusively is essential if any mRNA ablating anti-CTGF strategy is chosen. Given efficacy of the ASOs to reduce both haze and CTGF, it does appear that the “effector” CTGF is derived from cells in the cornea as opposed to a source outside of the cornea (i.e. tear fluid). Future work in this area will be done using conditional knockout mice which allow semi-selective genomic ablation of CTGF in the cornea using the same tissue specific Cre-recombinase system as was used in the cell tracing experiments. By using a panel

of promoters specific for the different cells layers in the cornea the source of pro-fibrotic CTGF in the cornea can be determined more conclusively.

Haze Fibrogenesis

The key observation leading to the new theory of haze fibrogenesis was made possible by the novel haze imaging and measuring technique developed herein. The fact that the haze begins in two distinct loci within the wound and then spreads from these loci of nucleation calls into question the currently espoused theory that underlying keratocytes spiral upwards into the wound, differentiate, and then adopt a light reflecting phenotype. If this was the case, then it is expected that the haze would have uniformly appeared and gradually increased in intensity. The histological evidence of fibroblasts accumulating along the stromal lamellae at the wound margin is evidence that the haze forming cells migrate into the wound interface from the periphery. This mechanism is consistent with the observed lateral spread of haze since the peripheral fibroblasts have to migrate a longer distance to get to the more central regions of the wound. Given a constant rate of migration, haze would appear to spread as the migrating fibroblasts made progress towards the center of the wound.

The separate haze initiation at the center of the wound is not as consistent in occurrence or location as the haze at the margin, indicating an element of randomness in the nucleating event. The image data from the CTGF antisense experiments indicated that the haze at the margin was sensitive to CTGF reduction while the central haze was refractory. The gross histological and cell tracing evidence demonstrated that the migrating epithelial cells can enter the stroma along incompletely removed lamellae. Given that the epithelial invasion of the stroma is expected to be independent of CTGF, it is possible that the epithelial invasion serves as another mechanism by which the

central haze is initiated and propagated. In the cell tracing experiment in the mouse cornea, and in study of the corneas from post-mortem human LASIK patients[23], the total contribution to haze of these epithelial islands appears to be minimal. While, the gross histological data from the rabbits indicate that the invading structures can be more substantial, it is not clear whether the observed larger epithelial inclusions persist, and the degree to which they contribute to the central haze. Since the rabbit PTK model is the more relevant model for transepithelial stroma-penetrating lesions, the degree of contribution to the central corneal haze of the epithelial inclusions is the focus of studies currently being planned.

Expected Clinical Impact

The majority of the findings presented here are expected to have their initial impact in the research and testing of new haze preventing agents; any clinical impact would be contingent upon the outcomes of those research projects. Of these findings, the new insights into the mechanism of haze formation is expected to have the largest, long-range, clinical impact. That said, some of the other findings have the potential for immediate clinical impact.

The first of these findings with immediate potential arises from the hypothesis that edema might be necessary for CTGF to be introduced into the wound. While this hypothesis is still immature scientifically, the approach and agents for testing it are already used in the clinic and are relatively benign. Currently, hypertonic saline is commonly used to reduce corneal swelling following the placement of corneal grafts. Given its clinical availability and nearly non-existent toxicity (compared to mitomycin C), a trial of topically applied hypertonic saline as a means of preventing corneal haze in wounds could have an immediate and drastic clinical impact.

While the wound photography and quantification technique is expected to be most useful in a research and testing environment, the technique could be used to make the data in a patient's chart more robust. Using standard commercial off-of-the shelf equipment, high resolution, highly detailed images of the lesion (fluorescein stained) or of the scar/opacity could be recorded and tracked with time. The greatest anticipated clinical value of including such images in the charts is that the complete coverage of the wound with a high resolution image, or series of images, would greatly facilitate consultation with more experienced colleagues from all over the globe (via telemedicine). Additionally, the inclusion of these images into medical records would create an invaluable repository for future medical research and training.

Closing Remarks

The work presented here severely undercut some initial hypotheses, validated others, and led to several newly generated ones as well. While the data presented here have provided further insight into, and immediately testable hypothesis about, the process of haze formation in the cornea, the data did not provide a definitive solution for the prevention or reversal of corneal haze. While the ultimate goal of medical research is to solve problems pertaining to human health and wellness, progress in medical research is measured by a reduction in the ambiguity surrounding any given medical problem. By this standard, I submit that the research presented herein was fruitful.

LIST OF REFERENCES

1. Border, W.A. & Ruoslahti, E. Transforming growth factor-beta in disease: the dark side of tissue repair. *J Clin Invest* **90**, 1-7 (1992).

2. Ito, Y.*, et al.* Expression of connective tissue growth factor in human renal fibrosis. *Kidney Int* **53**, 853-861 (1998).

3. Gressner, A.M., Weiskirchen, R., Breitkopf, K. & Dooley, S. Roles of TGF-beta in hepatic fibrosis. *Front Biosci* **7**, d793-807 (2002).

4. Lijnen, P.J., Petrov, V.V. & Fagard, R.H. Induction of cardiac fibrosis by transforming growth factor-beta(1). *Mol Genet Metab* **71**, 418-435 (2000).

5. Thompson, N.L.*, et al.* Transforming growth factor beta-1 in acute myocardial infarction in rats. *Growth Factors* **1**, 91-99 (1988).

6. Chegini, N. The role of growth factors in peritoneal healing: transforming growth factor beta (TGF-beta). *Eur J Surg Suppl*, 17-23 (1997).

7. Igarashi, A.*, et al.* Connective tissue growth factor gene expression in tissue sections from localized scleroderma, keloid, and other fibrotic skin disorders. *J Invest Dermatol* **106**, 729-733 (1996).

8. Sherwood, M.B. A sequential, multiple-treatment, targeted approach to reduce wound healing and failure of glaucoma filtration surgery in a rabbit model (an American Ophthalmological Society thesis). *Trans Am Ophthalmol Soc* **104**, 478-492 (2006).

9. Connor, T.B., Jr.*, et al.* Correlation of fibrosis and transforming growth factor-beta type 2 levels in the eye. *J Clin Invest* **83**, 1661-1666 (1989).

10. Moller-Pedersen, T., Cavanagh, H.D., Petroll, W.M. & Jester, J.V. Neutralizing antibody to TGFbeta modulates stromal fibrosis but not regression of photoablative effect following PRK. *Curr Eye Res* **17**, 736-747 (1998).

11. Esson, D.W.*, et al.* Expression of connective tissue growth factor after glaucoma filtration surgery in a rabbit model. *Invest Ophthalmol Vis Sci* **45**, 485-491 (2004).

12. Krachmer, J.H.M., Mark J.; Holland, Edward J. *Cornea*, (Elsevier Mosby, 2005).

13. Gordon-Thomson, C., de Iongh, R.U., Hales, A.M., Chamberlain, C.G. & McAvoy, J.W. Differential cataractogenic potency of TGF-beta1, -beta2, and -beta3 and their expression in the postnatal rat eye. *Invest Ophthalmol Vis Sci* **39**, 1399-1409 (1998).

14. Hales, A.M., Chamberlain, C.G., Dreher, B. & McAvoy, J.W. Intravitreal injection of TGFbeta induces cataract in rats. *Invest Ophthalmol Vis Sci* **40**, 3231-3236 (1999).

15. Lee, E.H. & Joo, C.K. Role of transforming growth factor-beta in transdifferentiation and fibrosis of lens epithelial cells. *Invest Ophthalmol Vis Sci* **40**, 2025-2032 (1999).

16. Zadunaisky, J.A. Active transport of chloride in frog cornea. *The American journal of physiology* **211**, 506-512 (1966).

17. Zadunaisky, J.A. Active transport of chloride across the cornea. *Nature* **209**, 1136-1137 (1966).

18. Hodson, S. & Miller, F. The bicarbonate ion pump in the endothelium which regulates the hydration of rabbit cornea. *The Journal of physiology* **263**, 563-577 (1976).

19. Dohlman, C.H. The function of the corneal epithelium in health and disease. The Jonas S. Friedenwald Memorial Lecture. *Invest Ophthalmol* **10**, 383-407 (1971).

20. Wilson, S.E. & Kim, W.J. Keratocyte apoptosis: implications on corneal wound healing, tissue organization, and disease. *Invest Ophthalmol Vis Sci* **39**, 220-226 (1998).

21. Zieske, J.D. Extracellular matrix and wound healing. *Curr Opin Ophthalmol* **12**, 237-241 (2001).

22. Kuo, I.C. Corneal wound healing. *Curr Opin Ophthalmol* **15**, 311-315 (2004).

23. Dawson, D.G.*, et al.* Ex vivo confocal microscopy of human LASIK corneas with histologic and ultrastructural correlation. *Ophthalmology* **112**, 634-644 (2005).

24. Moller-Pedersen, T. Keratocyte reflectivity and corneal haze. *Exp Eye Res* **78**, 553-560 (2004).

25. O'Brart, D.P.*, et al.* Night vision after excimer laser photorefractive keratectomy: haze and halos. *Eur J Ophthalmol* **4**, 43-51 (1994).

26. O'Brart, D.P.*, et al.* Disturbances in night vision after excimer laser photorefractive keratectomy. *Eye* **8 (Pt 1)**, 46-51 (1994).

27. Moller-Pedersen, T., Cavanagh, H.D., Petroll, W.M. & Jester, J.V. Corneal haze development after PRK is regulated by volume of stromal tissue removal. *Cornea* **17**, 627-639 (1998).

28. Long, Q.*, et al.* Correlation between TGF-[beta]1 in tears and corneal haze following LASEK and Epi-LASIK. *American Journal of Ophthalmology* **143**, 195-195 (2007).

29. Stramer, B.M., Zieske, J.D., Jung, J.C., Austin, J.S. & Fini, M.E. Molecular mechanisms controlling the fibrotic repair phenotype in cornea: implications for surgical outcomes. *Invest Ophthalmol Vis Sci* **44**, 4237-4246 (2003).

30. Alio, J.L.*, et al.* Ten-year follow-up of photorefractive keratectomy for myopia of more than -6 diopters. *Am J Ophthalmol* **145**, 37-45 (2008).

31. Alio, J.L.*, et al.* Ten-year follow-up of photorefractive keratectomy for myopia of less than -6 diopters. *Am J Ophthalmol* **145**, 29-36 (2008).

32. Boulton, M., Singh, A., Wong, HC., and McLeod, D. Dexamethasone directly and indirectly inhibits the proliferation of retinal microvascular endothelial cells. *Invest ophthalmol vis sci* **29**, 243 (1988).

33. Tuft, S.J., Zabel, R.W. & Marshall, J. Corneal repair following keratectomy. A comparison between conventional surgery and laser photoablation. *Invest Ophthalmol Vis Sci* **30**, 1769-1777 (1989).

34. Gartry, D.S., Kerr Muir, M. & Marshall, J. The effect of topical corticosteroids on refraction and corneal haze following excimer laser treatment of myopia: an update. A prospective, randomised, double-masked study. *Eye* **7 (Pt 4)**, 584-590 (1993).

35. Baek, S.H., Chang, J.H., Choi, S.Y., Kim, W.J. & Lee, J.H. The effect of topical corticosteroids on refractive outcome and corneal haze after photorefractive keratectomy. *J Refract Surg* **13**, 644-652 (1997).

36. Agren, M.S., Mirastschijski, U., Karlsmark, T. & Saarialho-Kere, U.K. Topical synthetic inhibitor of matrix metalloproteinases delays epidermal regeneration of human wounds. *Exp Dermatol* **10**, 337-348 (2001).

37. Vetrugno, M., Maino, A., Quaranta, G.M. & Cardia, L. The effect of early steroid treatment after PRK on clinical and refractive outcomes. *Acta Ophthalmol Scand* **79**, 23-27 (2001).

38. Tomasz, M. Mitomycin C: small, fast and deadly (but very selective). *Chem Biol* **2**, 575-579 (1995).

39. Tomasz, M. & Palom, Y. The mitomycin bioreductive antitumor agents: cross-linking and alkylation of DNA as the molecular basis of their activity. *Pharmacology & therapeutics* **76**, 73-87 (1997).

40. Roh, D.S. & Funderburgh, J.L. Impact on the corneal endothelium of mitomycin C during photorefractive keratectomy. *J Refract Surg* **25**, 894-897 (2009).

41. Kopp, E.D. & Seregard, S. Epiphora as a side effect of topical mitomycin C. *The British journal of ophthalmology* **88**, 1422-1424 (2004).

42. Coppens, G. & Maudgal, P. Corneal complications of intraoperative Mitomycin C in glaucoma surgery. *Bulletin de la Societe belge d'ophtalmologie*, 19-23 (2010).

43. Zhivov, A., Beck, R. & Guthoff, R.F. Corneal and conjunctival findings after mitomycin C application in pterygium surgery: an in-vivo confocal microscopy study. *Acta ophthalmologica* **87**, 166-172 (2009).

44. Ferguson, M.H., GF. Marsupial models of scarless fetal wound healing. in *Fetal Wound Healing* (ed. Adzick, N.L.M.) 95-124 (Elsevier, New York, 1992).

45. Longaker, M.T.*, et al.* Adult skin wounds in the fetal environment heal with scar formation. *Ann Surg* **219**, 65-72 (1994).

46. Shah, M., Foreman, D.M. & Ferguson, M.W. Neutralisation of TGF-beta 1 and TGF-beta 2 or exogenous addition of TGF-beta 3 to cutaneous rat wounds reduces scarring. *J Cell Sci* **108 (Pt 3)**, 985-1002 (1995).

47. Van Obberghen-Schilling, E., Roche, N.S., Flanders, K.C., Sporn, M.B. & Roberts, A.B. Transforming growth factor beta 1 positively regulates its own expression in normal and transformed cells. *The Journal of biological chemistry* **263**, 7741-7746 (1988).

48. Bascom, C.C.*, et al.* Complex regulation of transforming growth factor beta 1, beta 2, and beta 3 mRNA expression in mouse fibroblasts and keratinocytes by transforming growth factors beta 1 and beta 2. *Mol Cell Biol* **9**, 5508-5515 (1989).

49. Jester, J.V., Barry-Lane, P.A., Petroll, W.M., Olsen, D.R. & Cavanagh, H.D. Inhibition of corneal fibrosis by topical application of blocking antibodies to TGF beta in the rabbit. *Cornea* **16**, 177-187 (1997).

50. Whitby, D.J. & Ferguson, M.W. Immunohistochemical localization of growth factors in fetal wound healing. *Dev Biol* **147**, 207-215 (1991).

51. Saika, S. TGF-beta signal transduction in corneal wound healing as a therapeutic target. *Cornea* **23**, S25-30 (2004).

52. Tuli, S.S.*, et al.* Immunohistochemical localization of EGF, TGF-alpha, TGF-beta, and their receptors in rat corneas during healing of excimer laser ablation. *Curr Eye Res* **31**, 709-719 (2006).

53. Vesaluoma, M., Teppo, A.M., Gronhagen-Riska, C. & Tervo, T. Release of TGF-beta 1 and VEGF in tears following photorefractive keratectomy. *Curr Eye Res* **16**, 19-25 (1997).

54. Yoshino, K., Garg, R., Monroy, D., Ji, Z. & Pflugfelder, S.C. Production and secretion of transforming growth factor beta (TGF-beta) by the human lacrimal gland. *Curr Eye Res* **15**, 615-624 (1996).

55. Laping, N.J.*, et al.* Tumor-specific efficacy of transforming growth factor-beta RI inhibition in Eker rats. *Clinical cancer research : an official journal of the American Association for Cancer Research* **13**, 3087-3099 (2007).

56. Franch, H.A., Shay, J.W., Alpern, R.J. & Preisig, P.A. Involvement of pRB family in TGF beta-dependent epithelial cell hypertrophy. *The Journal of cell biology* **129**, 245-254 (1995).

57. Igarashi, A., Okochi, H., Bradham, D.M. & Grotendorst, G.R. Regulation of connective tissue growth factor gene expression in human skin fibroblasts and during wound repair. *Mol Biol Cell* **4**, 637-645 (1993).

58. Frazier, K., Williams, S., Kothapalli, D., Klapper, H. & Grotendorst, G.R. Stimulation of fibroblast cell growth, matrix production, and granulation tissue formation by connective tissue growth factor. *J Invest Dermatol* **107**, 404-411 (1996).

59. Grotendorst, G.R. Connective tissue growth factor: a mediator of TGF-beta action on fibroblasts. *Cytokine Growth Factor Rev* **8**, 171-179 (1997).

60. Garrett, Q.*, et al.* Involvement of CTGF in TGF-beta1-stimulation of myofibroblast differentiation and collagen matrix contraction in the presence of mechanical stress. *Invest Ophthalmol Vis Sci* **45**, 1109-1116 (2004).

61. Daniels, J.T.*, et al.* Mediation of transforming growth factor-beta(1)-stimulated matrix contraction by fibroblasts: a role for connective tissue growth factor in contractile scarring. *Am J Pathol* **163**, 2043-2052 (2003).

62. Bradham, D.M., Igarashi, A., Potter, R.L. & Grotendorst, G.R. Connective tissue growth factor: a cysteine-rich mitogen secreted by human vascular endothelial cells is related to the SRC-induced immediate early gene product CEF-10. *J Cell Biol* **114**, 1285-1294 (1991).

63. Blalock, T.D.*, et al.* Connective tissue growth factor expression and action in human corneal fibroblast cultures and rat corneas after photorefractive keratectomy. *Invest Ophthalmol Vis Sci* **44**, 1879-1887 (2003).

64. Baldwin, H.C. & Marshall, J. Growth factors in corneal wound healing following refractive surgery: A review. *Acta Ophthalmol Scand* **80**, 238-247 (2002).

65. He, S.*, et al.* Connective Tissue Growth Factor as a Mediator of Intraocular Fibrosis. *Invest. Ophthalmol. Vis. Sci.*, iovs.07-1302 (2008).

66. Hinton, D.R.*, et al.* Accumulation of NH2-terminal fragment of connective tissue growth factor in the vitreous of patients with proliferative diabetic retinopathy. *Diabetes Care* **27**, 758-764 (2004).

67. Brigstock, D.R.*, et al.* Purification and characterization of novel heparin-binding growth factors in uterine secretory fluids. Identification as heparin-regulated Mr 10,000 forms of connective tissue growth factor. *J Biol Chem* **272**, 20275-20282 (1997).

68. Grotendorst, G.R. & Duncan, M.R. Individual domains of connective tissue growth factor regulate fibroblast proliferation and myofibroblast differentiation. *FASEB J* **19**, 729-738 (2005).

69. Grotendorst, G.R., Rahmanie, H. & Duncan, M.R. Combinatorial signaling pathways determine fibroblast proliferation and myofibroblast differentiation. *FASEB J* **18**, 469-479 (2004).

70. Dawson, D.G., Kramer, T.R., Grossniklaus, H.E., Waring, G.O., 3rd & Edelhauser, H.F. Histologic, ultrastructural, and immunofluorescent evaluation of human laser-assisted in situ keratomileusis corneal wounds. *Arch Ophthalmol* **123**, 741-756 (2005).

71. Smiddy, W.E.*, et al.* Transforming growth factor beta. A biologic chorioretinal glue. *Arch Ophthalmol* **107**, 577-580 (1989).

72. Cuenoud, B. & Szostak, J.W. A DNA metalloenzyme with DNA ligase activity. *Nature* **375**, 611-614 (1995).

73. Dass, C.R., Choong, P.F. & Khachigian, L.M. DNAzyme technology and cancer therapy: cleave and let die. *Molecular cancer therapeutics* **7**, 243-251 (2008).

74. Famulok, M., Hartig, J.S. & Mayer, G. Functional aptamers and aptazymes in biotechnology, diagnostics, and therapy. *Chem Rev* **107**, 3715-3743 (2007).

75. Khan, A.U. Ribozyme: a clinical tool. *Clinica chimica acta; international journal of clinical chemistry* **367**, 20-27 (2006).

76. Maruyama, N., Fukuda, N., Okada, K. & Matsumoto, K. [Development of gene therapy for encapsulating peritoneal sclerosis by a chimeric DNA-RNA hammerhead ribozyme targeting TGF-beta1 mRNA]. *Nippon Jinzo Gakkai Shi* **49**, 113-120 (2007).

77. Wu, Y.*, et al.* Inhibition of bcr-abl oncogene expression by novel deoxyribozymes (DNAzymes). *Hum Gene Ther* **10**, 2847-2857 (1999).

78. Yusa, J.*, et al.* Inhibition of growth of human gingival fibroblasts by chimeric DNA-RNA hammerhead ribozyme targeting transforming growth factor-beta 1. *J Periodontol* **76**, 1265-1274 (2005).

79. Santoro, S.W. & Joyce, G.F. A general purpose RNA-cleaving DNA enzyme. *Proc Natl Acad Sci U S A* **94**, 4262-4266 (1997).

80. Bock, L.C., Griffin, L.C., Latham, J.A., Vermaas, E.H. & Toole, J.J. Selection of single-stranded DNA molecules that bind and inhibit human thrombin. *Nature* **355**, 564-566 (1992).

81. Huizenga, D.E. & Szostak, J.W. A DNA aptamer that binds adenosine and ATP. *Biochemistry* **34**, 656-665 (1995).

82. Ellington, A.D. & Szostak, J.W. In vitro selection of RNA molecules that bind specific ligands. *Nature* **346**, 818-822 (1990).

83. Waring, R.B., Scazzocchio, C., Brown, T.A. & Davies, R.W. Close relationship between certain nuclear and mitochondrial introns. Implications for the mechanism of RNA splicing. *J Mol Biol* **167**, 595-605 (1983).

84. Cotten, M., Schaffner, G. & Birnstiel, M.L. Ribozyme, antisense RNA, and antisense DNA inhibition of U7 small nuclear ribonucleoprotein-mediated histone pre-mRNA processing in vitro. *Mol Cell Biol* **9**, 4479-4487 (1989).

85. Zamore, P.D., Tuschl, T., Sharp, P.A. & Bartel, D.P. RNAi: double-stranded RNA directs the ATP-dependent cleavage of mRNA at 21 to 23 nucleotide intervals. *Cell* **101**, 25-33 (2000).

86. Matzke, M.A. & Birchler, J.A. RNAi-mediated pathways in the nucleus. *Nat Rev Genet* **6**, 24-35 (2005).

87. Hermann, T. & Patel, D.J. Adaptive recognition by nucleic acid aptamers. *Science* **287**, 820-825 (2000).

88. Advances in CMV management: fomivirsen (Vitravene) approved. *Proj Inf Perspect*, 7 (1998).

89. Choi, Y.K.*, et al.* Prevention of tissue injury by ribbon antisense to TGF-beta1 in the kidney. *Int J Mol Med* **15**, 391-399 (2005).

90. Doh, K.O.*, et al.* Prevention of CCl4-induced liver cirrhosis by ribbon antisense to transforming growth factor-beta1. *Int J Mol Med* **21**, 33-39 (2008).

91. Liang, Z. & He, Z. [TGF-beta 1 antisense gene transfer into ito cells and suppressed extracellular matrix production]. *Zhonghua Yi Xue Za Zhi* **78**, 850-852 (1998).

92. Liu, X., Yang, L., Chen, D., Zhang, Z. & Qiang, O. [Inhibition of the activation and collagen production of cultured rat hepatic stellate cells by antisense oligonucleotides against transforming growth factor-beta 1]. *Hua Xi Yi Ke Da Xue Xue Bao* **31**, 42-45 (2000).

93. Liu, X., Zhang, Z., Yang, L., Chen, D. & Wang, Y. [Inhibition of the activation and collagen production of cultured rat hepatic stellate cells by antisense oligonucleotides against transforming growth factor-beta 1 is enhanced by cationic liposome delivery]. *Hua Xi Yi Ke Da Xue Xue Bao* **31**, 133-135, 142 (2000).

94. Lu, C.H.*, et al.* [Effects of antisense RNA of connective tissue growth factor expressing plasmid on rat liver fibrosis]. *Zhonghua Gan Zang Bing Za Zhi* **15**, 118-121 (2007).

95. Uchio, K., Graham, M., Dean, N.M., Rosenbaum, J. & Desmouliere, A. Down-regulation of connective tissue growth factor and type I collagen mRNA expression by connective tissue growth factor antisense oligonucleotide during experimental liver fibrosis. *Wound Repair Regen* **12**, 60-66 (2004).

96. Choi, B.M.*, et al.* Control of scarring in adult wounds using antisense transforming growth factor-beta 1 oligodeoxynucleotides. *Immunol Cell Biol* **74**, 144-150 (1996).

97. Excaliard Pharmaceuticals, I. Excaliard Announces Positive Data From Phase 2 Clinical Trial of Its Anti-Scarring Drug, EXC 001. Vol. 2010 A press release about the results of Excaliard Pharmaceuticals, Inc.'s phase 2 clinical trial. (Carlsbad, CA, U.S.A., 2010).

98. Gibson, D.J. Electromotive delivery of oligonucleotides into the cornea. (University of Florida, [Gainesville, Fla.], 2007).

99. Gibson, D.J. & Schultz, G. Optimization of Electrode Material and Placement for in vivo Iontophoretic Delivery of Oligonucleotides Into the Stroma. *Invest. Ophthalmol. Vis. Sci.* **49**, 3195- (2008).

100. Gibson, D.J. & Schultz, G. High Field Computer Controlled Pulse Iontophoresis of Oligonucleotides Into the Cornea. *Invest. Ophthalmol. Vis. Sci.* **47**, 1593- (2006).

101. Gibson, D.J. & Schultz, G.S. Trans-Corneal HEPES Buffered Iontophoresis for Delivery of Oligonucleotides Into the Stroma. *Invest. Ophthalmol. Vis. Sci.* **48**, 5879- (2007).

102. Berdugo, M.*, et al.* Delivery of antisense oligonucleotide to the cornea by iontophoresis. *Antisense Nucleic Acid Drug Dev* **13**, 107-114 (2003).

103. Kigasawa, K.*, et al.* Noninvasive delivery of siRNA into the epidermis by iontophoresis using an atopic dermatitis-like model rat. *Int J Pharm* (2009).

104. Butler, M.*, et al.* Spinal distribution and metabolism of 2'-O-(2-methoxyethyl)-modified oligonucleotides after intrathecal administration in rats. *Neuroscience* **131**, 705-715 (2005).

105. Dokka, S., Cooper, S.R., Kelly, S., Hardee, G.E. & Karras, J.G. Dermal delivery of topically applied oligonucleotides via follicular transport in mouse skin. *The Journal of investigative dermatology* **124**, 971-975 (2005).

106. Roux, J.*, et al.* Transforming growth factor beta1 inhibits cystic fibrosis transmembrane conductance regulator-dependent cAMP-stimulated alveolar epithelial fluid transport via a phosphatidylinositol 3-kinase-dependent mechanism. *J Biol Chem* **285**, 4278-4290 (2010).

107. Yang, Y.M., Wu, X.Y. & Du, L.Q. [The role of connective tissue growth factor, transforming growth factor and Smad signaling pathway during corneal wound healing]. *Zhonghua Yan Ke Za Zhi* **42**, 918-924 (2006).

108. Blake, J.*, et al.* The Mouse Genome Database (MGD): Premier Model Organism Resource for Mammalian Genomics and Genetics. *Nucleic Acids Res* **39**, D842-D848 (2011).

109. Kapoor, M.*, et al.* Connective tissue growth factor promoter activity in normal and wounded skin. *Fibrogenesis & tissue repair* **1**, 3 (2008).

110. Kim, J.H., Green, K., Martinez, M. & Paton, D. Solute permeability of the corneal endothelium and Descemet's membrane. *Experimental Eye Research* **12**, 231-238 (1971).

111. Chai, J.Y., Modak, C., Mouazzen, W., Narvaez, R. & Pham, J. Epithelial or mesenchymal: Where to draw the line? *Biosci Trends* **4**, 130-142 (2010).

112. Ikeda, A., Maisel, H. & Waggoner, D. An immunofluorescent study of cornea development in the chick. *Journal of embryology and experimental morphology* **33**, 279-290 (1975).

113. Gage, P.J., Rhoades, W., Prucka, S.K. & Hjalt, T. Fate maps of neural crest and mesoderm in the mammalian eye. *Investigative ophthalmology & visual science* **46**, 4200-4208 (2005).

114. Kalluri, R. & Neilson, E.G. Epithelial-mesenchymal transition and its implications for fibrosis. *The Journal of clinical investigation* **112**, 1776-1784 (2003).

115. Neilson, E.G. The Jeremiah Metzger lecture. The origin of fibroblasts and the terminality of epithelial differentiation. *Transactions of the American Clinical and Climatological Association* **121**, 240-250; discussion 250-241 (2010).

116. Dandachi, N.*, et al.* Co-expression of tenascin-C and vimentin in human breast cancer cells indicates phenotypic transdifferentiation during tumour progression: correlation with histopathological parameters, hormone receptors, and oncoproteins. *J Pathol* **193**, 181-189 (2001).

117. Sauer, B. & Henderson, N. Site-specific DNA recombination in mammalian cells by the Cre recombinase of bacteriophage P1. *Proceedings of the National Academy of Sciences of the United States of America* **85**, 5166-5170 (1988).

118. Soriano, P. Generalized lacZ expression with the ROSA26 Cre reporter strain. *Nature genetics* **21**, 70-71 (1999).

119. Joo, J.H., Kim, Y.H., Dunn, N.W. & Sugrue, S.P. Disruption of mouse corneal epithelial differentiation by conditional inactivation of pnn. *Investigative ophthalmology & visual science* **51**, 1927-1934 (2010).

120. Gore-Hyer, E.*, et al.* TGF-beta and CTGF have overlapping and distinct fibrogenic effects on human renal cells. *Am J Physiol Renal Physiol* **283**, F707-716 (2002).

121. Liu, B.C., Zhang, J.D., Zhang, X.L., Wu, G.Q. & Li, M.X. Role of connective tissue growth factor (CTGF) module 4 in regulating epithelial mesenchymal transition (EMT) in HK-2 cells. *Clinica chimica acta; international journal of clinical chemistry* **373**, 144-150 (2006).

122. Bejjani, R.A.*, et al.* Electrically assisted ocular gene therapy. *Surv Ophthalmol* **52**, 196-208 (2007).

BIOGRAPHICAL SKETCH

Daniel James Gibson was born in Sarasota, Florida in 1978. In 2001, he was honorably discharged from the United States Air Force after 4 years of duty as an Imagery Analyst. He attended Edison Community College shortly after his military service, and in May of 2003, he was awarded an associate of arts degree in general studies. He matriculated to the University of Florida immediately after leaving Edison and earned a bachelor of science degree in mechanical engineering in May of 2005. Daniel remained at the University and entered a master of science program in the Department of Molecular Genetics and Microbiology. In May of 2007, Daniel was awarded a master of science degree in medical sciences for his research in electromotive drug delivery. Currently, he is continuing to further broaden the scope of his knowledge in the field of biomedical sciences where he plans to bring all of his diverse knowledge to bear on problems of human health. His personal interests include his growing family, philosophy, Rachmaninoff, and commercializing technology.